

**DESIGN AND ANALYSIS OF ANTENNAS FOR WIRELESS
UNDERGROUND PROPAGATION**

**A THESIS SUBMITTED IN PARTIAL FULFILMENT OF THE
REQUIREMENTS FOR THE DEGREE OF DOCTOR OF
PHILOSOPHY**

SARATH KUMAR ANNAVARAPU

MZU REGN NO: 1900103

Ph.D. REGN NO: MZU/Ph.D./ 1446 of 12.08.2019



**DEPARTMENT OF ELECTRONICS & COMMUNICATION
ENGINEERING
SCHOOL OF ENGINEERING AND TECHNOLOGY**

OCTOBER 2023

**DESIGN AND ANALYSIS OF ANTENNAS FOR WIRELESS
UNDEGROUND PROPAGATION**

BY

SARATH KUMAR ANNAVARAPU

Department of Electronics & Communication Engineering

Name of Supervisor : Prof. L. LOLIT KUMAR SINGH

Name of Joint Supervisor : Prof. SUDIPTA CHATTOPADHYAY

Submitted

In partial fulfilment of the requirement of the Degree of Doctor of Philosophy in
Electronics and Communication Engineering of Mizoram University, Aizawl



**Department of Electronics and Communication
Engineering**

School of Engineering and Technology

MIZORAM UNIVERSITY

(A Central University)

Tanhril, Aizawl - 796 004, Mizoram

CERTIFICATE

This is to certify that the thesis entitled “**Design and Analysis of Antennas for Wireless Underground Propagation**” submitted to Mizoram University for the award of the degree of **Doctor of Philosophy Electronics and Communication Engineering** by **SARATH KUMAR ANNAVARAPU**, Ph.D. Registration No. **MZU/Ph.D./1446 of 12.08.2019**, is Ph.D. scholar in the Department of Electronics and Communication Engineering, under our guidance and supervision and has not been previously submitted for the award of any degree in any Indian or foreign University. He has fulfilled all criteria prescribed by the UGC (Minimum Standard and Procedure governing Ph.D. Regulations). He has fulfilled the mandatory publication (Publication enclosed) and completed Ph.D. course work. It is also certified that the scholar has been admitted in the Department through an entrance test, followed by an interview as per UGC Regulation of 2016.

Date:

Place: Aizawl

(Prof.L.LOLIT KUMAR SINGH)

Supervisor

(Prof.SUDIPTA CHATTOPADHYAY)

Joint Supervisor

DECLARATION

MIZORAM UNIVERSITY

Aizawl

(October 2023)

I, **SARATH KUMAR ANNAVARAPU**, hereby declare that the subject matter of this thesis entitled “**Design and Analysis of Antennas for Wireless Underground Propagation**” is the record of work done by me, that contents of this thesis did not form basis of the award of any previous degree to me or to do the best of my knowledge to anybody else, and that the thesis has not been submitted by me for any research degree in any other University/Institute.

This is being submitted to the Mizoram University for the degree of Doctor of Philosophy in **Electronics and Communication Engineering**.

(SARATH KUMAR ANNAVARAPU)
Candidate

(Prof. (Dr.) L. LOLIT KUMAR SINGH)
Supervisor



(Head of the Department)

(Prof. (Dr.) SUDIPTA CHATTOPADHYAY)
Joint Supervisor

Acknowledgement

Praise the **GOD** for his uncountable blessings and wisdom he has bestowed upon me, the strength and good health in order to finish this research work

I would like to express my sincere, heartfelt gratitude and indebtedness to my supervisors **Prof.L. Lolit Kumar Singh**, Professor, Department of Electronics and Communication Engineering, Mizoram University, Aizawl, Mizoram and Joint supervisor **Prof. Sudipta Chattopadhyay**, Professor, Department of Electronics and Communication Engineering, Mizoram University, Aizawl, Mizoram for their support, effective guidance and timely motivation, constant encouragement and valuable suggestions throughout the course of this research work.

I am also thankful to **Prof.Reshmi Maity**, Head of the Department of Electronics and communication Engineering, Mizoram University, Aizawl, Mizoram. I am grateful to **Dr. Abhijyothi Ghosh**, Associate Professor, Department of Electronics and Communication Engineering, Mizoram University, for his constant support, encouragement and planning during the course work.

I thank my doctoral committee members **Prof. N.P. Maity** and **Dr. Achinta Baidya** and the faculty members **Prof. P.V. Naganjaneyulu**, **Dr. Zonunmawii** for their suggestions and comments that have enabled me to complete my research work.

I thank **Lalbiakdiki** and **Zoremsiami** staff department of Electronics and communication Engineering for their support. I extend my thanks to **Dr. G. Tejeswara Rao**, Assistant Professor Department of Education, Mizoram University for his continuous support and suggestions. I also thank my senior **Dr. Tanmoy Sarkar** and my juniors **Vishakaha Yadav** and **C. Lalengkima** for their help and support.

I express my deep sense of gratitude for my parents **A. Hanumaiah**, **O. Lalitha** for the love, support, effort and sacrifices for educating me and preparing for my future.

I dedicate this work to my wife **Dr. R. Sirisha** and my daughters **Sai Srinidhi** and **Sai Sri Varsha** for their support, understanding and prayers during my course of

research work. I sincerely thank my sister **Mrs. Moumitha Chattopadhyay** who supported, stood as backbone and prayed for my entire research work. I would like to express my gratitude to my brothers **Satish Kumar, Hari Krishna** and **Usha Vardhani, Srilatha** for their constant support and motivation to keep up my spirits. I am thankful for the kids **Aashrith, Karthik** and **Chandana** for their wishes.

I owe my gratitude to my college **KKR and KSR Institute of Technology and Sciences**, Guntur, Andhra Pradesh for providing me opportunity and support due to which I was able to complete my research work.

Lastly, I would like to convey special thanks to one and all those who have directly or indirectly extended their helping hand in this endeavor.

(Sarath Kumar Annavarapu)

Table of Contents

Acknowledgement	(i)
Table of Contents	(iii)
List of Figures	(v)
List of Tables	(x)
Chapter 1 Introduction and Literature Review	1-13
1.1 Introduction	1
1.2 Basics of Microstrip Patch Antenna	3
1.3 Feeding Techniques for Microstrip Patch Antenna	5
1.4 Applications of Low frequency Microstrip Patch Antenna	8
1.4.1 Wireless Underground sensor Networks (WUSN)	9
1.5 Antenna design for wireless underground propagation	11
1.6 Conclusion	12
Chapter 2 Experimental Investigation on Determination of Frequency for Wireless Underground Sensor Networks	14-25
2.1 Introduction	14
2.2 Simulation of Underground Environment using two antenna Model	14
2.3 Experimental verification of received signal strength in air medium	17
2.4 Experimental verification of received signal strength in underground medium (soil medium)	21
2.5 Conclusion	24
Chapter 3 An Investigation on Low frequency miniaturized printed antenna design for Wireless underground sensor network	26-38
3.1 Introduction	26
3.2 Antenna design with shorting vias	27
3.2.1 Study of frequency variation with number of shorting vias	27
3.2.2 Study of frequency variation with position of shorting vias	32
3.3 Conclusion	38

Chapter 4	Theoretical and Experimental investigation on air-Artificial Magnetic Conductor composite substrate for wireless underground sensor network application	39-60
4.1	Introduction	39
4.2	Simulation based investigation of placement of sorting position and air-AMC composite substrate	41
4.3	Antenna design	44
4.4	Evolution Analysis	46
4.4.1	AMC unit cell and array	46
4.4.2	AMC resonance	47
4.4.3	Standalone Antenna (Reference Antenna)	49
4.5	Proposed Antenna on air-AMC composite substrate	51
4.6	Results and Discussions	56
4.7	Conclusion	59
Chapter 5	Design and Analysis of Transverse Electric mode Rectangular microstrip antenna for wireless Underground Sensor Networks	61-91
5.1	Introduction	61
5.2	AMC for possible multiband resonance	63
5.3	Antenna structure	68
5.4	AMC Integrated Antenna	70
5.4.1	Frequency Impact of AMC Integrated Antenna	70
5.4.2	Evolution of Dual band	71
5.4.3	Evolution of dual width cavity	72
5.5	Dual band Impedance matching	74
5.6	Radiation characteristics of TE RMA	78
5.7	Results and Discussion	84
5.8	Conclusion	91
Chapter 6	Conclusion and Scope of Future Scope	92-93
	References	94
	Brief Bio-data of candidate	107
	List of Publications	108
	Particulars of the candidate	109

List of Figures

Fig. 1.1	Basic geometry of Microstrip patch antenna (a) top view (b) side view	3
Fig. 1.2	Different geometries of patch (a) circular (b) semicircular (c) square (d)annular ring (e) square ring (f) triangular (g) right angle triangle (h) hexagonal (i) Rectangular.	4
Fig. 1.3	Fringing filed extension of RMA along the length.	5
Fig. 1.4	Coaxial fed rectangular patch antenna.	6
Fig.1.5	Types of line feeding techniques (a) inset feed (b) edge feed (c) quarter wave transformer	7
Fig.1.6	Aperture Coupled fed patch antenna	7
Fig.1.7	Proximity Coupled fed patch antenna	8
Fig.2.1	Conventional Rectangular Microstrip antenna with coaxial feed	15
Fig. 2.2	Two antennae with layer for underground environment simulation	15
Fig. 2.3	Variation in Received signal (S_{12}) with change of relative permittivity and frequency	16
Fig. 2.4	Variation in Received signal (S_{12}) for different permittivity ϵ_r values	17
Fig. 2.5	Transmitting and receiving antennas used for experiment (a) 3 element Yagi-Uda (b) Folded dipole	18
Fig. 2.6	Experimental setup for measurement of received signal strength in the air medium at distances (a)118 cm (b)204cm (c)270 cm	18-19
Fig. 2.7	Variation in received signal strength(dBm) with frequency in air medium	21
Fig. 2.8	Experimental setup for measurement of received signal strength in the underground	22
Fig.3.1	Quarter Wave Patch (QWP) with shorting vias	28
Fig.3.2	QWP with various number of shorting vias (a) 24 shorting vias (b)12 shorting vias (c)8 shorting vias and (d) 3 shorting vias.	29-30

Fig.3.3	Variation in resonant frequency of QWP with number of shorting vias	31
Fig.3.4	Quarter wave patch with varying shorting vias position (p) from the edge of the patch	32
Fig.3.5	Variation in resonant frequency of QWP with position (p) of shorting vias from the radiating edge	33
Fig.3.6	Electric field vector at the shorted edges of the patch (a) slots at $p = 0$ mm (b) slots at $p = 20$ mm	34
Fig.3.7	Frequency variation of QWP with number and position of shorting vias	35
Fig.3.8	Radiation pattern QWP for vias at $p=0$ (a) 24 shorting vias (b) 12 shorting vias (c) 6 shorting vias (d) 3 shorting vias	35-37
Fig. 3.9	Gains Vs Shorting positions for different numbers of vias	38
Fig.4.1	Quarter wave patch at 453 MHz	41
Fig.4.2	Reflection coefficient of the QWP antenna at 453 MHz	41
Fig.4.3	Gain of QWP antenna at 453 MHz	42
Fig.4.4	AMC structure at 453 MHz (a) unit cell (b) reflection coefficient	42
Fig. 4.5	Schematic of Air -AMC Antenna at 385 MHz	43
Fig. 4.6	Reflection Coefficient of antenna resonance at 385 MHz	43
Fig. 4.7	Gain of antenna at 385 MHz	44
Fig.4.8	Proposed antenna (PA) structure at 413 MHz (a) Top view (b) Side view	45
Fig.4.9	(a) AMC unit cell, (b) 2×3 AMC array	46
Fig.4.10	Equivalent circuit of AMC	47
Fig.4.11	(a) Susceptance of AMC array as a function of frequency, (b) Reflection phase angle of unit cell and array.	48
Fig.4.12	Equivalent circuit of standalone reference antenna (RA) with shorting vias	50
Fig.4.13	Equivalent circuit of proposed antenna (PA).	51
Fig.4.14	(a) Plot of equation (4.10) to extract solution for frequency and simulated $ S_{11} $ profile of PA, (b) Simulated reflection phase of AMC in complete structure.	52

Fig. 4.15	(a) Simulated tangential H field magnitude on AMC surface of the PA, (b) Simulated radiation patterns of the RA and PA, (c) Simulated fringing E field vector at patch radiating edge for PA, (d) Simulated fringing E field vector at patch radiating edge for RA. [at $f = 414$ MHz for all cases]	53-54
Fig. 4.16	Comparison of radiation pattern of PA, RA and traditional RMA. (a) E plane, (b) H plane.	55
Fig. 4.17	The fabricated prototype of the PA, (a) AMC array, (b) AMC array on the ground plane, (c) proposed antenna (PA) structure.	56
Fig. 4.18	Results of PA and RA, (a) Measured $ S_{11} $, (b) Radiation efficiency	57
Fig. 4.19	Comparison of simulated and measured radiation pattern of RA and PA. (a) H-plane. (b) E-plane.	58
Fig. 5.1	(a) Magnitude of electric surface current on simple square metallic AMC unit cell with zero strip, and (b) Magnitude of electric surface current on proposed AMC unit cell with 12 strips (c) Reflections phase characteristics of AMC unit cells with different strips (zero, 5, and 12)	64-65
Fig. 5.2	A 3×3 AMC patch (a) Top view (b) Reflections phase characteristics	66
Fig. 5.3	A 5×5 AMC ground (a) Top view (b) Reflections phase characteristics	67
Fig. 5.4	Schematic representation of proposed antenna. (a) Top view, (b) side view (c) Bottom view. $w_s = 2$, $g_1 = 2$, $g_2 = 4$, $h_{SUB} = 30$, $h_{AMC} = 3.2$, $S_W = 5$, $S_L = 3.2$, $L_v = 28.3$, $L_h = 44.3$, $W = 150$, $L = 150$. Unit: mm.	69
Fig. 5.5	Reflection coefficient (S_{11}) profile of the AMC integrated TE patch, Resonant frequency variations of the AMC integrated TE patch as a function of the patch width W (from 100 mm to 350 mm), while parameter L is kept constant at 150 mm.	71

Fig.5.6	(a) Approximately zero Magnetic field vector distribution on the entire 3×3 AMC surface at $f_1 = 517$ MHz, indicating the entire patch is having AMC properties. (b) Approximately zero Magnetic field vector distribution on the central section of the 3×3 AMC surface at $f_2 = 778$ MHz, indicating the central portion of the patch retains the AMC property. (c) Physical illustrations of upper radiating edge magnetic field vector at $f_1 = 517$ MHz, (d) same as (c) at $f_2 = 778$ MHz, (e) simulated fringing magnetic field vector at radiating edge at $f_1 = 517$ MHz, (f) same as (e) at $f_2 = 778$ MHz	73
Fig.5.7	Simulated results of the proposed TE-RMA with and without loading the four corner dielectric strips, (a) reflection coefficient, (b) magnetic-field (H-field) distribution under the 3×3 AMC patch cavity at higher frequency band (f_2) for TE-RMA without corner dielectric strips, (c) magnetic-field (H-field) distribution under the 3×3 AMC patch cavity Proposed TE-RMA with corner dielectric strips at higher frequency band (f_2).	75-76
Fig.5.8	Smith chart diagrams (a)without dielectric strips, and (b) with dielectric strips	77
Fig.5.9	Simulated results of the proposed TE-RMA at low frequency (f_1), (a) radiation patterns, with and without loading the four dielectric strips, (b) H-field distribution under the 3×3 AMC patch cavity without loading the four dielectric strips, (c) H-field distribution under the 3×3 AMC patch cavity with loading the four dielectric strips.	78-79
Fig.5.10	Simulated radiation patterns of the proposed antenna (TE-RMA) at low frequency $f_{1p} = 569$ MHz and high frequency $f_{2p} = 782$ MHz	80
Fig.5.11	Computed radiation profile for E- and H-planes of the proposed antenna, (a) $f_{1p} = 569$ MHz, and (b) $f_{2p} = 782$ MHz.	83
Fig.5.12	Pictures of the fabricated prototype, (a) top view of proposed antenna, and (b) bottom view of 3×3 AMC (Top), revealing the 3×3 AMC patch structure.	85
Fig.5.13	Simulated and measured reflection coefficient (S_{11}) of the proposed antenna.	85

- Fig.5.14 Simulated and measured radiation patterns (co-pol and cross-pol) across the E- and H-planes, where the simulated $f_1 = 570$ MHz and $f_2 = 782$ MHz, and the measured $f_1 = 572$ MHz and $f_2 = 768$ MHz, (a) E-plane (f_1), (b) H-plane (f_1), (c) E-plane (f_2), and (d) H-plane (f_2) 86-87
- Fig.5.15 Variation of radiation performances of the proposed antenna across the two operating frequency bands (f_1 and f_2), (a) gain variation, and (b) efficiency variation. 88

List of Tables

Table 2.1	Received signal for different frequencies at different value of relative permittivity (ϵ_r)	16
Table 2.2	Received signal strength in the air medium for different distances	20
Table 2.3	Received signal strength in the underground for different distances	23
Table 3.1	Design Parameters used in QWP	28
Table 3.2	Frequency Vs Number of shorting vias	31
Table 3.3	Frequency Vs Position of shorting vias	33
Table 4.1	Performance comparison of proposed antenna with References	49
Table 4.2	Comparison of proposed antenna with other low frequency antennas	59
Table 5.1	Comparison of existing reports of TE-RMA till date	90
Table 5.2	Performance comparison of proposed TE antenna with other relevant reports for low frequency underground communications	91

CHAPTER

1

Introduction and Literature Survey

1.1 Introduction

In the modern era of communication, transmitting and receiving the signal through wireless has become prominent. With the development of the latest technologies such as Internet of Things (IoT), wireless sensor networks (WSN) these type of wireless technologies becomes essential. For data to transmit in wireless mode the system requires an antenna which is capable of transmitting and receiving Radio Frequency signals. Depending on the design aspects, antennas can be designed for the applications such as sensing application in the range of few meters to satellite applications ranging thousands of kilo meters. Design of Antennas for such varying range of applications is an important task. The operating frequency of antenna is a very important parameter in antenna design for different applications. The operating frequency of antenna depends on antenna geometry, which decreases with increase in the antenna size.

Antennas have been constructed with a wide variety of forms over the years, including aperture antennas, wire antennas, loop antennas, planar patch (Microstrip) antennas, and slot antennas. The demand for smaller as well as planar antennas grows with the advent modern wireless underground sensor networks or IoT applications. Furthermore, the mobility of wireless devices has become critical, necessitating the development of antennas suitable with miniaturised handheld devices. This imposes the use of antennas that are small in weight, low in profile, compact, and inexpensive. In this scenario, a microstrip antenna is found to be most suitable option for meeting most of the criteria of today's wireless world.

Microstrip antenna as a kilomegacycle range transmission technology is introduced by Greig and Engleman in 1952 and as a radiator was first perceived by Deschamps in 1953[1]-[2]. The Microstrip antenna and its application is first patented

in 1955 by Gutton and Bassinot [3]. Various perspectives of stripline discontinuities and radiation were reported between 1955 to 1969 by different researchers [4]-[7]. However, for the next five years, until 1975, researchers such as Byron, Howell, Munson, and others pioneered research in the fields of printed antennas or microstrip antennas by analysing the radiation of a conducting stripline like copper clads with dielectric substrate of few wavelengths in between [8]-[15]. Due to the advantageous features of microstrip antenna its usage has become prominent in the missile satellite industry and airborne systems [16]-[21]. The developments in microstrip antenna various geometries and analysis were drafted by in 1980 by Bahl and Bhartia [22]. The parametric studies and analysis of microstrip antenna are elaborated in book of James, Hall and Wood [23] in 1981. Another book released in 1981 by James et al [23] expanded the analyses and designs to incorporate parametric investigations. A well-reviewed study by Carver and Mink [24] also spelled forth the key characteristics and aspects of microstrip antennas, to which reference is still made. The fundamental and significant expressions of input impedance, radiation resistance, and radiation fields were expressed [25], but they were only applicable to centre fed patches and so could not be used in many real antenna configurations.

Lo et al. [26]-[29] presented a more generalised expression based on modal-expansion techniques for different geometries such as rectangular, triangular, circular, semicircular, and so on. Advanced analysis and techniques were also presented by Shen [30], Carver and Coffey [31]-[34], and it focused on calculating the mutual and self impedance and limitations of microstrip antenna when integrated to form array antenna. Different authors and researchers have reported on different approaches of analysis, such as the aperture field model [35], vector potential approach [36], wire grid model [37], Dyadic Green's function (DGF) techniques [38], and so on, to describe the radiation characteristics.

From the 1980s through the year 2000, the second phase of printed antenna development took place. During this period, the basic radiation process was studied and realised utilising cavity model analysis. This research is widely reported in the literature, including [39]-[40]. The growing interest in printed antennas has resulted in the creation of small, wideband antennas for novel wireless applications. The latest

publications [41]-[42] reflect this. contemporary handbooks and collections [43]-[45] on printed antenna design have included modern innovations, including CAD-based approaches. These efforts are laying the groundwork for today's commercial and academic research and development.

Moving on to the third and most recent phase, breakthroughs in material technology and exotic material fabrication have permitted the development of sophisticated microstrip antennas. Among the most notable are (a) antennas with metamaterials [46]-[52], (b) Defected ground structures for printed antennas [53]-[60], and (c) Defected patch structures using AI-generated forms. (d) Electrically miniaturised antennas for mobile communication [61-69], and (e) printed antennas for RFID systems [70]-[77] etc, both with and without active power.

1.2 Basic structure of Microstrip Patch Antenna

Microstrip patch antenna of Length (L) and width (W) lying on a height (h) substrate. The co-ordinate axis is chosen so that the length runs along the x axis, the width runs along the y axis, and the height runs along the z axis. With the length of the patch nearing to the $\frac{1}{2}$ wavelength then patch radiates at the desired frequency.

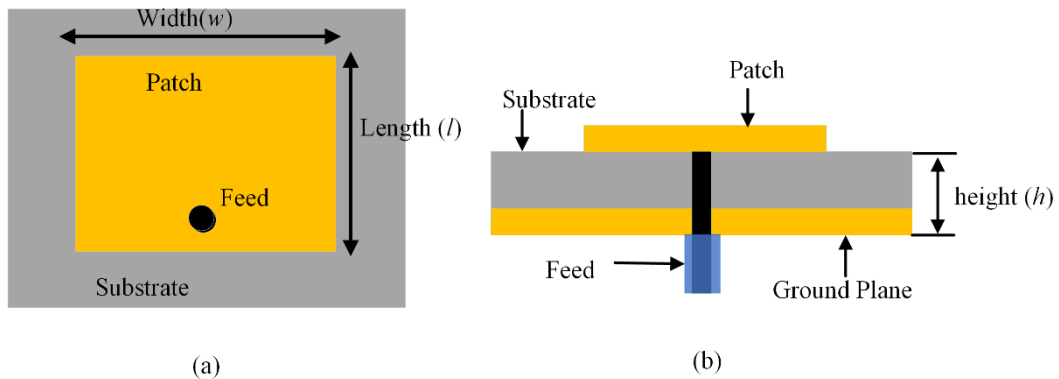


Fig.1.1. Basic geometry of coaxial fed Microstrip patch antenna (a) top view (b) side view

Basic Microstrip antenna with coaxial feed is depicted in Fig.1.1. The fundamental mode of the rectangular patch antenna is TM_{10} mode, and the patch to operate at that mode the length should be approximately equal to $\lambda/2$ where λ is the wavelength which can be determined by free space wavelength λ_0 as $\lambda_0/\epsilon_{\text{reff}}$ where ϵ_{reff} is the relative dielectric constant of the medium. This TM_{10} mode indicates the field variation along the patch length varies with one $\lambda/2$ per cycle. Various regular geometries of patch

such as circular, triangular, square, annular ring, semi-circular etc are used. Different shapes of the patch are depicted in Fig.1.2.

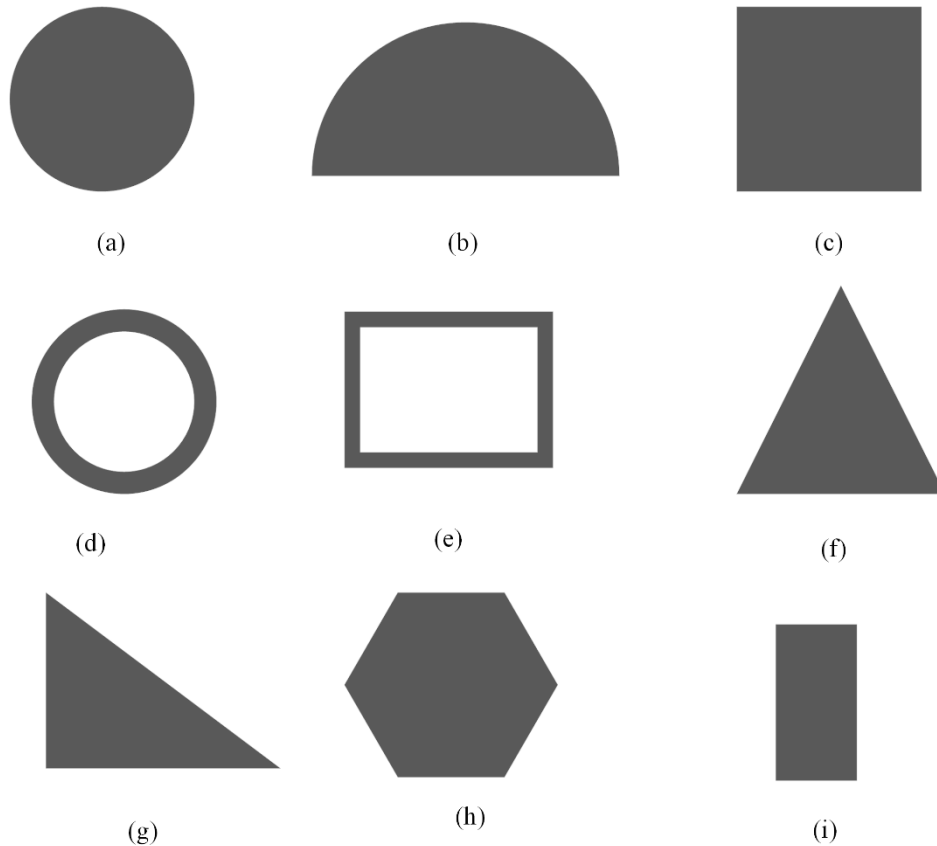


Fig.1.2. Different geometries of patch (a) circular (b) semi-circular (c) square (d)annular ring (e) square ring (f) triangular (g) right angle triangle (h) hexagonal (i) rectangular

To function in the fundamental TM_{10} mode, the patch length must be slightly less than $\lambda/2$ where λ is the dielectric medium wavelength. The TM_{10} mode suggests that the field fluctuates one $\lambda/2$ cycle along its length but not along its patch width. The microstrip patch antenna is shown in Fig. 1.3 by two slots separated by a transmission line of length L and open circuited at both ends. Because of the open ends, the voltage is highest along the width of the patch and the current is lowest. The fields at the edge can be divided into normal and tangential components with respect to the ground plane.

Because the patch is $\lambda/2$ long, the normal components of the electric field at the two edges along the width are in different directions and hence out of phase, and thus cancel each other in the broadside direction. Because the tangential components are in phase, the resultant fields combine to generate the greatest radiated field normal to the structure's surface. As a result, the width's edges may be represented as two radiating slots that are $\lambda/2$ apart, excited in phase, and radiate in the half space above the ground plane. The fringing fields throughout the width will be treated as radiating slots, and the patch of the microstrip antenna appears larger than its physical dimensions electronically. The patch's dimensions throughout its length have now been stretched by a distance ΔL on either end, as illustrated in Fig. 1.3.

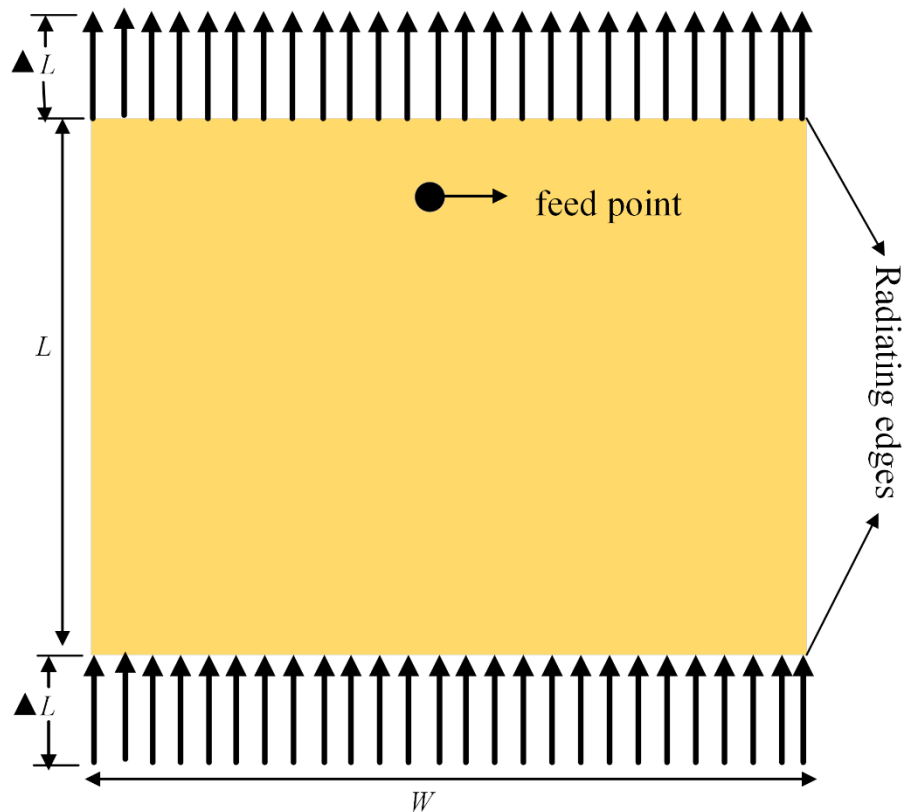


Fig.1.3. Fringing field extension of RMA along the length

1.3 Feeding Techniques for Microstrip Patch Antenna

For microstrip patch antennas, many feeding mechanisms have been employed. Feeding strategies are classified as contact or non-contacting. Radio Frequency power is provided directly to the patches in the contact type feeding. The categories that come

under contact feed are line feed and coaxial feed. Non-contact feeds, on the other hand, use field coupling methods to transmit power. This category includes aperture and proximity couples. The location of the feed on the patch is critical for obtaining adequate impedance matching between the patch and feed. The following are some examples of feeding strategies.

Coaxial feed

This is also referred to as probe feed. The inner conductor is routed through the dielectric substrate and to the patch using this technique. This inner wire is shielded by an exterior conductor connected to the antenna ground plane. Fig. 1.4 shows a schematic illustration of coaxial feed.

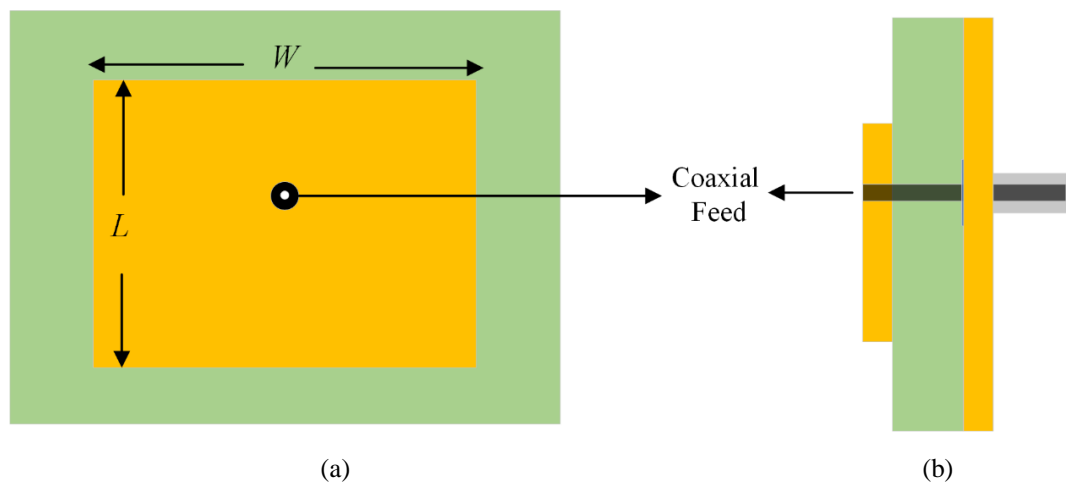


Fig.1.4. Coaxial fed rectangular patch antenna

Microstrip line feed

As illustrated in Fig. 1.5 a conducting strip is linked directly to the border of the Microstrip patch. The patch extends beyond the conducting strip. As a result, the feed can be etched on the same substrate, resulting in a planar structure.

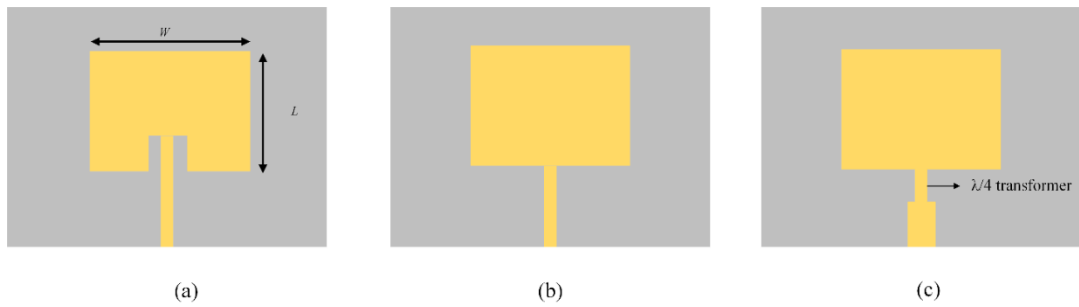


Fig.1.5. Types of line feeding techniques (a) inset feed (b) edge feed (c) quarter wave transformer

Aperture coupled feed

By using two dielectric substrates separated by a ground plane, an aperture coupled antenna avoids the direct electrical connection between the feed and radiating conductors. As illustrated in Fig.1.6, the signal is connected to the patch via an aperture in the ground plane. This enables for independent optimisation of the microstrip transmission line feed as well as the radiating pattern.

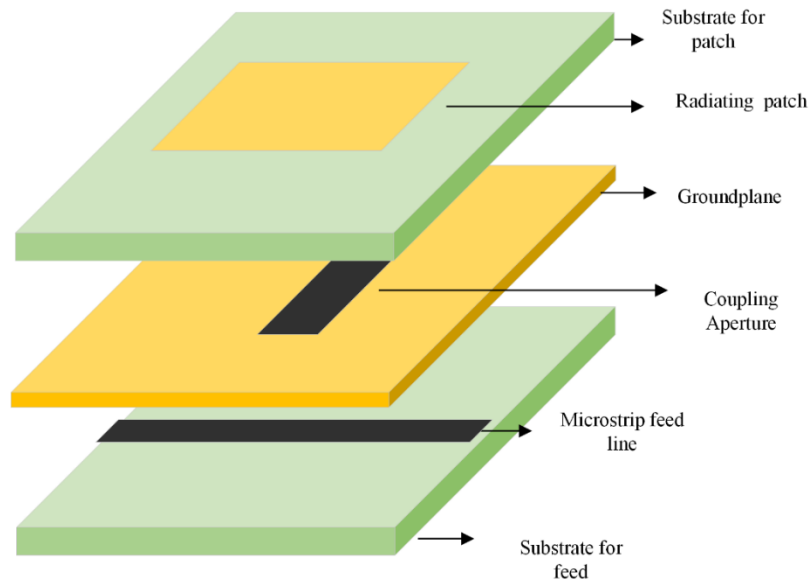


Fig.1.6. Aperture Coupled fed patch antenna

Proximity coupled feed

The electromagnetic coupling strategy is another name for the proximity linked feed technology. The feed line is located between the two dielectric substrates, and the radiating patch is located on top of the upper substrate. Two substrates with varying dielectric constants are used in this method of feeding as illustrated in Fig.1.7.

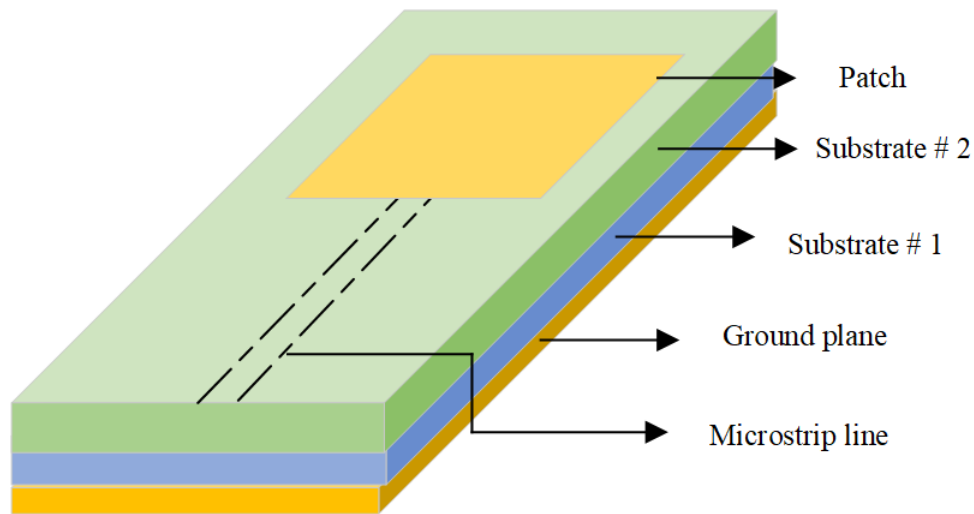


Fig.1.7 Proximity Coupled fed patch antenna

1.4 Applications of Low frequency Microstrip patch antenna

The shape and size of the patch determine the frequency of operation and performance of the antenna. The most common geometries viz. rectangular and circular geometries are extremely useful for industries and modern applications. Nevertheless, for low frequency, these patch antennas are typically larger in size. In spite of their several shortcomings, these antennas are very useful because of its planar form and ease of conformality with the surfaces of aeroplanes, spacecraft, satellites, missiles, and even portable mobile devices.

Microstrip patch antennas are used in a variety of wireless communication. For example, in Satellite communication, we need circularly polarised radiation patterns, which may be produced using either a square or circular patch microstrip antenna. The Circularly polarised microstrip antennas are employed in global positioning satellite (GPS) systems. Microstrip antennas with 2.45 GHz are used in telemedicine applications. Typically, an antenna with a gain of 6.7 dB, a front-to-back ratio of 11.7 dB, and a resonant frequency of 2.45 GHz is appropriate for telemedicine applications. RFID (radio frequency identification), mobile communication employs different types of microstrip antennas. A type of Wearable microstrip antennas are appropriate for wireless body area networks. Microstrip antennas are used in WiMax communication equipment, Radio altimeters, command and control systems, remote sensing and

environmental instrumentation, feed elements in complex antennae, satellite navigation receivers, mobile radio, integrated antennae, biomedical radiators and intruder alarms.

Patch antennas have become more important in sensing applications since the introduction of the internet of things. The frequency of operation of the antenna is dictated by the application. Ad hoc wireless sensor networks (WSN) are often utilised for short-range sensing applications. This thesis focuses on the design of planar antennas for underground Electromagnetic propagation. These are also known as Wireless underground sensor networks (WUSN).

A wireless sensor network (WSN) is a collection of spatially distributed sensor nodes that are interconnected by wireless communication. The sensor nodes are deployed in an ad-hoc manner to monitor the physical or environmental conditions of a particular area. Each sensor node has a processor, a memory, a transceiver, and one or more sensors. The sensor nodes collect data from the environment and transmit it to the base station, which is a central node that processes and stores the data. The base station can also be connected to the internet to share the data with other systems.

Applications of WSN:

- Internet of Things (IoT)
- Agriculture
- Environmental temperature, humidity, and air pressure
- Landslide Detection
- Medical applications like patient monitoring
- Surveillance and Monitoring for security, threat detection.

1.4.1. Wireless Underground sensor networks (WUSN)

Wireless underground sensor networks (WUSNs) are a promising application of communication for the cutting-edge technology compared to the other applications stated in the earlier section. The design of antenna for WUSN is less explored topic. Also, this topic is very challenging because of the application and its inherent restriction of low frequency operation. This WUSNs are a specialized type of WSN

that focus on using sensors in the underground region of the soil. For a long time, this region has been used to bury sensors for irrigation and environmental monitoring applications, but without wireless communication capabilities. WUSNs promise to fill this gap and provide the infrastructure for new applications. The main difference between WUSNs and terrestrial WSNs is the communication medium. The propagation of electromagnetic (EM) waves in soil is significantly different from that in air, so a complete characterization of the underground wireless channel was only recently developed. Despite the potential advantages of WUSNs, there are several challenges that need to be addressed before they can be widely deployed. The main challenge is the realization of efficient and reliable underground wireless communication between buried sensors. This is because the underground environment has significant impact on communication performance. For example, changes in temperature, weather, soil moisture, soil composition, depth, distance etc. can affect underground communication. The characterization of the wireless underground channel is essential for the development of antennas for WUSNs. By understanding how EM waves propagate in soil, we can design antennas that are more efficient and reliable. Some specific examples of applications for WUSNs are Precision agriculture, Structural health monitoring, Natural disaster monitoring etc. Wireless underground sensor networks is an emerging application as stated above and has been explored extensively [78]-[119]. Amongst them [109]-[119] is very much prominent for the present investigation to design planar microstrip antenna for such cutting edge WUSN/WIoT application. The determination of design frequency is critically dependent in soil properties. Experiments are performed to determine the dielectric behavior of wet soil [78]-[79] at the range of 1.4 to 18 GHz. Real and imaginary parts of relative dielectric constants of soils for the frequency range of 0.3-1.3 GHz range is presented in [80]-[83]. Single ended monopole antenna is designed with appropriate efficiency and wide range for different soil moisture measurement at frequency of 869 MHz in [84]. Electromagnetic wave transmission and effect of dielectric characteristics of soil on the signal propagation are shown in [93]. Communication issues and the appropriate channel modelling due to various types of material present in the soil environment are shown in [94]-[95]. Application of sensor networks for measurement of soil water content and various channelization techniques are

elaborated in [96]-[101]. Application of sensor networks in oil reservoirs, water saving and automated precision agriculture is depicted in [102]-[107]. Capacity profile of underground wireless channel is determined with empirical return loss from the antenna and frequency responses for channel for different types of soil for Internet of Underground things in [108]. Diversity in the reception along with antenna beamforming approach and energy aware routing in WUSN has been investigated in [109]-[111]. Measurement of received signal strength and antenna such as dipole, MIMO and other application of sensor networks in field of Wireless internet of things are elaborated in [112]-[119].

1.5 Antenna design for wireless underground propagation

Low frequency antennas are becoming more popular due to their wide range of applications, including underground sensing, mining, smart agriculture, and environmental monitoring. Because high frequencies are absorbed by the earth's surface, low frequency signal transmission is critical in underground environments. A comprehensive description of wireless underground communication is provided in [120]. Influence of various soil factors on received signal intensity at various frequencies is elaborated in [121]. Investigation of pattern reconfigurable antennas to enhance communication connectivity in mines is described in [123]. Furthermore, because the size of the antenna increases as the operating frequency decreases, miniaturization is required for low frequency antenna design in order to make it small. Miniaturized dipole antenna for low frequency ground penetrating radar is proposed in [124]. miniaturized antennas for applications such as card size indoor readers and meander printed circuit board antennas operating at 433 MHz are explored in [125]-[126]. In [127], another low frequency antenna at 430 MHz is created for digestive system surveillance. The gain and other parameters of the antenna are affected by miniaturization. The issues in miniaturizing antennas for personal communication systems, as well as gain considerations, are discussed in [128]-[129].

A sort of meta material known as Artificial Magnetic Conductor (AMC) can be used to improve the gain and other features of low frequency antennas. An AMC is a composite material with an electronic band gap (EBG) structure and in phase reflection

capabilities. developments in the EBG structure and its potential in the construction of microstrip patch antennas are discussed in [130]. The design and analysis of an AMC unit cell are reported in [131]. An overview of the use of AMC for various antenna applications is provided in [132]. the practical validation of AMC performance using dipole antennas are reported in [133] the use of AMC for low profile and low frequency antenna applications are described in [134]-[135].

1.6 Conclusion

The fundamentals of microstrip antennas are presented in the literature review firstly. Following that, contemporary advances in antenna design for wireless sensor networks and wireless underground sensor networks are discussed. The issues related with low frequency antenna design has been documented in elaborate manner to facilitate the planar antenna design for recent applications. According to the current literature, developing planar antennas for low frequencies is a difficult issue with a wide range of possibilities for design and implementation. Hence in this thesis planar antennas operating at low frequencies suitable for underground sensor networks with good gain are designed and analyzed. At the same time, miniaturization techniques are incorporated to make the proposed antenna compatible with portable devices.

The organization of thesis is as follows

In **Chapter 2** an analysis of electromagnetic wave propagation in various media is carried out, including simulation and practical validation. Received signal strength analysis is carried out for three different distances practically in the air medium and underground medium. The results indicate the feasibility of low frequency for different medium.

In **Chapter 3** miniaturization technique using shorting vias for patch antenna is thoroughly investigated. This patch is termed as quarter wave patch. The variation in the operating frequency with different positions and number of shorting vias are analysed and presented. This shorting vias technique considered as miniaturization technique to design the antennas for low frequencies.

In **Chapter 4** the quarter wave patch gain is enhanced by utilizing artificial magnetic conductor (AMC) as composite substrate. The position of AMC is judiciously placed so that the in-phase reflections from it will enhance the overall gain of the proposed antenna. Along with gain enhancement further miniaturization of QWP is obtained with the use of AMC.

In **Chapter 5** the AMC has been utilized in patch and ground plane to form AMC patch and AMC ground plane. The structure of AMC is designed in such a way the dual periodicity exists once the array is formed. These dual periodic AMC array when incorporated in the patch and ground plane forms a dual band Transverse Electric (TE) mode excited antenna. This TE antenna is dual of the conventional Transverse magnetic (TM) antenna that is formed with PEC ground and PEC patch. The characteristics the TE antenna is further enhanced by incorporating four dielectric strips at the corners of the patch. Complete analysis of the TE antenna is presented mathematically and practically.

Finally, a conclusion and future scope of this research work has been documented.

CHAPTER

2

Experimental Investigation on Determination of Frequency for Wireless Underground Sensor Networks

2.1 Introduction

Electromagnetic waves may travel across all media, including air, water, and underground (soil). Each media has various dielectric characteristics and, as a result, varied relative permittivity (ϵ_r). The propagation of an electromagnetic wave is affected by various factors, one of which is the dielectric constant of the medium. To analyze the effect of frequency with varying dielectric constants of the experiments are carried out using EM simulation software, in the laboratory and underground experimental set up in this chapter. In all the cases intensity of received signal strengths are observed and plotted. Received signal strength is observed in following cases (a) By simulation of underground environment using two antenna model (b) Experimental measurement of received signal in air medium and (c) Experimental measurement of received signals strength in the Underground environment

2.2. Simulation of Underground Environment using two antenna model

For performing the simulation, a simple Rectangular microstrip antenna (RMA) with coaxial feed is employed. The key advantage of this sort of feeding technique is that the feed may be positioned anywhere inside the patch to achieve impedance matching. This feed mechanism is simple to fabricate and produces little spurious radiation. As seen in Fig.2.1, the RMA are made up of a metallic ground plane, a dielectric substrate, and a metallic patch.

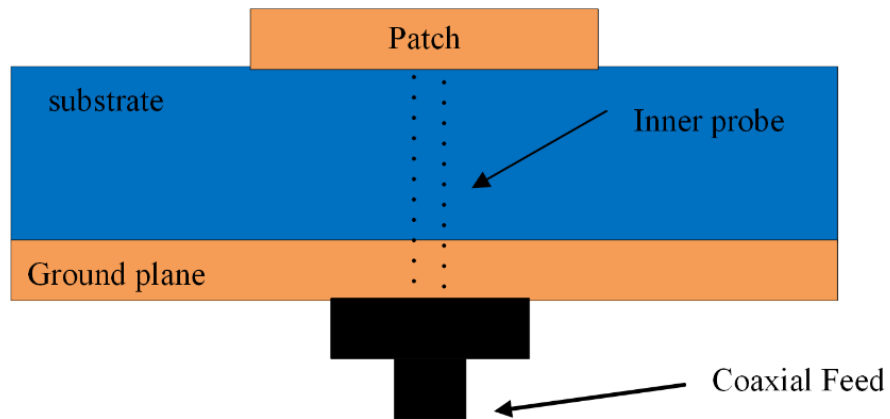


Fig.2.1. Conventional Rectangular Microstrip antenna with coaxial feed

For simulating different conditions two antennas are constructed facing each other so that each antenna can transmit and receive the signal between them. A box is placed such that the two antennas are within the box to facilitate different soil conditions. The simulation setup with two antennas inside the box is depicted in Fig.2.2.

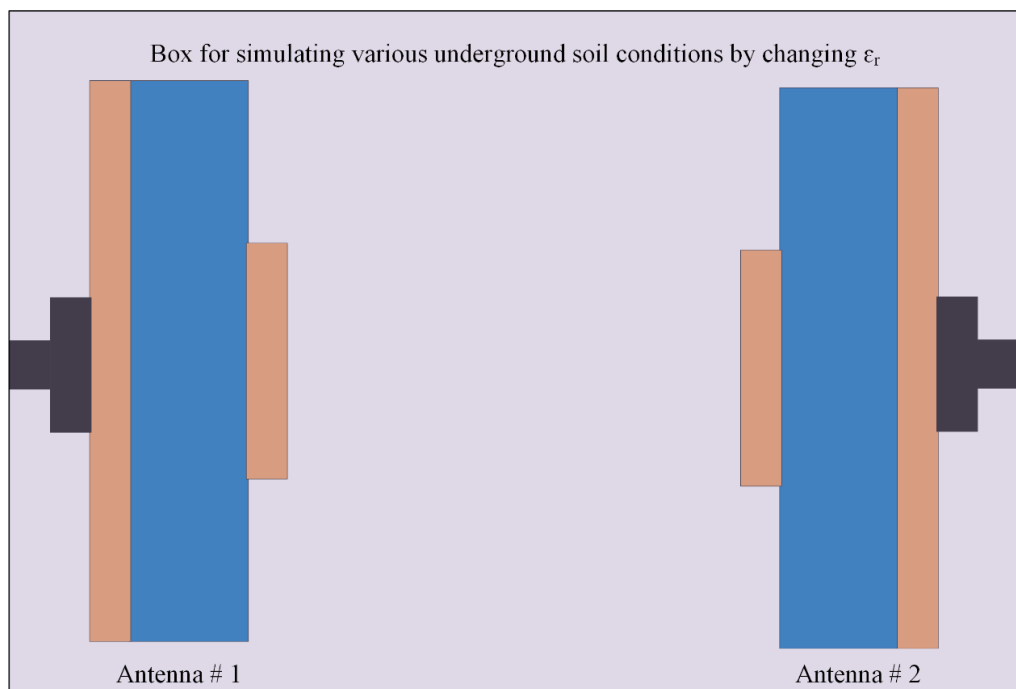


Fig. 2.2. Two antennas with layer for underground environment simulation

Relative permittivity of different soils ranging from 3 to 40 [136] are assigned to the box to simulate different soil conditions between the two antennas. Then, each

antenna is tuned to operate at different frequencies ranging from 300 MHz to 2000 MHz's to check effect of frequency on antenna performance under soil.

The received signal intensity (S_{12}) is observed and recorded in each case as indicated in Table.2.1.

Table 2.1.

Received signal for different frequencies at different value of relative permittivity (ϵ_r)

Frequency in MHz	Received signal S_{12} by varying the Relative permittivity of layer					
	$\epsilon_r = 3$	$\epsilon_r = 5$	$\epsilon_r = 15$	$\epsilon_r = 25$	$\epsilon_r = 35$	$\epsilon_r = 40$
2000	-6.5	-7.5	-10.6	-11.7	-10.3	-9.4
1000	-5.1	-6.9	-6.02	-7	-9.4	-9.6
900	-5.0	-5.4	-5.8	-6.2	-7.9	-8.5
800	-4.9	-5.3	-5.6	-6.0	-6.6	-6.9
700	-4.8	-5.1	-5.5	-5.8	-6.4	-6.7
600	-4.3	-5.0	-5.4	-5.6	-6.0	-6.2
500	-4.0	-4.6	-5.0	-5.4	-5.7	-6.0
400	-3.9	-4.3	-4.8	-5.3	-5.2	-5.7
300	-3.3	-4.0	-4.7	-5.0	-4.6	-5.4

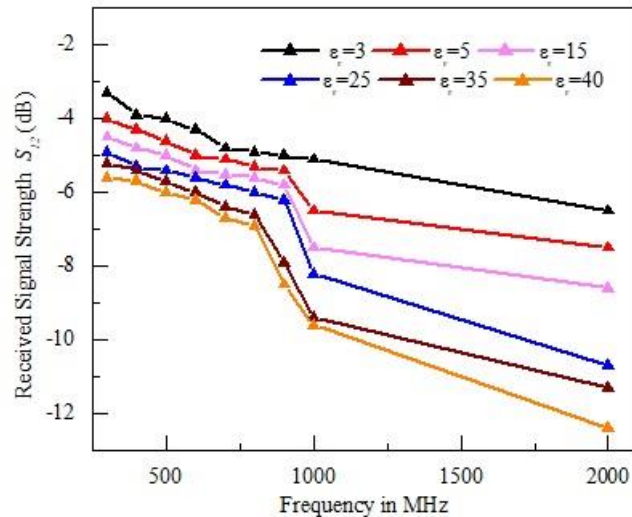


Fig.2.3. Variation in Received signal (S_{12}) with frequency

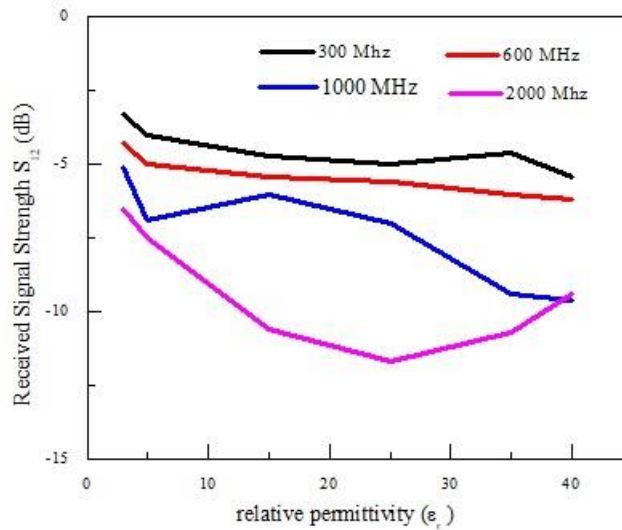


Fig.2.4. Variation in Received signal (S_{12}) for different permittivity values

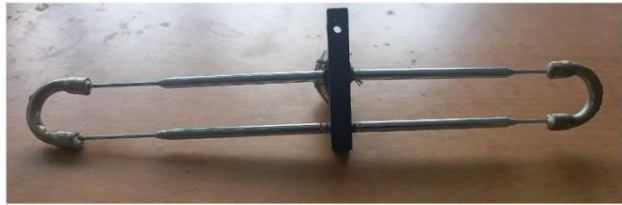
The variation in S_{12} with frequency for various values of ϵ_r is seen in Fig.2.3. It can be shown that for all relative permittivity levels, the best values are attained at lower frequencies. In Fig. 2.4, the same data is displayed between received signal intensity and relative permittivity for four distinct frequencies, indicating that at lower frequencies, signal strength almost constant for different values of permittivity compared to higher frequencies.

2.3 Experimental verification of received signal strength (air medium)

Experiment is performed to determine the received signal strength of antenna in the air. Two antennas are used for these experiments (i) Three element Yagi-Uda antenna as transmitter and (ii) Folded dipole antenna as receiver. The experiment is carried out by making both the antennas to operating at different frequency ranges and observing the received signal strength in each case. The experiment is carried out with three different distances between the transmitting and receiving antenna. These distances are 118 cm ,204 cm and 270 cm respectively. These distances are selected in such a way to compare the effect of the same in the underground propagation as explained in next section. The transmitting and receiving antenna pictures are shown in Fig.2.4



(a)



(b)

Fig.2.5. Transmitting and receiving antennas used for experiment (a) 3 element Yagi-Uda (b) Folded dipole

The experimental setup for observing the received signal strength of antenna in the air medium with three different distances are shown in the Figs.2.5(a) (b) and (c). The Amitec ATS-10 wireless and mobile communication analyzer is used to feed the antenna and to measure the signal strength.



(a)



(b)



(c)

Fig.2.6. Experimental setup for measurement of received signal strength in the air medium at distances (a)118 cm (b)204cm (c)270 cm

Table.2.2 depicts the value of received signal strength in the air with three different distances of 118 cm ,204 cm and 270 cm. Experiment is performed by varying the operating frequency from 300 MHz to 660 MHz. The frequency ranges are selected based on the available resources at Laboratory during the time of measurement. For each frequency received signal strength for the three distances are measured and noted. The received signal strength is measured in dBm. The variations in the received signal strength with respect of frequency is depicted in Fig.2.6

Table.2.2

Received signal strength in the air medium for different distances

Distance (cm)	Frequency (MHz)	Received Signal strength (dBm)
118	300	72
	320	70
	380	69
	440	75
	540	70
	580	65
	600	62
	660	60
204	300	67
	320	64
	380	63
	440	61
	540	60
	580	56
	600	55
	660	52
270	300	60
	320	58
	380	56
	440	54
	540	53
	580	52
	600	48
	660	45

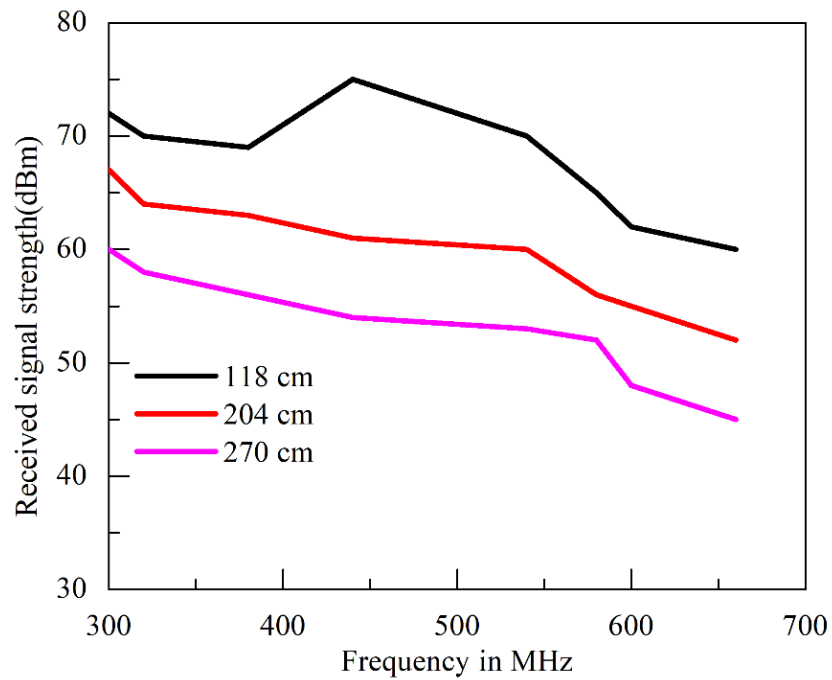


Fig.2.7 Variation in received signal strength(dBm) with frequency in air medium

From the Fig. 2.7 it is observed that lower frequency shows better performance as compared with higher frequency in the air medium for the different distances between transmitting and receiving antennas.

2.4 Experimental verification of received signal strength in underground (soil medium)

Three holes of two feet depth were dug at the Department of Electronics and Communication Engineering, Mizoram University. The holes were dug in such a way that three different distances of 118 cm, 204 cm, and 270 cm could be obtained between them. The same experimental setup that was used to measure signal strength in air (as mentioned in Section 2.3) was used for the underground measurement. The overall experimental setup for performing underground received signal strength analysis is depicted in Fig.2.8. The transmitting antenna (transmitter) was placed in the Hole #1. The distances between the transmitter and receiver were varied by moving the receiver (Receiving antenna) to the second Hole #2 and Hole #3. This covers the distance of 204 cm and 270 cm between the antenna.

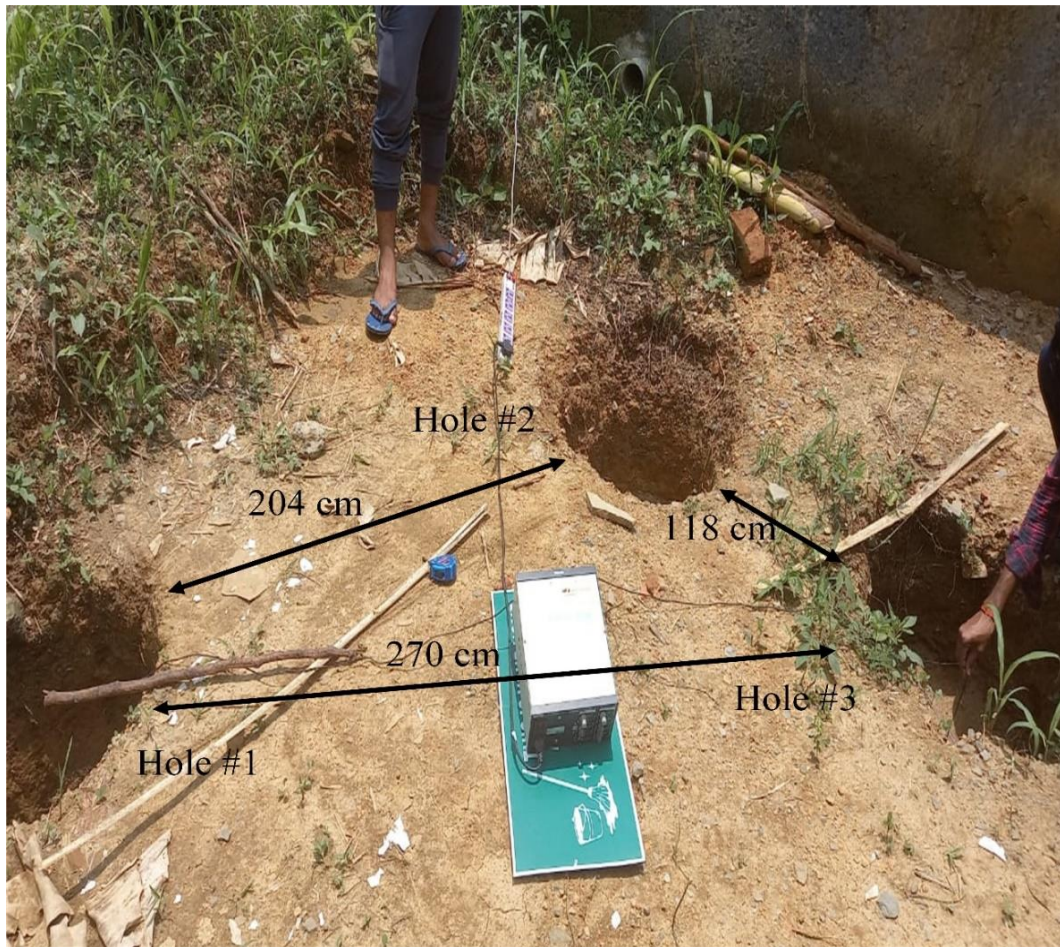


Fig.2.8. Experimental setup for measurement of received signal strength in the underground

Then the transmitting antenna is kept in the second hole and receiving antenna at third hole so that the distance between them is 118 cm. The received signal strength was measured for different frequency between 300MHz to660 MHz. The variation of frequency is restricted between 300 MHz to 660 MHz due to the limitation of available system in the laboratory at that time of measurement. The results of the experiments showed that the received signal strength decreased as the distance between the transmitter and receiver increased. This is because the soil absorbs electromagnetic radiation, which reduces the strength of the signal as it travels through the soil. The results of this experiment provide experimental verification of the theoretical models that have been developed to predict the received signal strength in soil.

Table.2.3

Received signal strength in the underground for different distances

Distance (cm)	Frequency (MHz)	Received Signal strength (dBm)
118	300	65
	320	62
	380	60
	440	63
	540	59
	580	55
	600	61
	660	58
204	300	60
	320	58
	380	55
	440	56
	540	53
	580	50
	600	56
	660	53
270	300	58
	320	53
	380	53
	440	50
	540	52
	580	49
	600	42
	660	40

These results can be used to design wireless sensor networks that are deployed underground. Similar procedure performed in the section 2.3 for the air medium for received signal strength is repeated for underground environment.

The values are noted by varying the frequency similar to the air medium. Table.2.3 depicts the values of received signal strength for each frequency and for the various distances. Variation in the received signal strength for different frequencies with distances in the underground is depicted in Fig.2.8. From the Fig.2.8 it can be observed that the signal strength received in the underground is less compared to that of air.

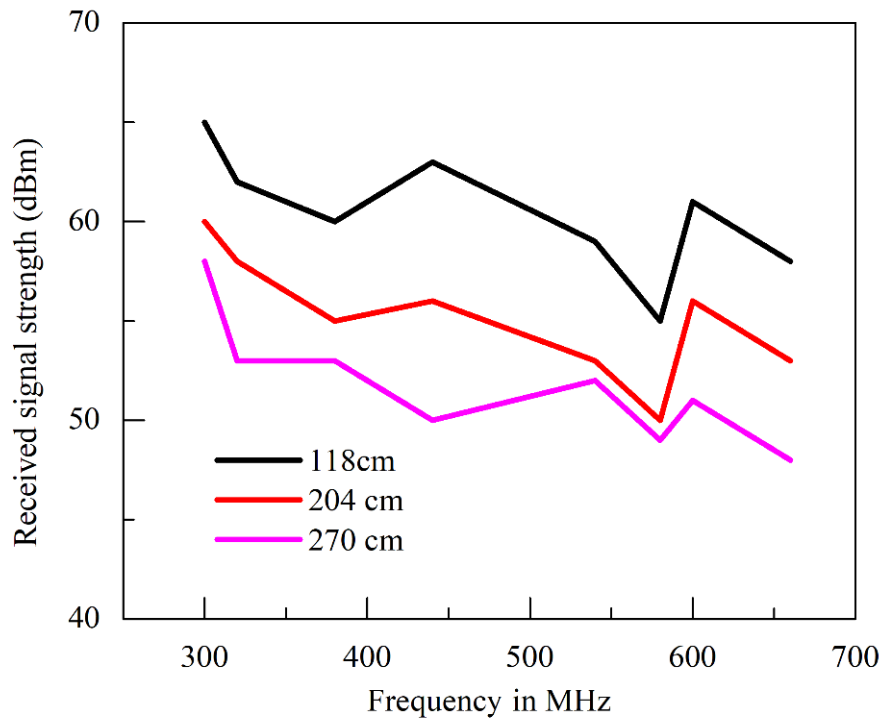


Fig.2.9. Variation in received signal strength(dBm) with frequency in soil (underground) medium

This is due to the different permittivity values of soil compared to that of air. It is also found that lower frequency has better signal reception as compared with higher frequency under same soil condition during the measurement.

2.5. Conclusion

The propagation of electromagnetic waves in three different scenarios is investigated and the results are reported. Two antennas are simulated by altering the relative dielectric medium between them. Experimental validation of received signal

intensity in air for three distances and measured the received signal strength in soil (underground) for three distances same as in air.

Based on the results, it can be inferred that low frequency signal strength in the order of MHz is good enough compared to higher frequencies, and that for lower frequencies, the signal strength remains almost constant for changes in relative permittivity values. The results indicate the importance of low frequencies for underground propagation. It is also evident from the results that at low frequencies the received signal strength remains constant with change in the relative permittivity values.

CHAPTER

3

An investigation on low frequency miniaturized printed antenna design for Wireless Underground Sensor Networks

3.1 Introduction

Wireless Underground Sensor Networks (WUSNs) are important for monitoring soil, habitats, oil, and other underground components. However, electromagnetic waves at high frequencies are absorbed by the Earth's surface and are not useful for underground propagation. Therefore, lower frequencies in the megahertz (MHz) range are preferred. Designing a Rectangular microstrip patch antenna (RMA) at such low frequencies is a challenge, as the antenna size becomes larger. Miniaturization techniques can be used to reduce the size of RMA. Use of wireless underground sensor for oil refinery and its limitations are briefed in [137]. A compact and broadband RMA with shorted patch, stacked shorted patch, and slot loading patch is presented in [138]. Several works have reported the use of shorting techniques to reduce the size of MPAs. In [139], miniaturization techniques such as material loading, reshaping the antenna, shorting and folding techniques, slots, and defected ground structure are reported. In [140], a simple folding operation of a wall shorted patch resulting in a stacked shorted patch is designed for the industrial, scientific, and medical (ISM) band. Specifically, in [141], dielectric loading technique is used to reduce the patch size that produces circular polarization for a CubeSat payload operating at 436 MHz. In [142], an H-shaped microstrip antenna is studied through a transmission line model and analysed using the method of moments. Miniaturization and tuning of a patch antenna using a stacked superstrate layer is reported in [143]-[145], where short circuit posts are used for miniaturization. In this chapter, shorting vias are explored in terms of number and position on the patch for low frequency applications in the P band.

3.2. Antenna design with shorting vias

The resonance frequency of a microstrip patch antenna (MPA) is inversely related to the length of the patch. Conventionally, MPA with a length of 396 mm and a width of 410 mm on air substrate of 10 mm thickness is required to resonate at 365 MHz. However, such a big antenna is not feasible for the majority of applications due to constraint of space. In this chapter, we see about how shorting vias may be used to miniaturise MPA. Shorting vias are tiny holes carved into the antenna's ground plane that link the patch to the ground plane. When shorting vias are placed in proper positions, they can efficiently decrease the patch size without compromising the electric field distribution. When the patch antenna is shorted at the end, the current at the end is no longer compelled to be zero. As a result, the current-voltage distribution of this antenna is identical to that of a half-wave patch antenna. However, the radiation-causing fringing fields are shorted at the far end, so only the fields closest to the transmission line radiate. As a result, the antenna gain is lowered, but the patch antenna has the same basic features as a half-wavelength patch while being 50% smaller in area. As a result, we may design MPAs that are much smaller than conventional MPAs of the same frequency. The shorting vias can be thought of as a parallel inductance to the reference model of the patch. A number of approaches, including the method of moments, may be used to estimate this inductance. The simulation results indicate that miniaturised MPAs perform at an acceptable level. One of the probable options for miniaturising MPAs for low-frequency applications appears to be shorting vias. This chapter discusses a thorough examination with the number and position of sorting vias in the quarter wave patch (QWP).

3.2.1. Study of Frequency variation with number of shorting vias

Initially, a patch with dimensions $L_p \times W_p = 155 \text{ mm} \times 186 \text{ mm}$ on a ground plane with dimensions $L \times W = 225 \text{ mm} \times 286 \text{ mm}$ is being investigated. The dimensions are computed in such a way that the lowest operating frequency of 365 MHz is obtained. To make patch to QWP, shorting vias of dimension $D = 2 \text{ mm}$ and length of 10 mm are integrated at the patch's edge, as illustrated in Fig.3.1. The antenna's design specifications are shown in Table 3.1. The number of shorting vias on the patch are

varied from 24 to 3 as depicted in the Fig.3.2 and the variation in the resonant frequencies is observed for each case.

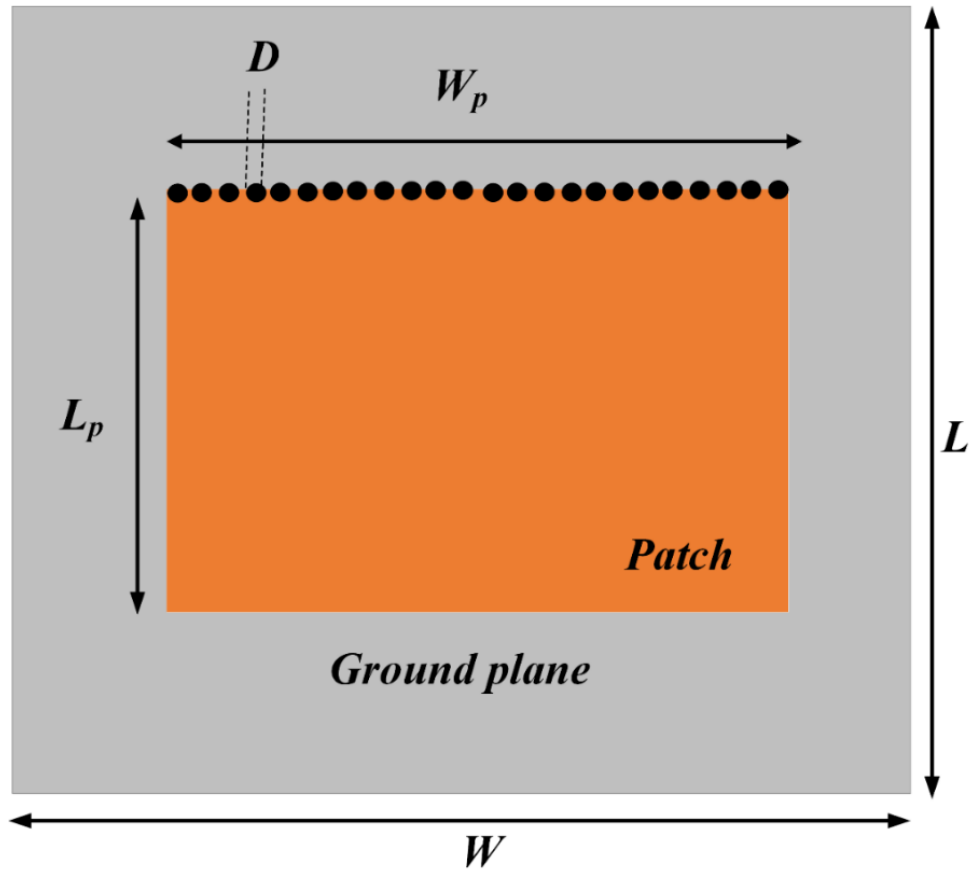
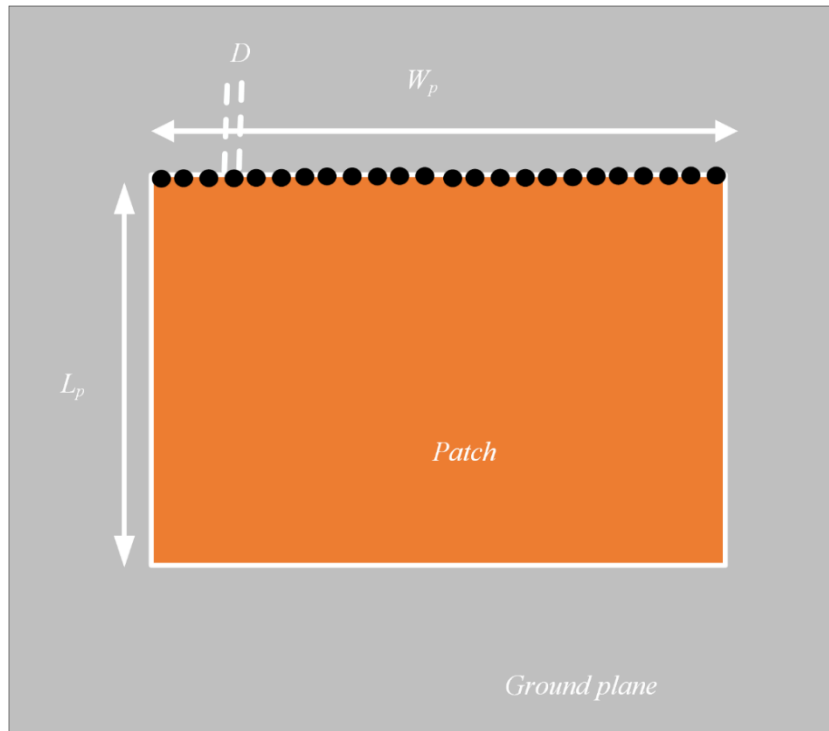


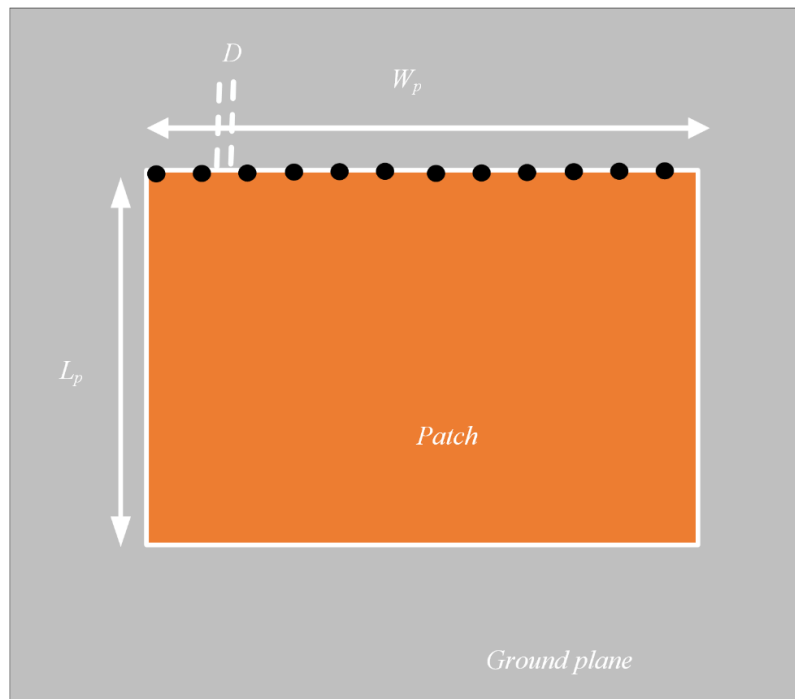
Fig.3.1. Quarter Wave Patch (QWP) with shorting vias

Table 3.1.
Design Parameters used in QWP(Fig.3.1)

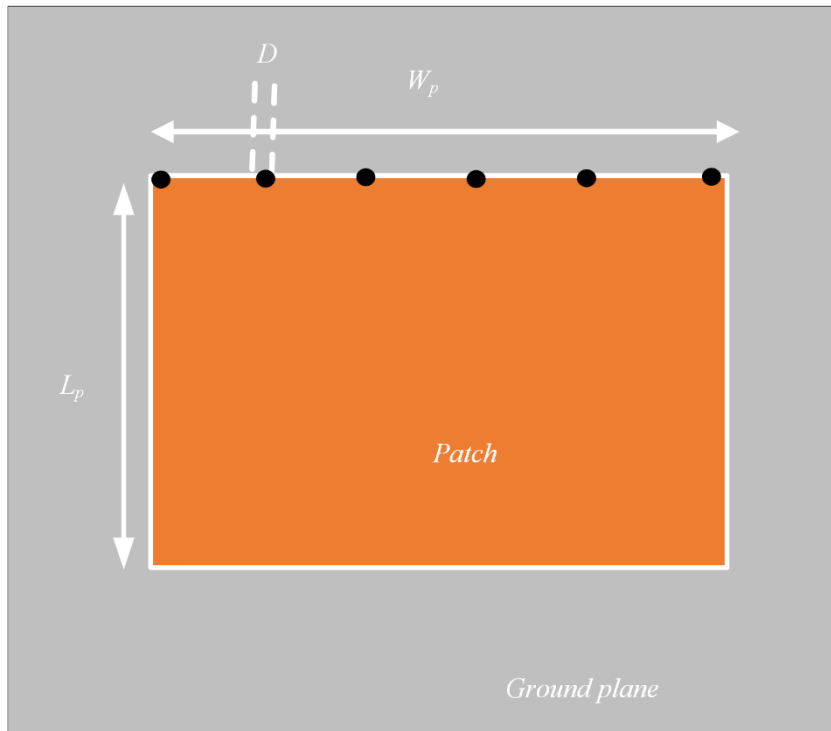
L (mm)	W (mm)	L_p (mm)	W_p (mm)	D (mm)
225	286	155	186	2



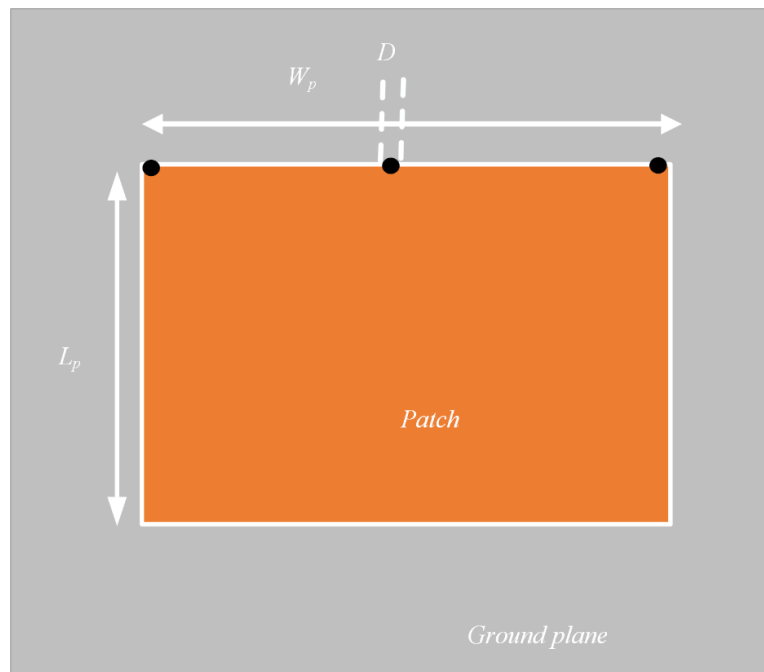
(a)



(b)



(c)



(d)

Fig.3.2. QWP with various number of shorting vias (a) 24 shorting vias (b)12 shorting vias (c) 6 shorting vias and (d) 3 shorting vias

Table 3.2.
Frequency Vs Number of shorting vias

Number of shorting vias	Operating Frequency (MHz)
3	362
6	414
12	425
24	440

Resonant frequency in all the cases by varying the number of shorting vias position at the edge of patch is observed. It is clearly evident from the Fig.3.3 that as the number of shorting vias decreases resonant frequency decreases.

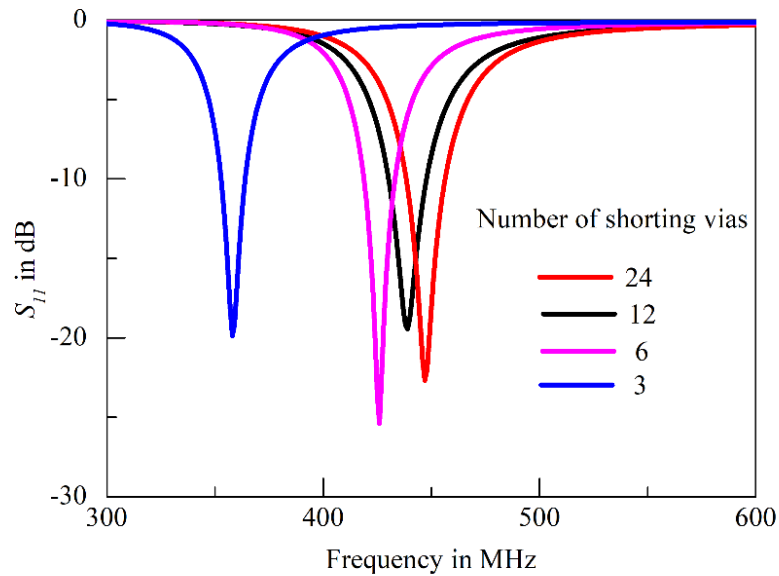


Fig.3.3. Variation in resonant frequency of QWP with number of shorting vias

As shown in Table 3.2, the simulation results show a noticeable frequency shift from 440 MHz to 362 MHz when the number of shorting vias is reduced from 24 to 3. Figure 3.3 depicts a graphical illustration of the same. The results show that changing the number of shorting greatly changes the operating frequency of the QWP. Furthermore, effects of resonant frequency by varying of shorting via position are studied in the next section.

3.2.2. Study of Frequency variation with position of shorting vias

With varying number of shorting vias at particular position of patch varies the operating frequency of the patch as discussed in the previous section. Another factor that the frequency of shorted QWP is varying with positions of the shorting vias. In this section miniaturized version with three shorting vias is further discussed for the frequency variation by varying the position of the shorting vias as shown in Fig.3.4.

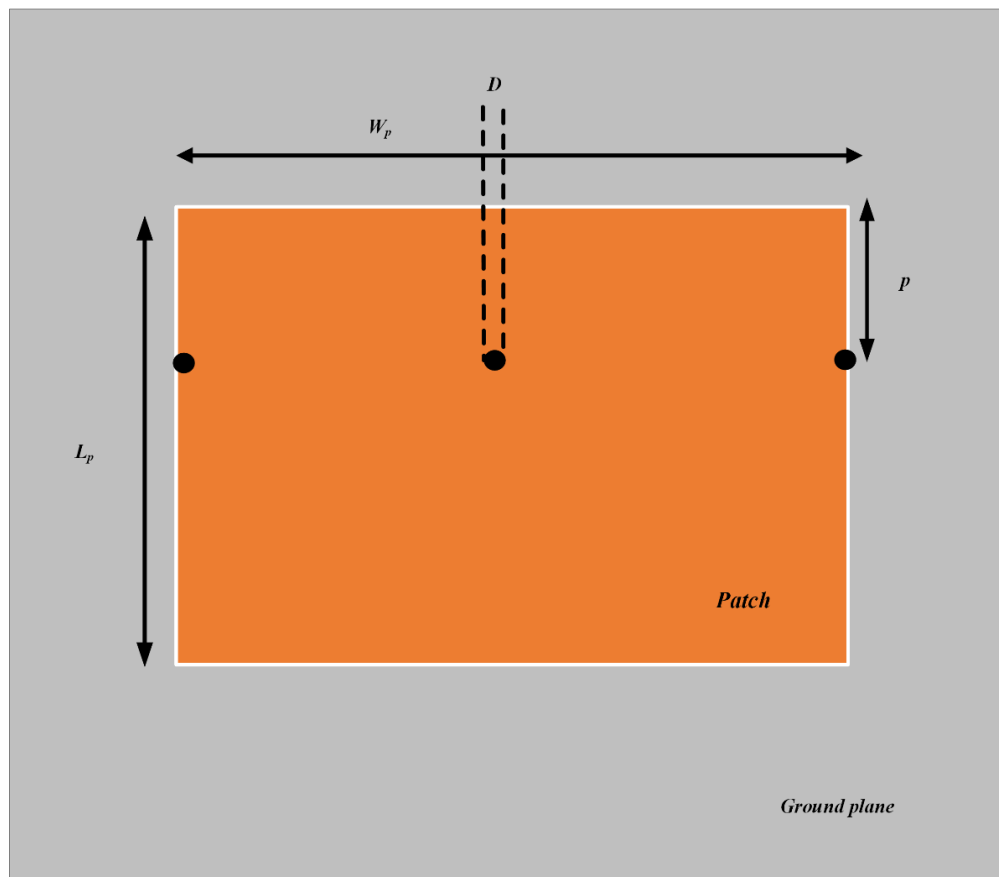


Fig.3.4. Quarter wave patch with varying shorting vias position (p) from the edge of the patch

Simulations are performed with varying the position of shorting vias (p). The values of p are varied from 0mm to 20 mm. In all the positions the frequency of the patch is observed and the S_{11} plots are depicted in Fig.3.5.

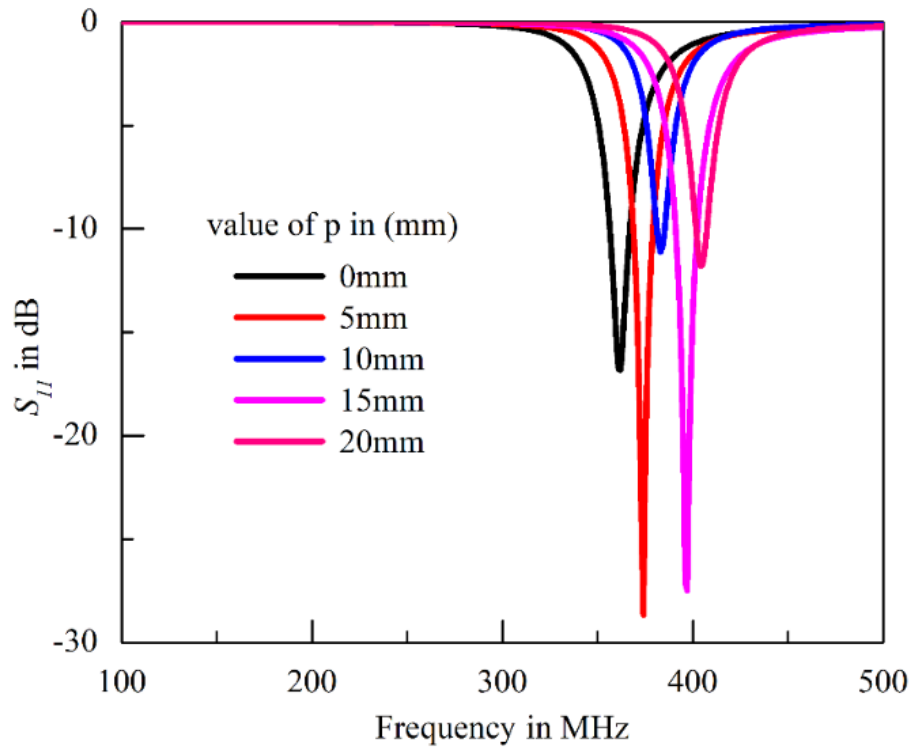


Fig.3.5. Variation in resonant frequency of QWP with position (p) of shorting vias from the radiating edge

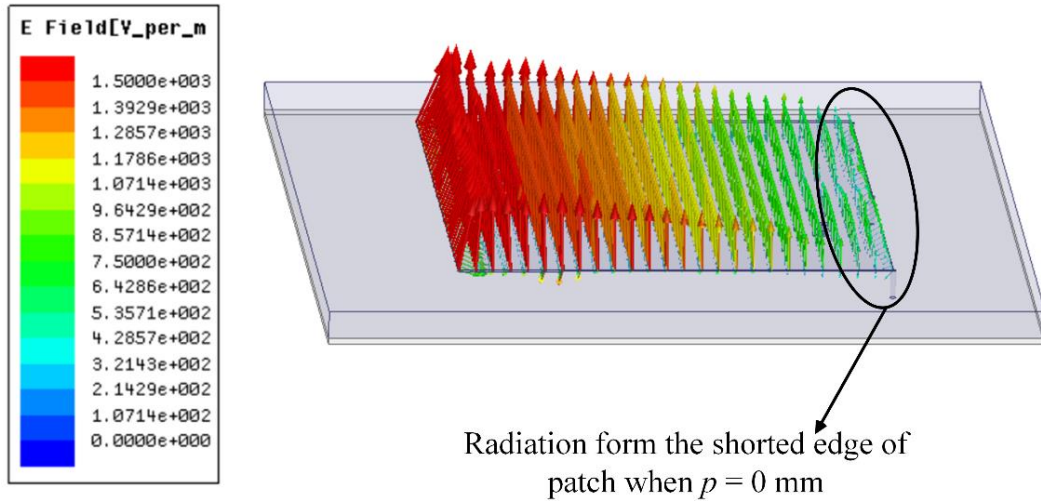
Table:3.3.

Frequency Vs Position of shorting vias

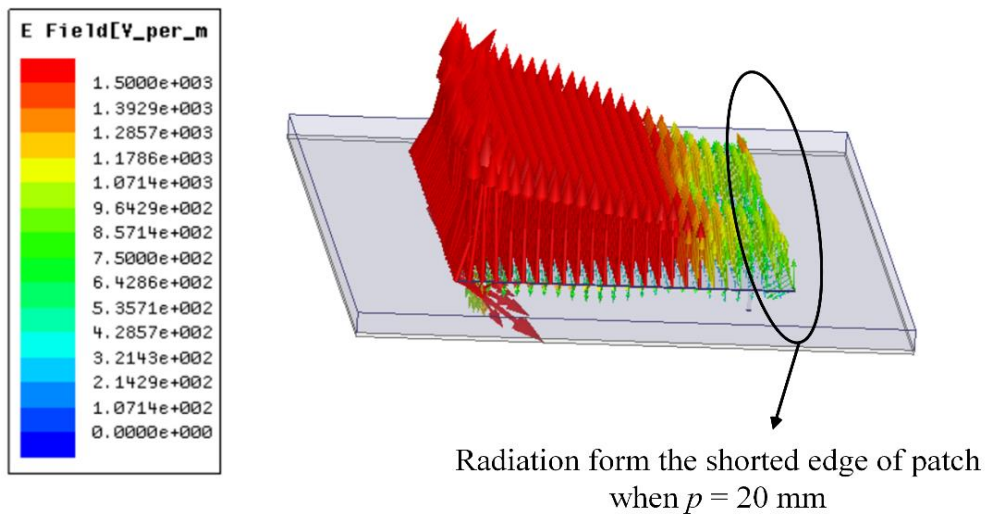
Position of shorting vias from edge of the patch (mm)	Operating Frequency (MHz)
0 (edge)	362
5	374
10	383
15	397
20	410

The operating frequency increases when the position of the shorting vias are shifted towards the center of the patch as shown in Fig.3.5. This rise in frequency with changing location is tabulated in Table3.3. When one of the patch's radiating edges is shorted with vias, the shorted edge does not radiate. As the point is shifted below the patch's edge, as seen in Fig.3.4, the shorted edge begins to radiate. The strength of radiation rises as the position of the vias is lowered downward. Because of the increase

in radiation from the shorted edge caused by the shift of the vias location, the patch resonates at a high frequency. The pattern of electric field from the shorting vias are depicted in the Fig 3.6.



(a)



(b)

Fig. 3.6. Electric filed vector at the shorted edges of the patch (a) slots at $p = 0$ mm (b) slots at $p = 20$ mm

As illustrated in Fig.3.6, repositioning the shorting vias causes an increase in the electric field at the patch's shorted edge, which raises the frequency of the patch. Figure 3.7 depicts the overall shifts of the frequency with the number and position of the shoring vias.

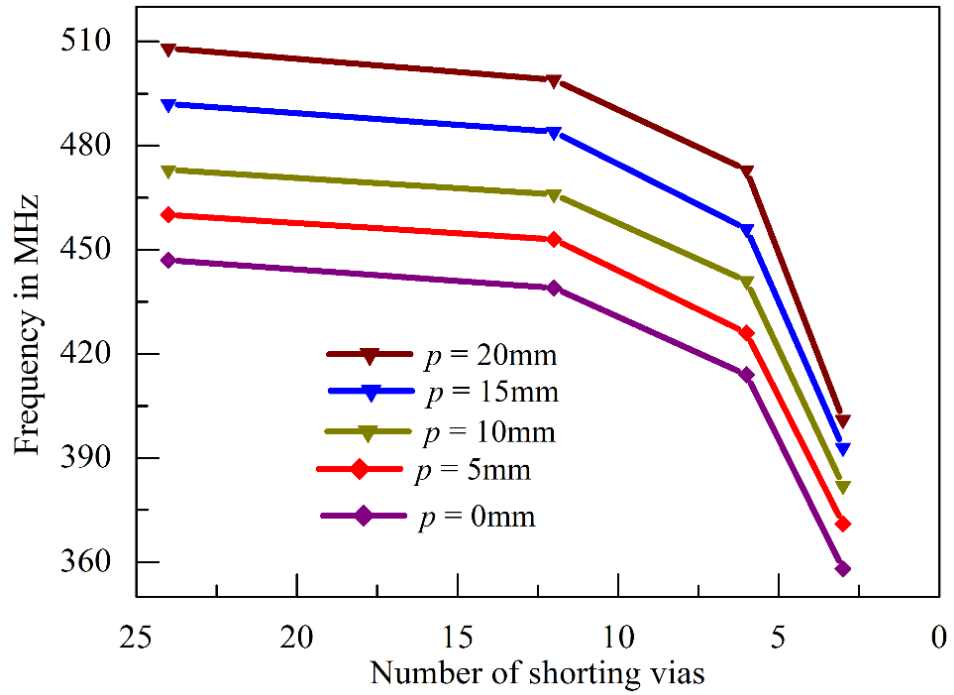
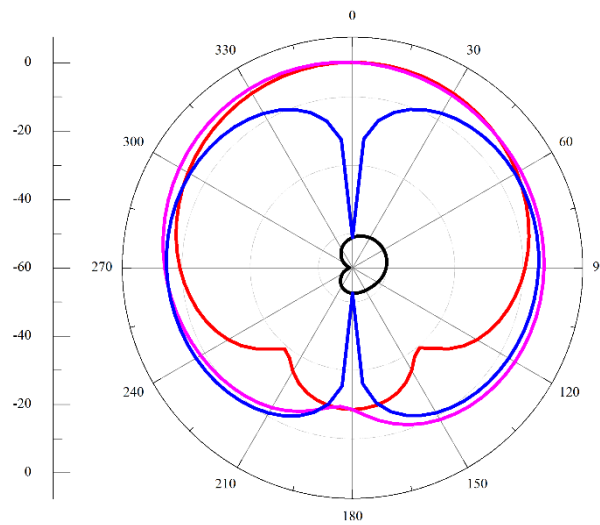
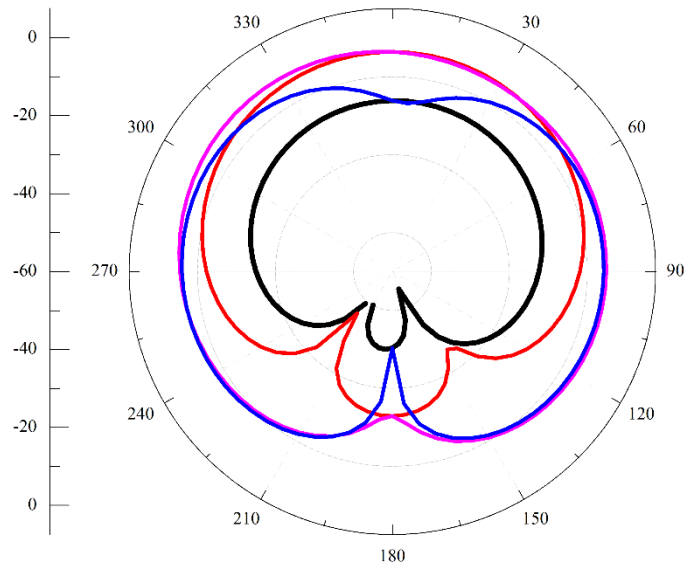


Fig.3.7. Frequency variation of QWP with number and position of shorting vias

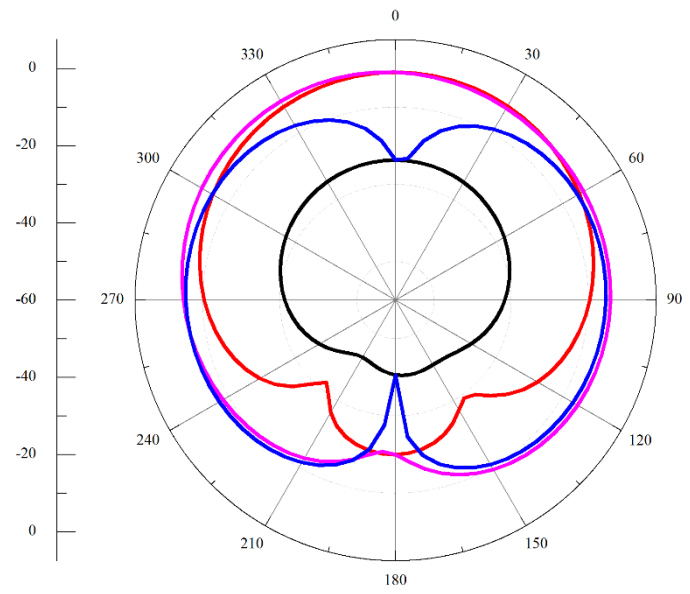
The gain pattern of the QWP with shorting vias are also observed. The gain profile of QWP with different number of shorting vias at the position $p=0$ is depicted in the Fig.3.8



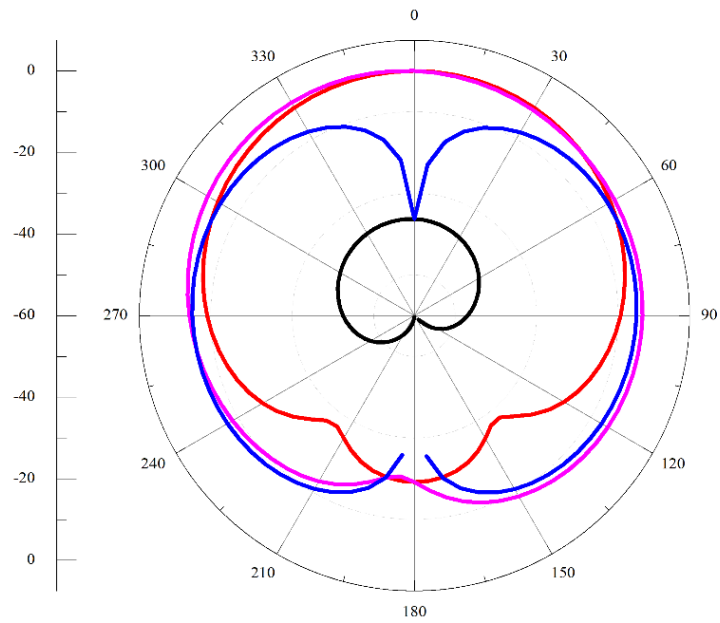
(a)



(b)



(c)



(d)

Fig. 3.8. Radiation pattern QWP for vias at $p = 0$ (a) 24 shorting vias (b) 12 shorting vias (c) 6 shorting vias (d) 3 shorting vias

The gains for different shorting vias at different positions are depicted in the Fig.3.9. The gain pattern shows that QWP yields lower gain than the traditional antenna at the same frequency. From the Fig. 3.9 it is evident that the gain of QWP for different combinations of vias position and number yields the gains ranging from -2.5dBi to 2.5dBi

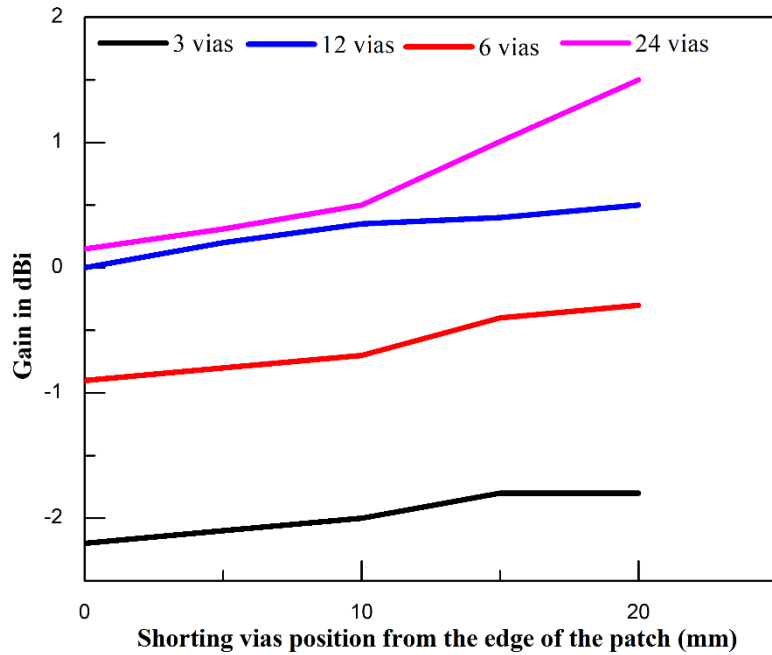


Fig. 3.9. Gains Vs Shorting positions for different numbers of vias

3.3. Conclusion

The observation described in this chapter involves changing the position and the number of shorting vias on a Quarter Wave patch. The simulation results indicate that a Quarter Wave patch may be made to work at different frequencies by altering the number and position of shorting vias. A miniaturization can be produced as a result of the previously described Quarter Wave patch concept. Aside from compactness, the gain of QWP is lower when compared to conventional antennas. As a result of this observation, we can infer that QWP with shorting vias is one of the miniaturization approaches used to minimize patch size. Further investigation is done to improve gain characteristics for these structure by incorporating a meta material having in phase reflection properties known as an Artificial Magnetic Conductor (AMC) is implanted with this QWP to achieve better gain.

CHAPTER

4

Theoretical and Experimental investigation on Air-Artificial Magnetic Conductor composite substrate for Wireless Underground Sensor Network Application

4.1 Introduction

Designing a miniaturized antenna for Wireless Underground Sensor Network (WUSN) or ground penetrating radar (GPR) is a challenging task for antenna researchers. These antennas typically operate in the range of 250 MHz to 900 MHz [86],[95],[119], specifically those in the P band that usually exhibit negative gains and low efficiency. In [84],[148]-[151], different antennas are reported for low frequency (above 500 MHz) underground applications such as simple monopole with Defected Ground Structure [84], Vivaldi antennas [148], a concrete-backed ground plane and a concrete superstrate loaded rectangular microstrip antenna (RMA) and extended slot loaded RMA [149] yielding very poor gain from -1 dBi to -12.9 dBi. Notably, fewer efforts were investigated with Rectangular Microstrip Antenna design below 500 MHz. Designing a compact size antenna for WUSN below 430MHz is very promising as the classical miniaturization techniques such as slot-loading or quarter-wave patch (QWP) severely degrades the gain. Notably, the antennas operating at 433 MHz for WUSN applications such as helical [152] and square spiral [153] usually suffer from negative gain of -5 dBi and -13 dBi. Investigations with planar meander line antennas operating at 433 MHz have also been reported in [154]-[156]. Amid these designs, [154] and [155] have reported a slightly modified meander line printed monopole that is suitable for WUSN application in the Mica2 (commercially available sensor node for WUSN) sensor node. Here, the utilization of trans-receiver box and modified feeding position is used to attain -4.4 dBi gain. To enhance the antenna gain, a similar antenna with a double-layer capacitive strip cut with inter-digital slots is reported in

[155], yielding 1.2 dBi gain. In [156], similar antenna with a capacitive strip is designed via feed battery pad, but a distorted radiation pattern with poor gain (-1 to -0.7 dBi) was obtained.

To address the lacunae of earlier studies, in the present investigation, a Rectangular Microstrip Antenna with 4 shorting pins loaded along with a composite substrate (air dielectric-AMC) is employed to yield positive gain and better efficiency at frequency < 430 MHz. In another report RMA with shorting pins are widely used to achieve 38% miniaturization with dual band operation, low gain (1 dBi with 28% efficiency) [157] and for circular polarization with better gain [158]-[160]. Shorting vias for wideband and to attain polarization purity are reported in [161]-[163]. AMC as ground plane has been used to enhance bandwidth, multi-band operation, miniaturization and high gain [164]-[167]. Nevertheless, the aforementioned RMA with shorting pins or AMC ground plane is designed for frequencies above 1 GHz. Therefore, neither any attempt is made to design an RMA below 430 MHz nor has AMC been used as a composite substrate. Notably, the use of AMC as a part of the composite substrate in an RMA is a completely new technique that is adopted in the present investigation.

In this chapter a simple miniaturized patch is designed on a composite substrate (dielectric-Artificial Magnetic Conductor (AMC)), in which an air gap is introduced as the dielectric. To achieve compact size for the proposed antenna, thoughtful choices of number of shorting vias and their placement is done based on the investigation done in chapter 3. Initially three shorting vias at the edge of the patch is taken for the QWP and simulation is performed and it yields a gain of 1.3 dBi at 385 MHz. This structure is altered such that number of vias is made to four and moved down 5mm from the edge so that the structure is operating at 413 MHz with a peak gain of 3.1 dBi.

4.2. Simulation based investigation of placement of sorting position and air-AMC composite substrate

A quarter wave patch with three shorting vias as discussed in chapter 3 is initially considered as shown in Fig.4.1. The dimensions of the QWP are selected in such that it resonates at frequency of 454 MHz with a gain of 0.7 dBi. The dimensions of QWP is $L_c \times W_c = 120 \text{ mm} \times 150 \text{ mm}$ on a ground plane of $L_g \times W_g = 350 \text{ mm} \times 350 \text{ mm}$. The structure of QWP its resonant frequency and gain plots are depicted in Figs.4.1, 4.2 and 4.3 respectively.

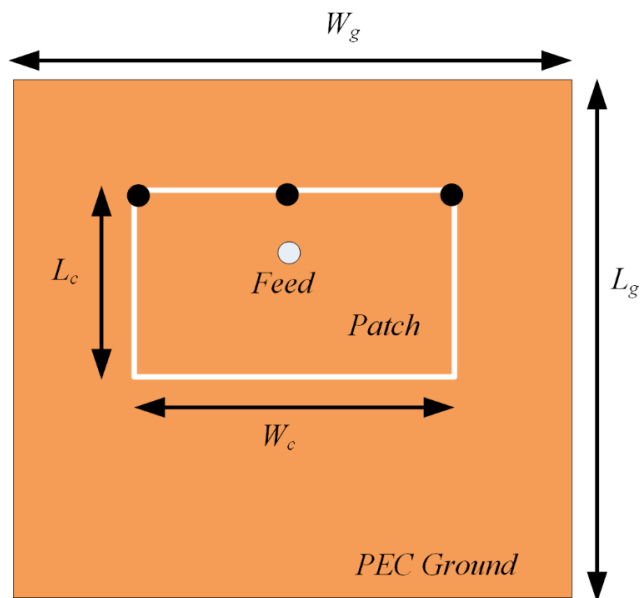


Fig.4.1. Quarter wave patch at 453 MHz

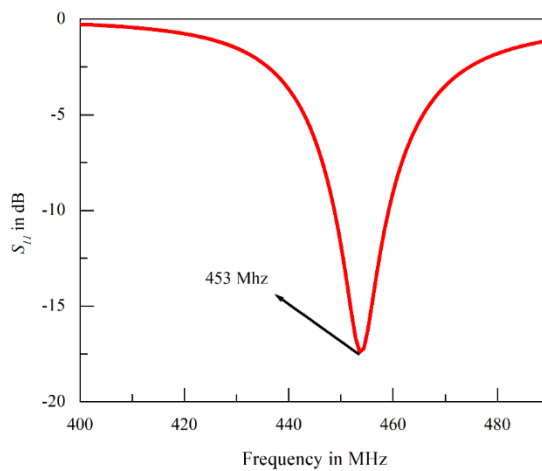


Fig.4.2. Reflection coefficient of the QWP antenna at 454 MHz

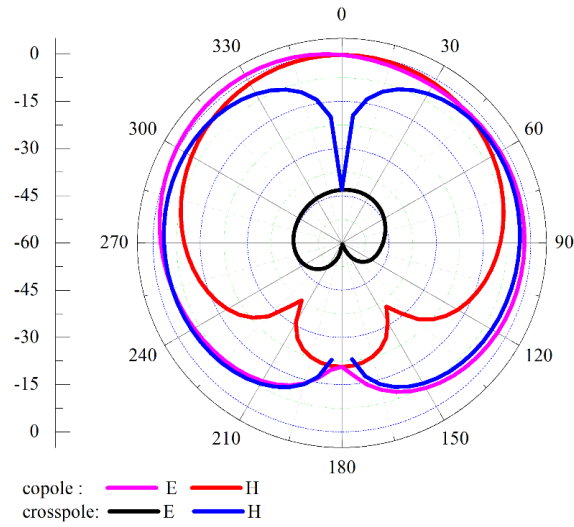


Fig.4.3. Gain of QWP antenna at 454 MHz

This QWP provides the miniaturized structure as discussed in the chapter 3. To increase the gain of this QWP, air-AMC composite substrate is embedded into it. An AMC unit cell of $L_{amc} \times L_{amc} = 100 \text{ mm} \times 100 \text{ mm}$ is built on a $S_{l_{amc}} \times S_{l_{amc}} = 104 \text{ mm} \times 104 \text{ mm}$ ground plane. A 3.2 mm thick substrate with a relative permittivity of $r = 10.2$ is put on top of this PEC ground plane. This AMC unit cell and its reflection coefficient at 453 MHz is shown in Fig.4.4, which corresponds to the frequency of the antenna designed.

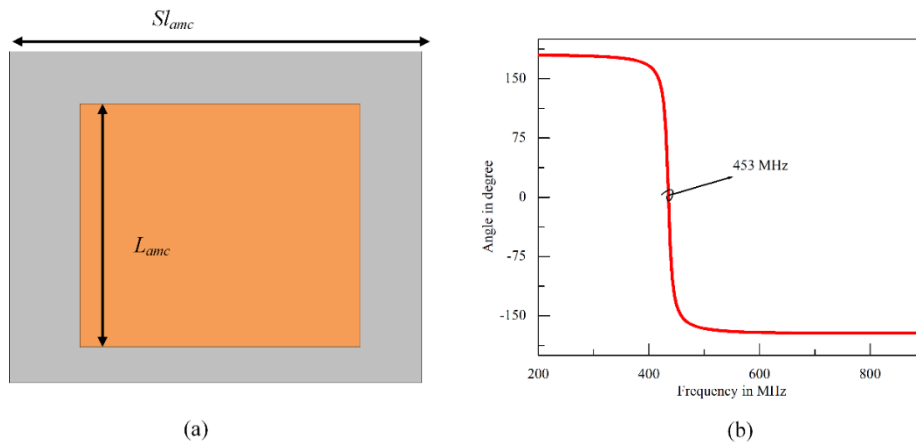


Fig.4.4. AMC structure at 453 MHz (a) unit cell (b) reflection coefficient

This AMC is made as 2×3 array to accommodate the patch size and form a composite substrate. With the integration of AMC, the antenna resonates at 385 MHz. The proposed antenna at 385 MHz is shown in the Fig.4.5.

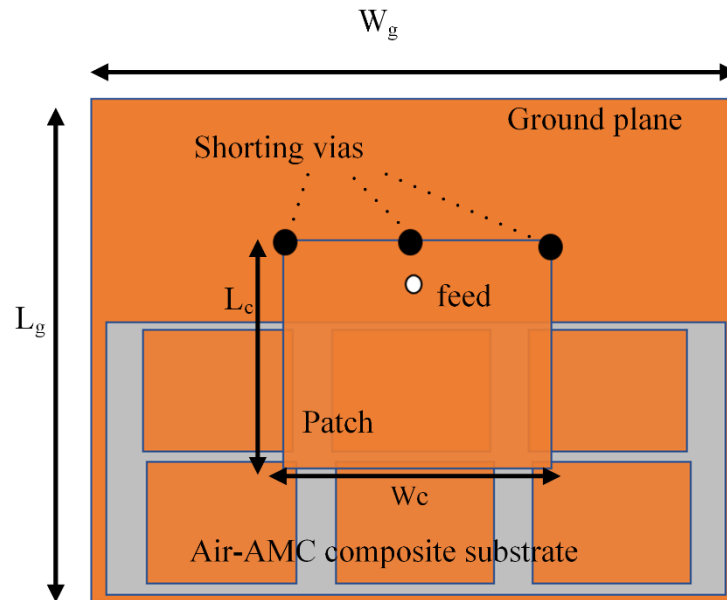


Fig.4.5. Schematic of Air -AMC Antenna at 385 MHz

By incorporation of Shorting vias and air-AMC composite substrate this structure is made to operate at 385 MHz where in general conventional RMA requires a dimension of $250 \text{ mm} \times 300 \text{ mm}$ patch size for same operating frequency. The reflection coefficient of this antenna depicted in Fig 4.6 confirms the resonance at 385 MHz

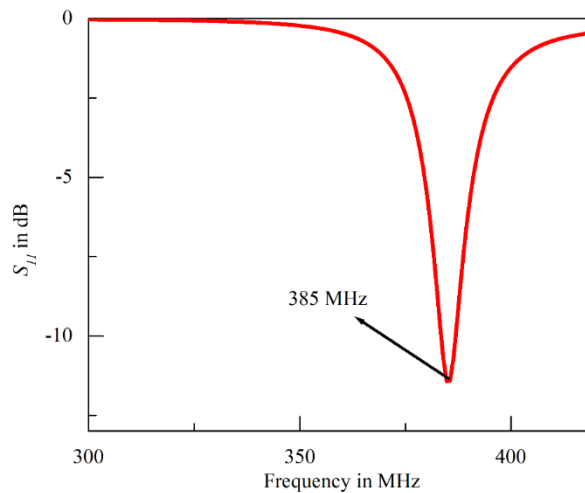


Fig.4.6. Reflection Coefficient of antenna resonance at 385 MHz

Incorporation of AMC as composite substrate enhances its gain from 0.7 dBi to 1.3 dBi and reduces frequency from 454 MHz to 385 MHz as depicted in the Fig.4.7.

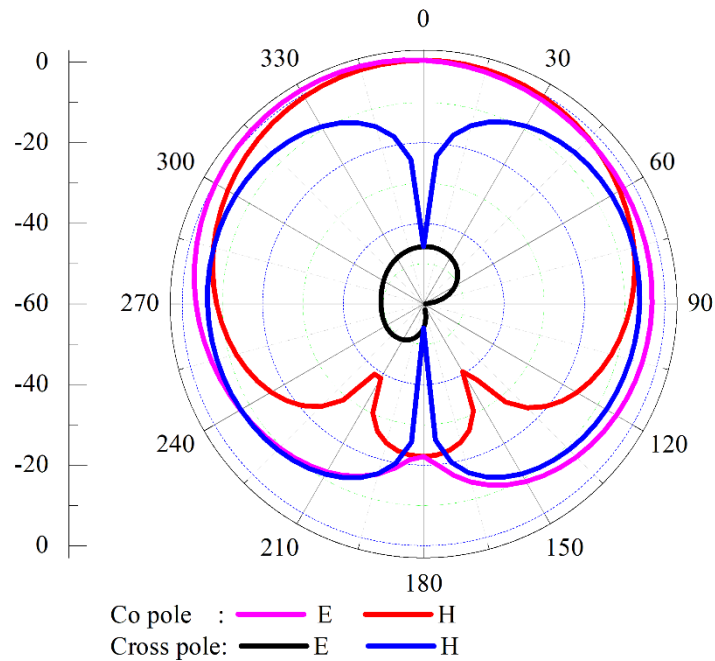


Fig.4.7. Gain of antenna at 385 MHz

Hence a QWP with air AMC composite substrate operating at 385 MHz is proposed and designed. The gain of this structure is 1.3 dBi, is useful for the low gain applications. However, for lossy ground for combating attenuation it would be better to have antenna gain more than at least 2dBi. Analogous structure with close resemblance is further analyzed by changing the shorting vias number and position to yield more better radiation performance. Through and methodical investigation has been carried out and documented in the next section

4.3 Antenna design

A simple miniaturized patch (smaller than classical QWP) is designed on a composite substrate (dielectric-Artificial Magnetic Conductor (AMC)), in which an air gap is applied as the dielectric, as shown in Fig. 4.8. To achieve compact size for the proposed antenna, thoughtful choices of shorting vias numbers and their corresponding placement positions are important as initially investigated in earlier chapter 3.

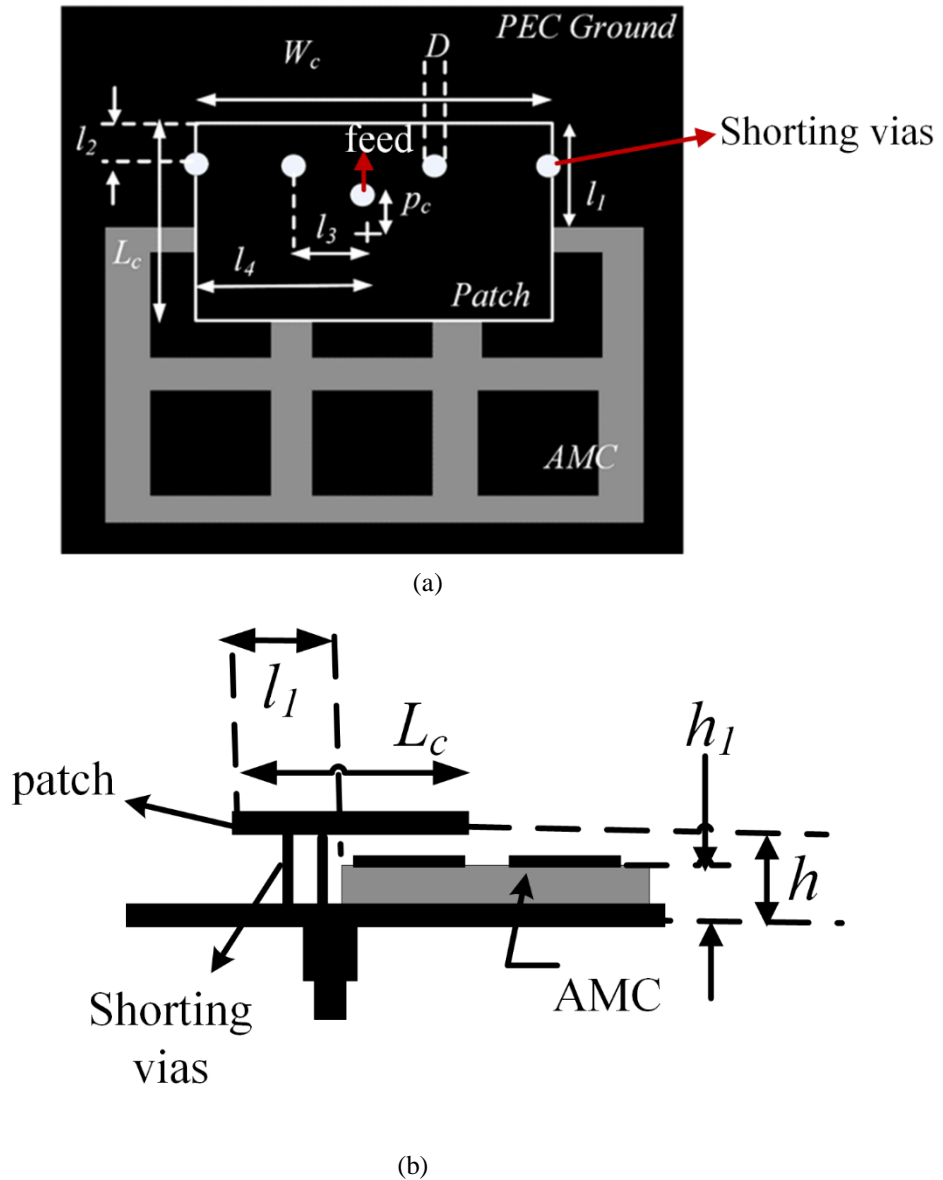


Fig.4.8. Proposed antenna at 413 MHz (PA) structure (a) Top view (b) Side view.

To further miniaturize the proposed antenna, a composite substrate (partial AMC) is incorporated, and the proposed antenna size can be reduced to $0.16\lambda_0 \times 0.20\lambda_0 \times 0.01\lambda_0$ (fabricated on a $0.47\lambda_0 \times 0.47\lambda_0$ ground plane). Where λ_0 is free space operating wave length. The proposed antenna can be useful not only for WUSN applications but also for other underground wireless applications and space applications in the range of 300 MHz to 1 GHz.

4.4 Evolution Analysis

4.4.1 AMC Unit Cell and Array:

An AMC unit cell in the form of high impedance surface (HIS) is initially designed by using a simple single square patch of side length $L_1 = 84 \text{ mm}$ ($\approx \lambda_{eff}/2$), and it is printed on an alumina substrate of size $D \times D = 88 \times 88 \text{ mm}^2$ and thickness (h_1) = 3.0 mm, permittivity (ϵ_r) = 10.0, as shown in Fig. 4.9 (a). The unit cell is designed at a slightly higher frequency of $f = 530 \text{ MHz}$, followed by extending it into an array type, in which a 2×3 AMC array is realized at the same frequency with a periodicity of 86 mm. The gap (g) of 2 mm between the AMC patches is maintained at, and the overall AMC substrate dimension is $260 \times 176 \text{ mm}^2$. Fig. 4.9(b) shows the 2×3 AMC array structure (at slightly higher frequency) with a view to attaining the desired resonant frequency below 430 MHz. The simulation study shows that the introduction of AMC as a substrate will lead to patch size miniaturization, and hence decreases the resonant frequency. As such, AMC as HIS presents both the high input resistance and reactance at its resonant frequency that obstructs electric currents to flow through it. In the present investigation, alumina with very low loss-tangent ($\tan \delta = 0.0001$) is used as the AMC substrate. For the lossless structure, the resonance condition can be defined by the frequency at which the AMC-HIS surface has ideally infinite reactance or zero susceptance [168].

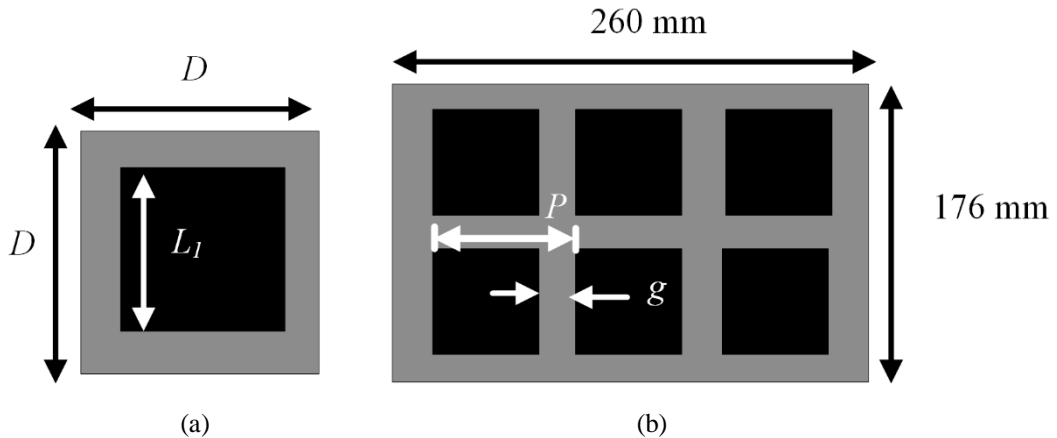


Fig. 4.9. (a) AMC unit cell, (b) 2×3 AMC array.

4.4.2 AMC resonance

The objective of the AMC unit cell and the 2×3 AMC array (at slightly higher frequency) is to eventually achieve a desired resonant frequency of below 430 MHz. For the lossless structure, the resonance condition can be defined by the frequency at which the AMC-HIS surface has ideally infinite reactance or zero susceptance [168]. This AMC array can be modeled by applying a series R-L-C resonant circuit backed by a grounded dielectric substrate. The complete AMC equivalent circuit is shown in Fig. 4.10 where Z_d is the input impedance of the grounded dielectric substrate, and it is parallel to the series R-L-C circuit. The input susceptance of the grounded dielectric substrate may be written as,

$$B_d = \frac{1}{Z_d} = \left(\frac{\eta_0}{\sqrt{\epsilon_r}} [\tan(k_0 h_1 \sqrt{\epsilon_{reff}})] \right)^{-1} = \frac{\eta_0}{\sqrt{\epsilon_r}} \left(\left[\tan \left(k_0 h_1 \sqrt{\frac{\epsilon_r + 1}{2}} \right) \right] \right)^{-1} \quad (4.1)$$

and using the equations of inductance (L) and Capacitance of AMC (C_{AMC}) from [168]-[169], the susceptance of the series R-L-C circuit of the AMC floor (Frequency Selective Surface) can be written as,

$$B_{FSS} = \frac{1}{X_{FSS}} = \left[\frac{1 - \omega^2 L C_{AMC} (\epsilon_r + 1)/2}{\omega C_{AMC} (\epsilon_r + 1)/2} \right]^{-1} \quad (4.2)$$

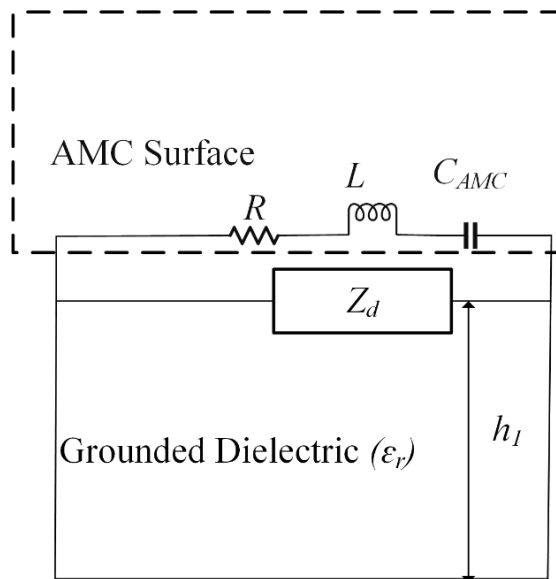
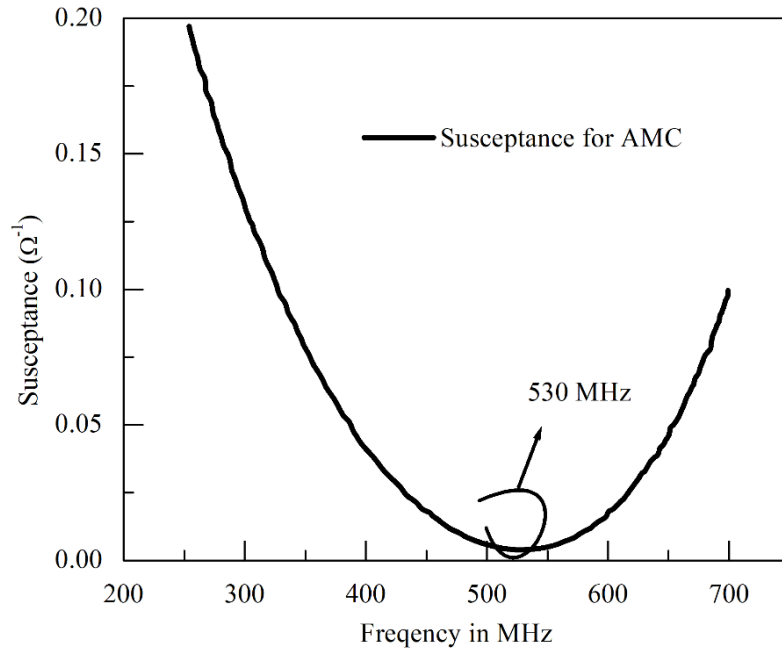


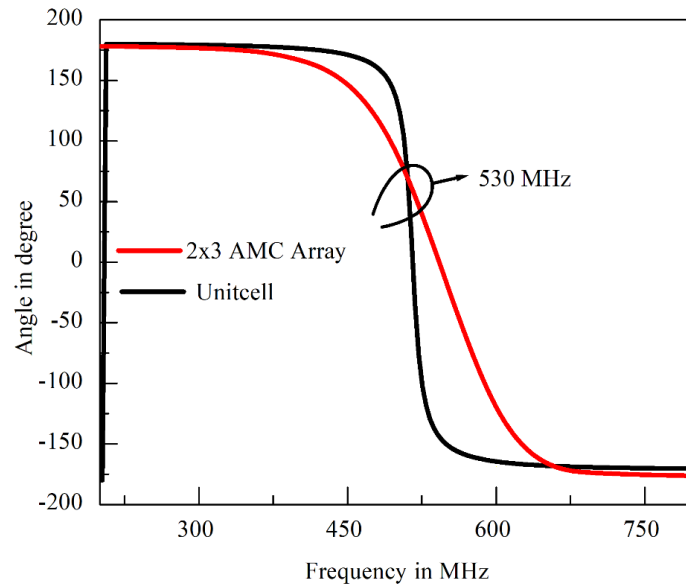
Fig. 4.10. Equivalent circuit of AMC

The equivalent susceptance of the AMC terminal (B_{AMC}) is a parallel combination of both B_d , B_{FSS} and at resonance,

$$B_{AMC} = \frac{1}{X_{AMC}} = B_d + B_{FSS} \rightarrow 0 \quad (4.3)$$



(a)



(b)

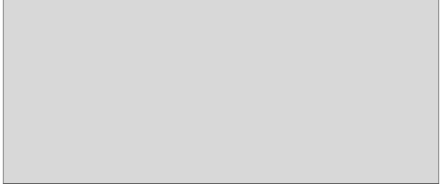


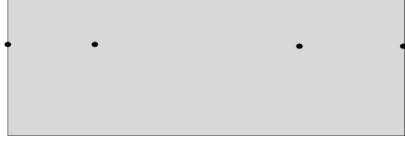
Fig. 4.11. (a) Susceptance of AMC array as a function of frequency, (b) Reflection phase angle of unit cell and array.

The resonance of AMC array obtained from equation (4.3) and that obtained from the simulated reflection phase characteristics is shown in Fig. 4.11 (a) and (b) respectively. Both the figures show close agreement amongst the predicted circuit model and the simulated result.

4.4.3 Stand Alone Antenna (Reference Antenna):

A conventional RMA (290 mm × 400 mm) with a square PEC ground plane of size 600 x 600 mm² suspended (10 mm) over air substrate resonates at $f = 530$ MHz is initially investigated from simulation. However, the dimension of this RMA is not feasible for any applications. Further investigation from the simulation has shown that if 68 shorting vias (diameter of 2 mm) are to be loaded along the central line of the patch, the patch size can be reduced to almost halve (160 mm × 200 mm). Consequently, a much smaller ground plane of size 400 x 400 mm² can be attained, with the antenna resonating at $f = 500$ MHz.

Table 4.1
Performances comparison of proposed antenna with references

Structure	Structures and patch size $L \times W$ (mm × mm)	Frequency in MHz
	290x400 (Conventional RMA)	530
	160x200 (Classical QWP with 68 shorting vias)	500
	160x200 (Compact QWP with 4 shorting vias)	460
	120x150 (RA)	520

This Quarter Wave Patch (QWP) is made more compact and inductive by reducing the numbers of shorting vias to 4, and then antenna is resonating at 460 MHz. Hence, to match the antenna frequency with the AMC, the length and width of the patch are shortened to $L_C = 120$ mm and $W_C = 150$ mm, respectively and the shorting vias are moved 5 mm toward centre from the edge of the QWP as shown in Fig.4.8.

This antenna structure is now denoted as reference antenna (RA) or standalone RA, and it has a smaller ground plane size of 350×350 mm². The step-by-step antenna structure design evaluation and the resonant frequencies are shown in Table:4.1. Here, the resulting RA structure resonates at 520 MHz as per the simulation. The equivalent circuit for RA with shorting vias is shown in Fig. 4.12.

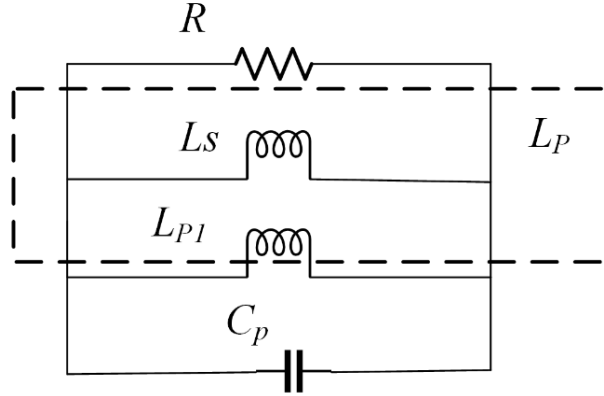


Fig. 4.12. Equivalent circuit of standalone reference antenna (RA) with shorting vias

To induce a resonance, the inductive reactance should be the same as the capacitive reactance of the patch. The inductive reactance (L_{p1}) and capacitive reactance (C_p) of RMA obtained from [169], [40] comes in parallel to 4 shorting posts with inductance (L_s) results in the total inductive reactance of RA

$$L_P = \frac{L_{P1}L_S}{(L_{P1}+L_S)} \quad (4.4)$$

Where L_s can be written as [162]

$$L_S = \frac{\eta_0}{4\sqrt{\epsilon_r}} \tan \left[\frac{2\pi h}{\lambda_0} \right] \quad (4.5)$$

and the condition for resonance

$$\omega L_P = \frac{1}{\omega C_P}. \quad (4.6)$$

The solution of equation (4.6) reveals that, the antenna is resonating at $f = 514$ MHz, which is in good agreement with the simulated result ($f = 520$ MHz).

4.5 Proposed Antenna on Air-AMC Composite Substrate

The proposed patch is suspended on a composite air-AMC substrate, in which the equivalent circuit of the AMC is parallel to the anti-resonant circuit of the patch. As the placement of air-AMC composite substrate presents different static capacitance in the anti-resonant circuit of the patch, the operating frequency of the Proposed Antenna (PA) structure is changed from 514 MHz to 414 MHz (as expected) [166] detail calculation is shown below, and its corresponding equivalent circuit is presented in Fig. 4.13.

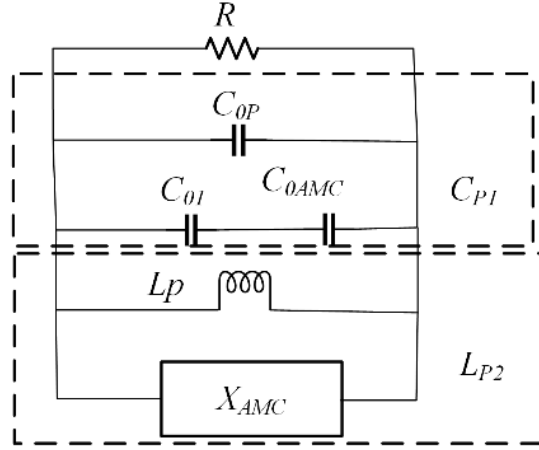


Fig. 4.13. Equivalent circuit of proposed antenna (PA).

From the present antenna structure shown in Fig. 4.8(a), the AMC is placed $l_1 = 15$ mm below the upper edge of the top patch. Therefore, in the specific region beneath the patch, there will be two series capacitances, namely, C_{0I} (between the patch and AMC) and C_{0AMC} (AMC part beneath the patch) that are parallel to another capacitance (C_{0P}) which is developed for the portion of the patch with full air substrate. Here,

$$\left. \begin{aligned} C_{0P} &= \frac{\epsilon_0 l_1 W_C}{2h} \\ C_{0I} &= \frac{\epsilon_0 (L_C - l_1) W_C}{2(h - h_1)} \end{aligned} \right\} \quad (4.7)$$

and

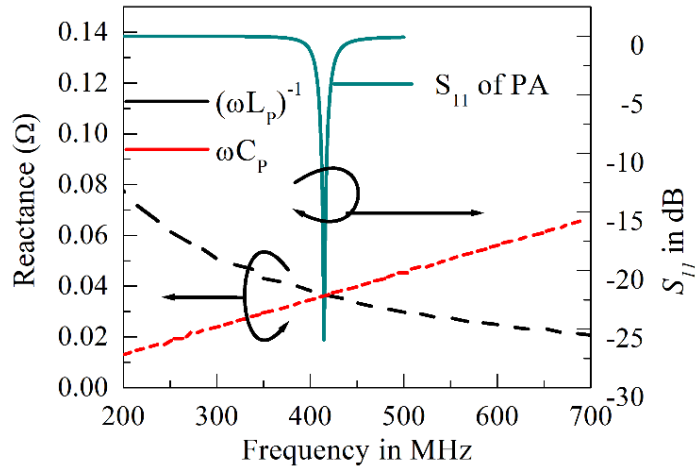
$$C_{0AMC} = \frac{\epsilon_0 \epsilon_r (L_C - l_1) W_C}{2h_1}$$

and the modified patch capacitance (C_{PI}) becomes,

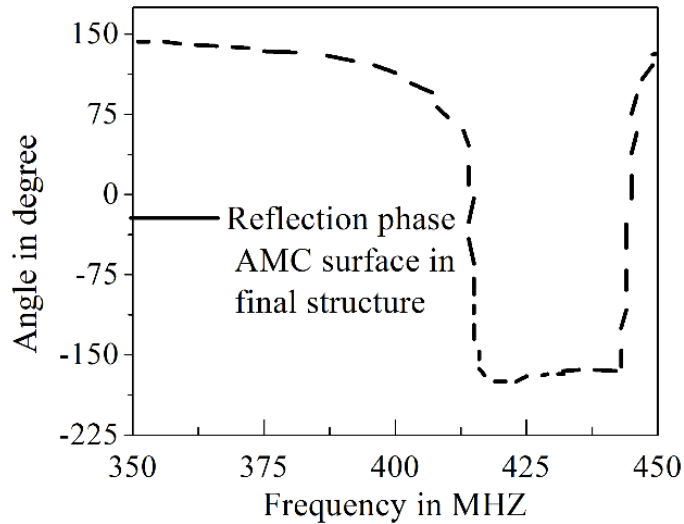
$$C_{P1} = \frac{C_{01}C_{0AMC}}{(C_{01}+C_{AMC})} + C_{op} \quad (4.8)$$

From close inspection of the AMC reactance (X_{AMC}), one can see that it is highly inductive at 414 MHz. Therefore, this AMC inductance (X_{AMC}) is also in parallel to the shorted patch inductance (L_P), as denoted in equation (4.4), and the resulting antenna structure possesses the inductance of,

$$L_{P2} = \frac{L_P X_{AMC}}{(L_{P1} + X_{AMC})} \quad (4.9)$$



(a)



(b)

Fig. 4.14. (a) Plot of equation (4.10) to extract solution for frequency and simulated $|S_{11}|$ profile of PA, (b) Simulated reflection phase of AMC in complete structure.

From close inspection of the AMC reactance (X_{AMC}), one can see that it is highly inductive at 414 MHz. Therefore, this AMC inductance (X_{AMC}) is also in parallel to the shorted patch inductance (L_P), as denoted in equation (4.4), and the resulting antenna structure possesses the inductance of,

$$L_{P2} = \frac{L_P X_{AMC}}{(L_{P1} + X_{AMC})} \quad (4.9)$$

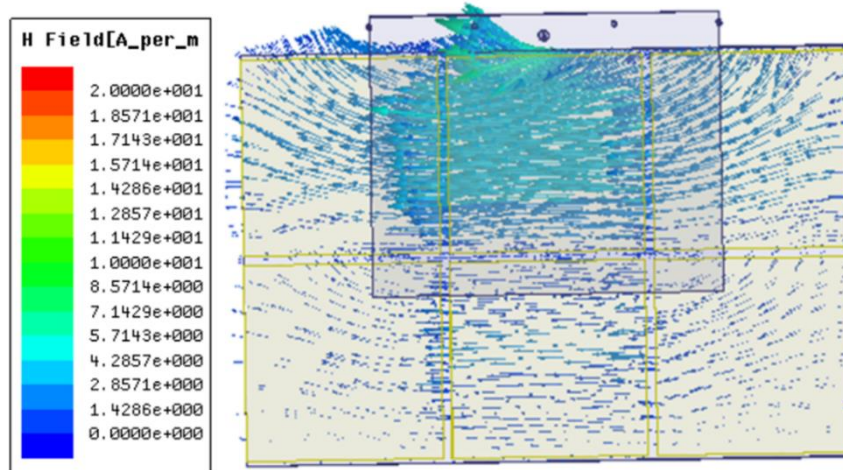
Finally, the resonance of the final antenna structure is,

$$\omega L_{P2} = \frac{1}{\omega C_{P1}} \quad (4.10)$$

The simulated $|S_{11}|$ profile of the PA indicating resonance at $f = 414$ MHz and the plots of Equation (4.10), depicted in Fig. 4.14(a), shows good agreement between the simulation and predicted results. Also, the designed AMC has a zero-reflection phase at the same frequency (Fig. 4.14(b)).

The concept of zero reflection phase is further confirmed through zero tangential H field vector on AMC surface of PA at $f = 414$ MHz as depicted in Fig. 4.15(a). The simulated radiation patterns and the fringing E field vectors at the patch radiating edge of the PA and RA are shown in Figs. 4.15(b),(c) and (d), respectively.

The horizontal extension of fringing fields in PA in comparison with RA is due to the incorporation of AMC surface beneath the patch which in turn enhance the gain. Furthermore, the same phase image current strengthens the radiation field and results in higher gain of the PA



(a)

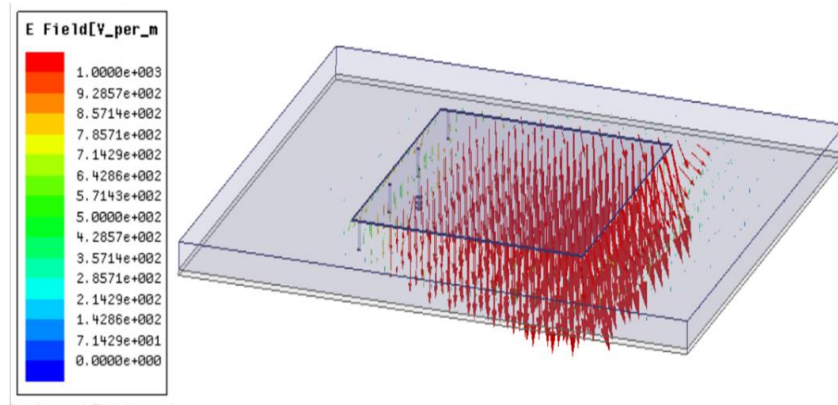
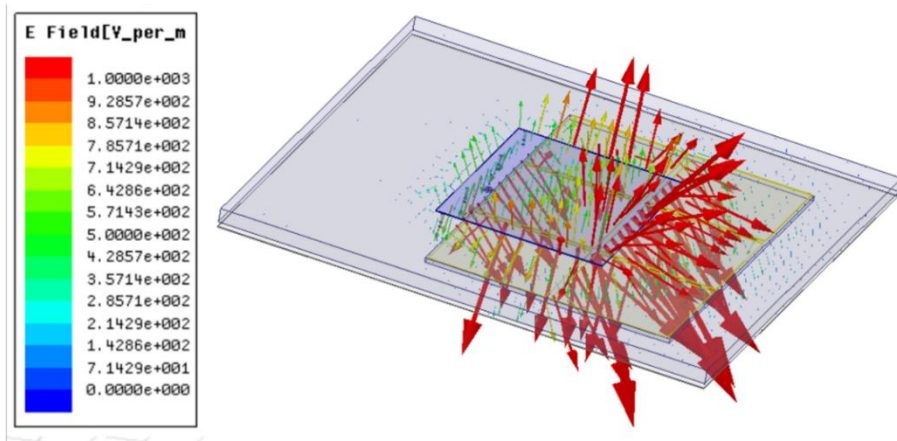
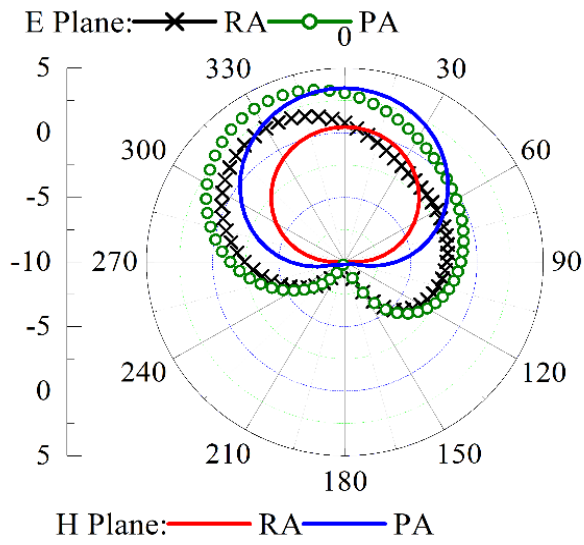


Fig. 4.15. (a) Simulated tangential H field magnitude on AMC surface of the PA, (b) Simulated radiation patterns of the RA and PA, (c) Simulated fringing E field vector at patch radiating edge for PA, (d) Simulated fringing E field vector at patch radiating edge for RA. [at $f = 414$ MHz for all cases]

The copolar radiation performance of PA, RA and traditional RMA of same frequency is presented in Fig.4.16. This depicts that around 2 dB of gain improvement with PA (gain 3.1 dBi) can be achieved in comparison with classical RMA (gain 1.1 dBi).

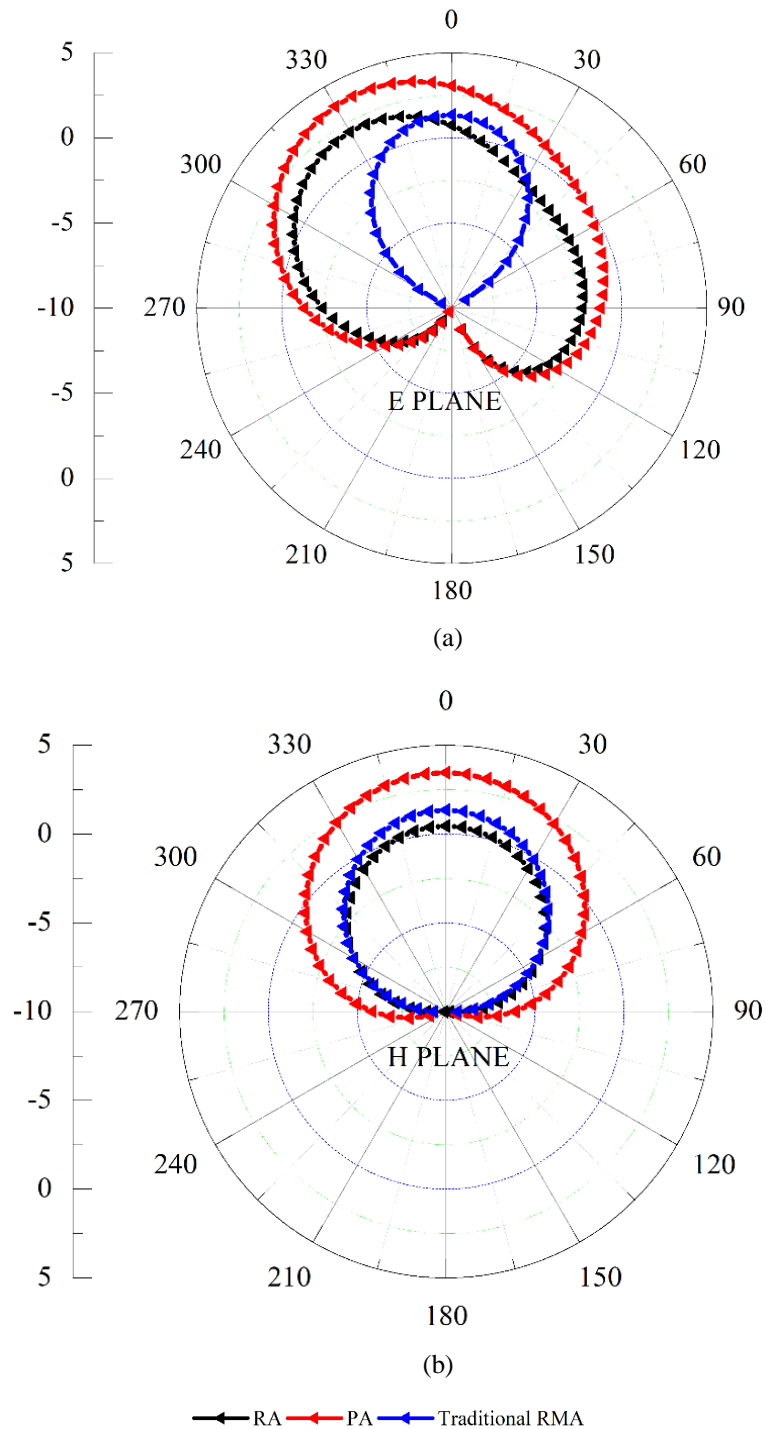


Fig. 4.16. Comparison of radiation pattern of PA, RA and traditional RMA. (a) E plane, (b) H plane.

It is very clear that the PA can give much better performance in gain in comparison with RA and Traditional RMA. The bandwidth of the PA is found about 2%. The experimental validation of performance limit of small antenna is classically explained in [172]. Here, PA is the miniaturized antenna for underground communication with such good radiation performance and it well follows the fundamental limits predicted in [172]. Nevertheless, the less bandwidth of PA in comparison to traditional RMA is expected as the antenna is much miniaturized. Notably, in spite of much miniaturization of patch, efficiency is good and that may be attributed to the use of AMC as composite substrate as discussed earlier.

4.6. Results and Discussions

The Fabricated prototype of the PA is shown in Fig.4.17. Notably, the PA with $120 \times 150 \text{ mm}^2$ is much smaller than the RA ($150 \times 187 \text{ mm}^2$) designed at the same frequency.

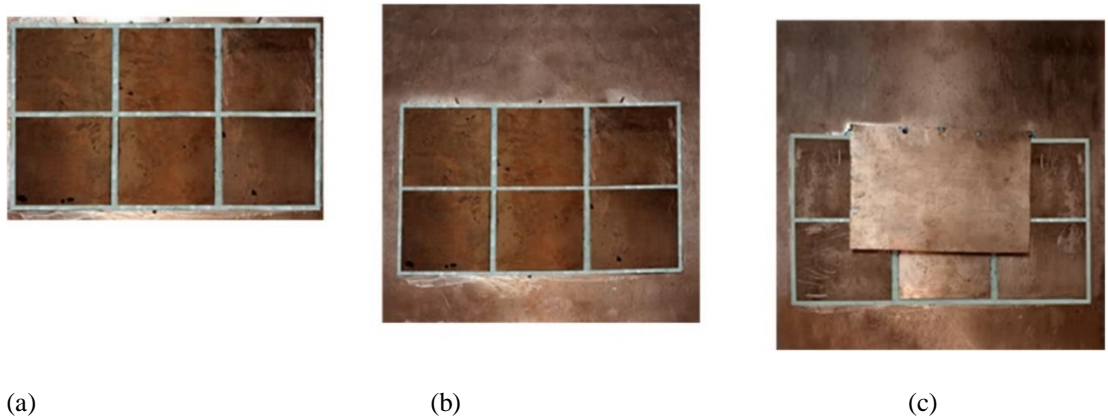
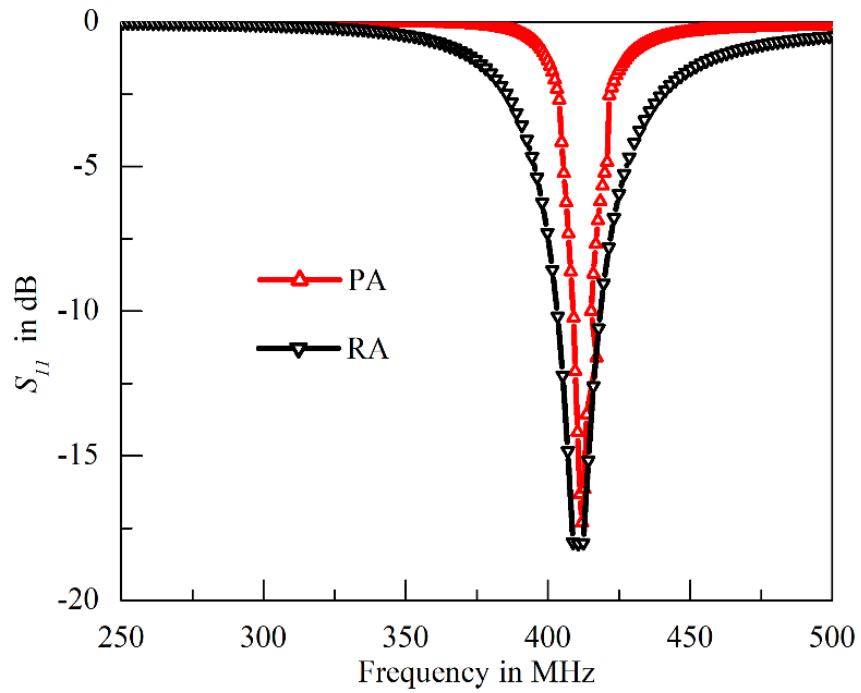
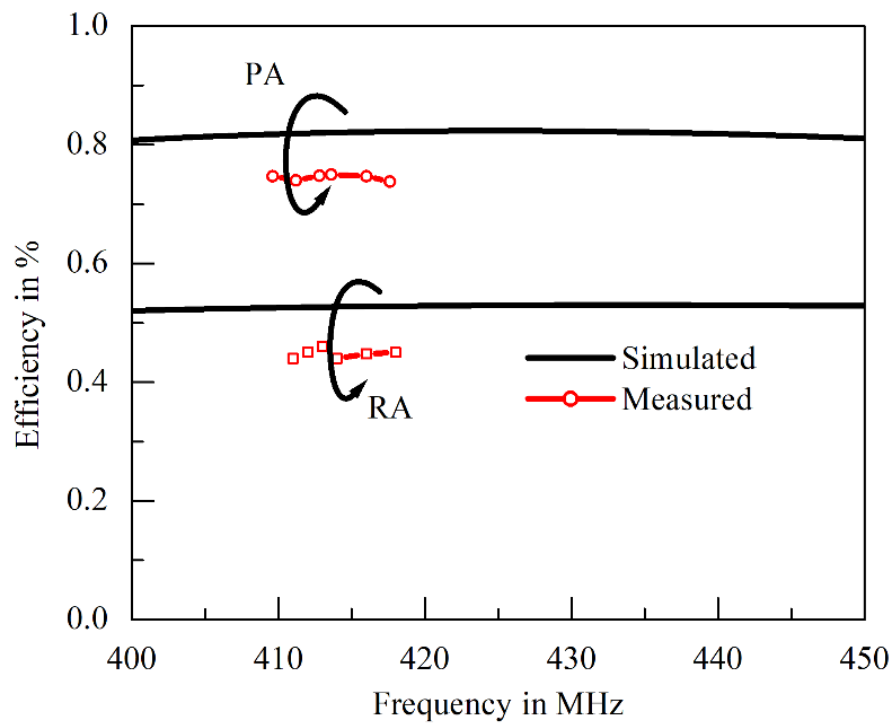


Fig. 4.17. The fabricated prototype of the PA, (a) AMC array, (b) AMC array on the ground plane, (c) proposed antenna (PA) structure.

Both the PA and RA are fed at 50 mm and 60 mm, respectively, from the patch center. The measured $|S_{11}|$ and efficiency of the PA and RA are depicted in Fig. 4.18 (a) and Fig.4.18 (b), respectively. The PA resonating at 413 MHz has exhibited a -10 dB impedance bandwidth from 408 to 416 MHz while the same for RA was from 402 to 417 MHz. The high dielectric constant of AMC substrate will reduce the surface wave results in the reduction in bandwidth and enhancement of gain and efficiency in PA compared with RA.



(a)



(b)

Fig. 4.18. Results of PA and RA, (a) Measured $|S_{11}|$, (b) Radiation efficiency.

It is also observed from Fig. 4.18 (b) that the measured radiation efficiency of the RA was 44%, while the same for PA was 75%. The complete radiation patterns observed from Fig.4.19, corroborates 2.05 dB of clear enhancement of PA gain from 1.05 dBi to 3.1 dBi in comparison with RA.

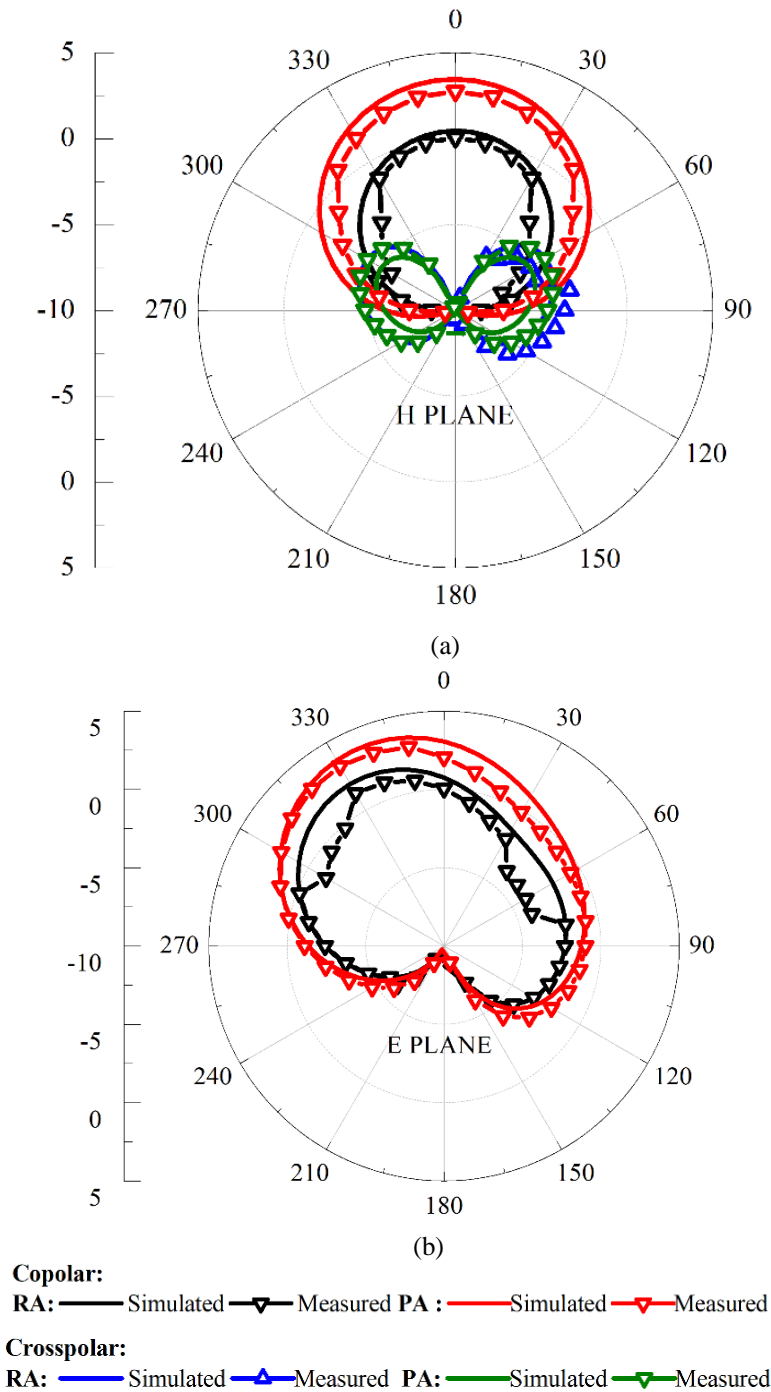


Fig. 4.19. Comparison of simulated and measured radiation pattern of RA and PA. (a) H-plane. (b) E-plane. (Cross pole is not visible due to scale)

Table 4.2 shows the performances of the PA in comparison with relevant references. It is observed that the PA can resonate at the lowest frequency in comparison to others which is apt for underground communication. Even though the PA exhibits slightly larger size, it still maintains a low profile of $0.01\lambda_0$ with good positive gain with better efficiency in spite of maintaining good bandwidth of 2% at such low frequency in comparison with other antennas.

Table 4.2

Comparison of proposed antenna with other low frequency antennas

Ref	Size (λ_0) ³ mm ³	Frequency (MHz)	Gain (dBi)	Band Width (%)	Eff
[148]	0.11×0.10×0.002	500	-13	2	-
[153]	0.07×0.04×0.002	434	-13	1.1	<40%
[154]	0.70×0.016×0.006	433	-4.3	1.3	-
[155]	0.12×0.04×0.002	4334	1.2	0.9	60.8%
[170]	0.20×0.20×0.05	410	0.4	-	50%
[171]	0.13×0.05×0.001	435	-1	0.6	55%
PA	0.16×0.20×0.01	413	3.1	2	75%

4.7. Conclusion

A simple shorted RMA with composite air-AMC substrate operating at relatively very low frequency 385 MHz is initially investigated. The impact of shorting vias on the frequency has been verified for two different structures. The structure operating at 385 MHz produces a gain of 1.3dBi. the same structure is made to operate at (413 MHz) for WUSN and other underground communication yield gain of 3.1 dBi as well as good radiation efficiency of 75% and has been successfully investigated and presented in the later section. The novelties of the proposed antenna are listed as follows

- The use of AMC as the substrate to yield composite substrate beneath the patch can improve the antenna performances such as miniaturization and higher gain.

- The proposed fabricated antenna that operates at 413 MHz is suitable for WUSN and other underground wireless applications. Furthermore, the miniaturization of the proposed antenna structure is better than that of the classical QWP.
- Even though the proposed antenna is operating at a very low frequency with higher gain such as 3.1 dBi can be achieved by incorporating the AMC property as shown in comparison Table 4.2.
- As far as the author's knowledge is concerned, the use of AMC has not been attempted at such low frequency. Furthermore, a very simple AMC structure is applied with patch arrays. The proposed antenna is simple to design, easy to manufacture, and could be analysed by applying an appropriate equivalent circuit model.

Design and Analysis of Transverse Electric mode excited Rectangular Microstrip Antenna for Wireless Underground Sensor Networks

5.1 Introduction

Artificial magnetic conductors (AMCs) are used in antennas to improve their performance as seen in previous chapter, where AMC was used as a composite substrate with air to enhance the gain of a low-frequency antennas. Conventionally Transverse Magnetic (TM) mode is excited by a perfect electric conductor (PEC) patch and ground plane. However, to generate Transverse Electric (TE) mode, a perfect magnetic conductor (PMC) patch and ground are required. As PMC materials are not available, AMC is used to create magnetic patch and ground that excite TE mode in the antenna. Embedding AMC in both the ground and patch makes the antenna operate in the TE mode instead of the TM mode.

In the present era, the key challenge for a low frequency planar antenna applied to a wireless underground sensor network (WUSN) and other underground wireless communication is to achieve positive gain with good efficiency. Besides that, a relatively wider bandwidth with more than one operating frequency is desirable for operational versatility. In the present chapter, a simple artificial magnetic conductor (AMC) integrated rectangular microstrip antenna (RMA) of size $0.28\lambda_0 \times 0.28\lambda_0 \times 0.07\lambda_0$ is employed. By meticulously exploiting a dual periodic AMC along with dielectric strips (AMC radiating patch and AMC ground plane) and proper utilization of an L-probe feed, two resonances at 572 MHz (low band) and 768 MHz (high band) can be yielded with a wide bandwidth of around 12% for both cases. Unlike the classical RMA design, a transverse electric mode (TE) excited RMA is proposed. The proposed

antenna can also achieve good positive gains of 4.3 dBi (572 MHz) and 6.1 dBi (768 MHz) across both bands with an efficiency of 71% and 75%, respectively.

Rapid development in underground sensing applications hankers the demand of designing a compact planar low frequency antenna for wireless Underground Sensor Networks (WUSN) (300-900 MHz) [86],[95],[119]. As such, in the era of the Wireless Internet of Things (WIOT), Cognitive Radio application (CRA), and Wireless Underground Sensor Networks (WUSN), multi-functional devices with compact planar antennas are very much essential. Indigenous antenna design with more than one operating frequency, improved bandwidth, and good positive gain is a thought-provoking task for the antenna scientific community. Nevertheless, designing a low frequency (300-1000 MHz) dual-band antenna for underground wireless communication with augmented positive gain and wider bandwidth is definitely beneficial to the scientific community and undeniably a current state-of-the-art-research. Furthermore, in the case of WUSN, the dual-band antenna has more versatility to operate for two different soil conditions. The antennas for low frequency wireless underground applications have been reported in [152]-[153], and they have yielded negative gain with poor bandwidth. Other antenna designs with different planar structures, such as printed monopole [154] and meander line structures [155]-[156] working at such a low frequency range, can attained a maximum gain of 1 dBi as per report. From the literature, it can be seen that very few efforts have been made to improve the gain and bandwidth of a planar rectangular microstrip antenna (RMA) design for low frequency underground wireless communication as far our knowledge. For example, the planar RMA with a concrete backing [150] has exhibited a low gain of -3 dBi to -6 dBi, while the slot loading planar RMA in [151] has displayed a low gain of 1 dBi. Besides showing low gain characteristics, both designs also have a narrow bandwidth of $< 2\%$ as well.

Recently, metamaterial and artificial magnetic conductor (AMC) techniques have been implemented in an RMA design to realize low frequency planar antennas suitable for underground wireless communication. In [173], the metamaterial array structure (with vias and partial ground plane) is incorporated into a meandered line RMA with two layers of substrate, yielding 2 dBi gain with 2% bandwidth. To further improve

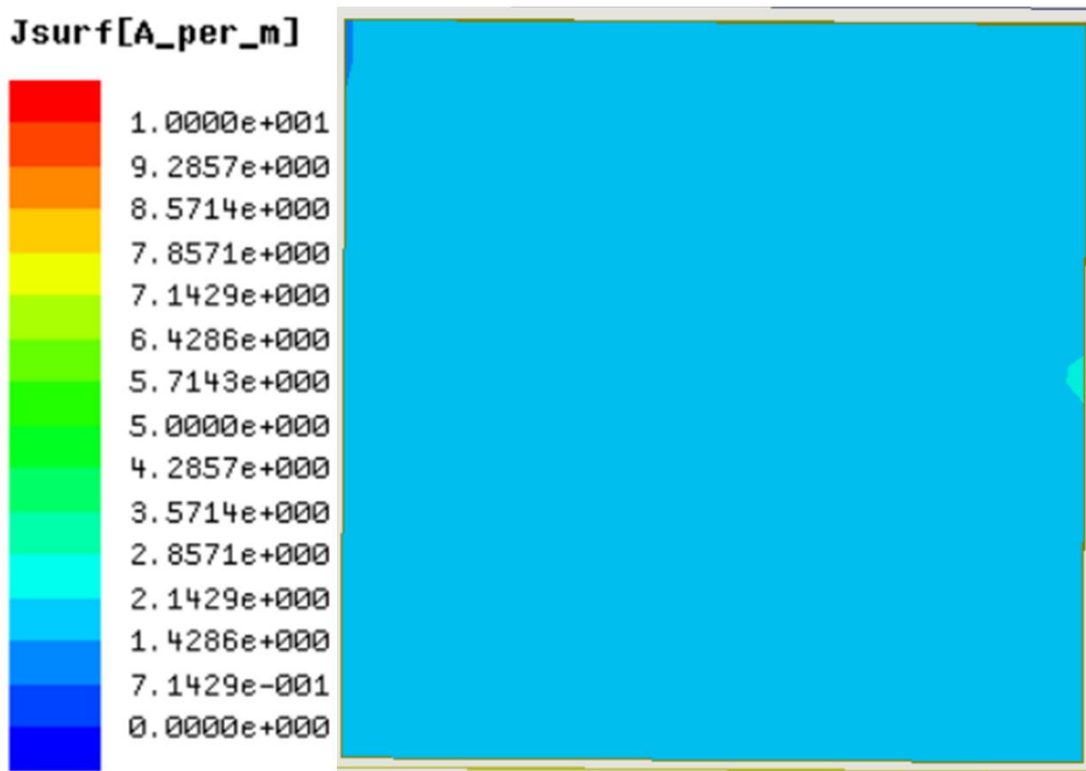
the gain to 3 dBi (with 2% bandwidth), has applied a new approach of using an air-AMC composite substrate on the RMA design in previous chapter. However, despite all these attempts, it is challenging for such antenna designs to operate in more than one frequency band with higher bandwidth; as a consequence, it lacks the diversity requirement for the WUSN or WIOT applications, which may need to operate on two frequencies depending on the circumstances of the subterranean soil. Furthermore, all the earlier designs have failed to improve the bandwidth of the RMA by up to 10%.

To alleviate the lacunae of earlier attempts, a relatively new approach is taken up in the present investigation. Here, instead of applying the classical RMA design that supports the TM_{10} mode, an AMC-integrated RMA design is proposed to support the TE mode instead of the transverse magnetic (TM) mode. The dominant mode of the proposed AMC-integrated RMA (referred to as TE-RMA) is TE_{10} mode. As such, the TE-RMA is hardly explored, and only two reports have been found in the open literature [174]-[175]. The possibility of TE mode excitation in RMA has been shown in [174]. Following [174], a proper realization of TE RMA has been documented in [175]. However, in [175], TE RMA has been designed and its characteristics have been verified based on duality. Further, the structure is single band (6% bandwidth) with lower gain than classical patch. Therefore, a more extensive investigation on such TE-RMA design is imminent to identify its advantages over classical RMA design. In the present work novel dual wideband TE-RMA design with good gain characteristics is investigated to achieve good positive gain along with dual wideband operations (of >10%) working in the wireless underground communication band and also in other cognitive radio, WUSN, or WIOT frequencies.

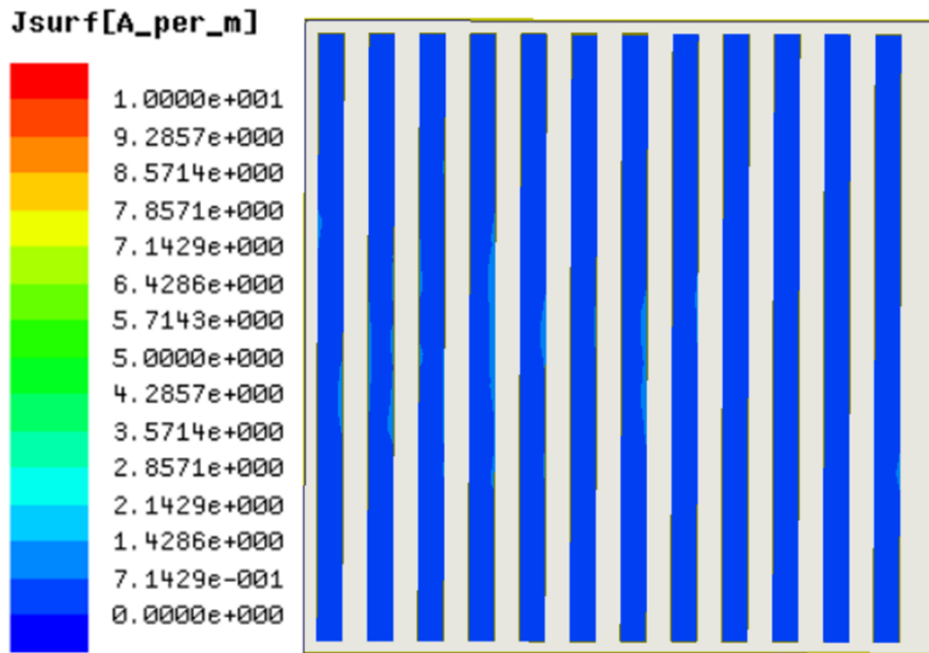
5.2 AMC for possible multiband resonance

Three cases are investigated, namely, zero strip (full metallic patch of size 48 mm \times 48 mm), 5 strips (size of each strip is 48 mm \times 10 mm), and 12 strips (size of each strip is 48 mm \times 2 mm). By further observing the simulated electric surface current magnitude in Figs.5.1(a) and Fig.5. 1(b), one can see that the surface of the final AMC unit cell design with 12 strips compared with a simple square metallic AMC unit cell with zero strip becomes more magnetic. It is evident with near zero electric surface

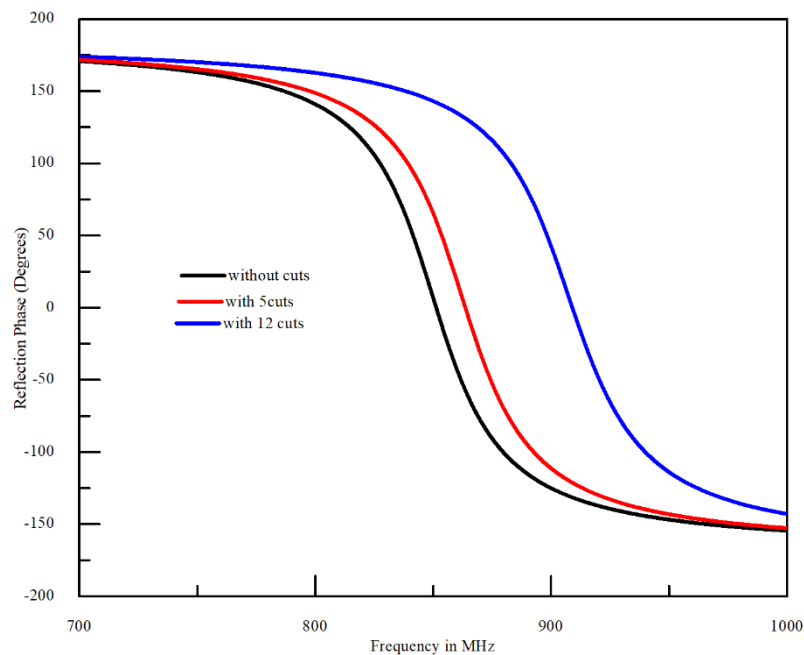
current for 12 strips (deep blue) compared to that of simple metallic AMC (less blue) in the Fig 5.1 (a) and 5.1 (b). The reflection phase characteristics of the AMC unit cell (or metallic patch) with different strip numbers are shown in Fig. 5.1 (c). In this figure, besides revealing that the AMC is resonating near 800–900 MHz, as the strip number increased from zero to 12, the bandwidth of the AMC unit cell is slightly enhanced from 4% to 7.7%, and the frequency (at zero degrees reflection phase) is shifted to near 900 MHz.



(a)



(b)

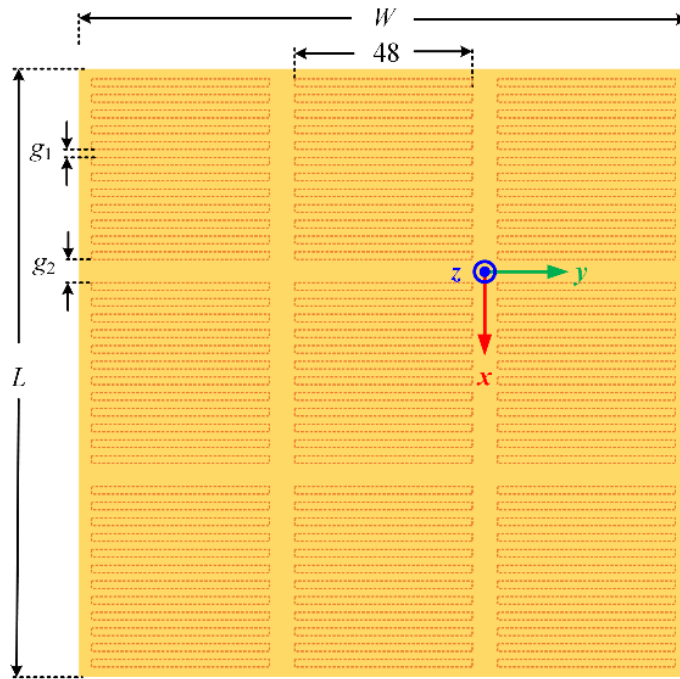


(c)

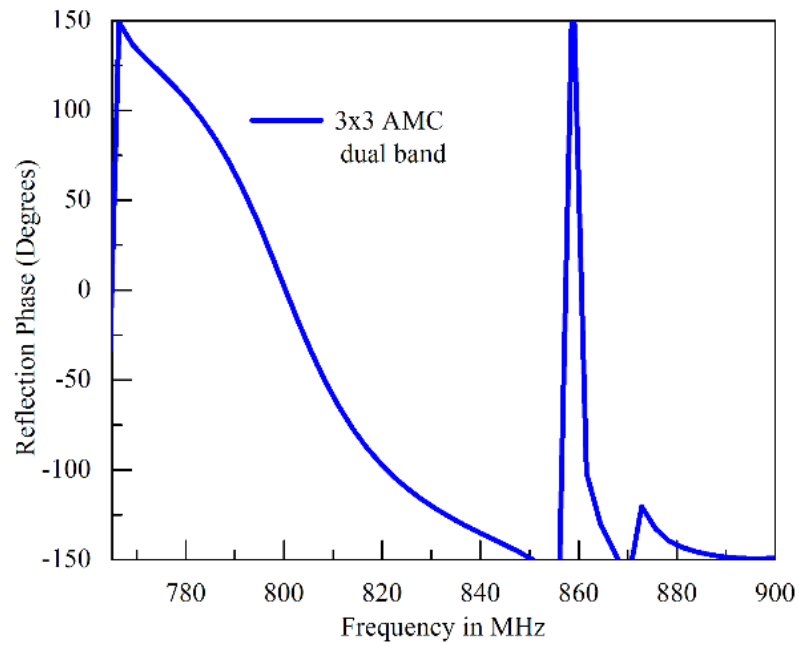
Fig. 5.1 (a) Magnitude of electric surface current on simple square metallic AMC unit cell with zero strip, and (b) Magnitude of electric surface current on proposed AMC unit cell with 12 strips (c) Reflections phase characteristics of AMC unit cells with different strips (zero, 5, and 12)

Interestingly, due to the dual periodic nature due to intercell and intracell spacings which is discussed in the next section, the reflection phase characteristics of the array structure (with a unit cell of 12 strips) may evolve the possibility of exciting two

resonances. As depicted in Figs.5.2(a) and Fig.5. 2(b), the 3×3 AMC array (with a unit cell of 12 strips) has dual resonances at 800 MHz and 860 MHz. This 3×3 AMC array is used as patch for the proposed antenna. This forms a patch of $150 \text{ mm} \times 150 \text{ mm}$.



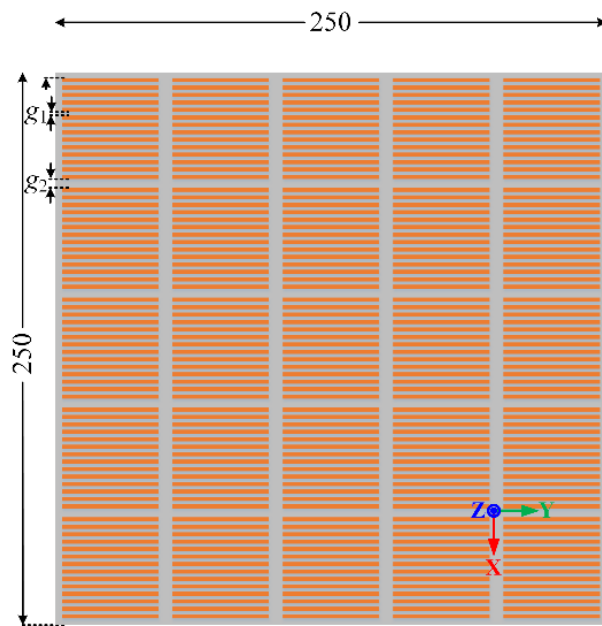
(a)



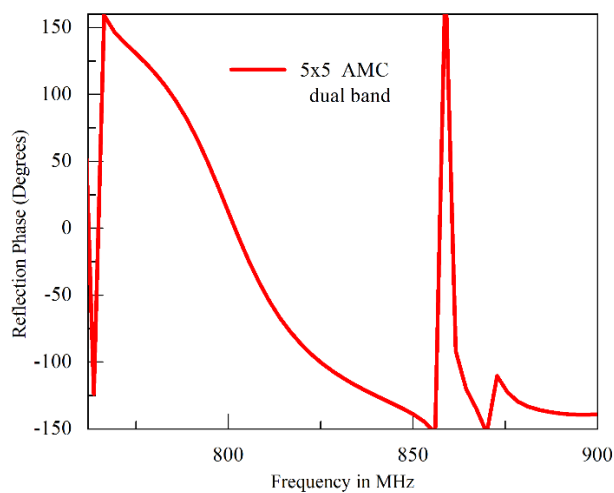
(b)

Fig. 5.2 A 3×3 AMC patch (a) Top view (b) Reflections phase characteristics

The ground plane is formed with a 5×5 AMC array with a size of $250 \text{ mm} \times 250 \text{ mm}$. The ground plane size is selected optimally to suffice the patch dimensions and to obtain better antenna performance. The top view of proposed 5×5 AMC ground and its reflection is shown in Fig.5.3 (a) and Fig 5.3 (b) respectively. It can be observed from this figures that the 5×5 Array ground also possess similar dual periodic property as that of the patch.



(a)



(b)

Fig. 5.3 A 5×5 AMC ground (a) Top view (b) Reflections phase characteristics

5.3 Antenna structure

The proposed TE antenna structure shown in Fig.5.4 mainly composed of three different sections, namely, AMC radiating patch, AMC ground plane, and an L -shaped feeding probe (or L -probe). The AMC radiating patch is 3-dimensional structure consisting of top metal sheet (0.5 mm thickness), alumina substrate (with a substrate thickness of $h_{AMC} = 3.2$ mm, and dielectric constant of $\epsilon_r = 10.2$), and array of 3×3 unit cells of metal-dielectric repeating structure. The planar dimension of AMC radiating patch is a $0.5 \lambda_g$, 150 mm (L) \times 150 mm (W). Here, each array element of this 3×3 AMC has a size of 48 mm \times 48 mm, so as to resonate at around 850 MHz. By further observing the unit cells of AMC specifically, the metal dielectric repeating surface, it comprises of 12 copper strips (each with length 48 mm and width $w_s = 2$ mm) with intra-cell strip-to-strip gap of $g_1 = 2$ mm, and the inter-cell gap of $g_2 = 4$ mm. The main reason for such design (with gap g_1 and g_2) and array arrangement is to attain wider operational bandwidth and dual-band operation. In addition, it enhances the magnetic property of AMC, which will be discussed in the next section. It may be noted that, with the final AMC unit cell of 12 strips, its corresponding array structure will give rise to a dual periodic nature due to (a) cell periodicity (where, gap g_2 between unit cells is $0.012 \lambda_0$) and (b) intra-cell periodicity (where, gap g_1 between the strips is $0.006 \lambda_0$). By further observing Fig.5.1, the AMC ground plane has a planar size of 250 mm \times 250 mm. It is also 3-dimensional structure like radiating patch as discussed above with 5×5 AMC array. To firmly attach the AMC radiating patch right in the middle above the AMC ground plane with an air substrate height of $h_{AIR} = 30$ mm (approximately $0.07 \lambda_0$), four dielectric strips (alumina substrate) with height $h_s = 34.2$ mm and a cross-sectional area of $S_w \times S_L$ (5 mm \times 3.2 mm) are applied to the four corners of the AMC radiating patch. Besides attaining structural rigidity, incorporating the four dielectric strips can also aid in achieving better impedance matching and higher gain. Finally, to excite the proposed antenna with good impedance matching, an L -shaped feeding probe is applied [176]-[177], in which this L -probe (of diameter $\emptyset = 1.25$ mm) is optimally positioned (offset from center) with a vertical height (L_v) of 28.3 mm and horizontal length (L_h) of 44.3 mm. Notably the horizontal section of this

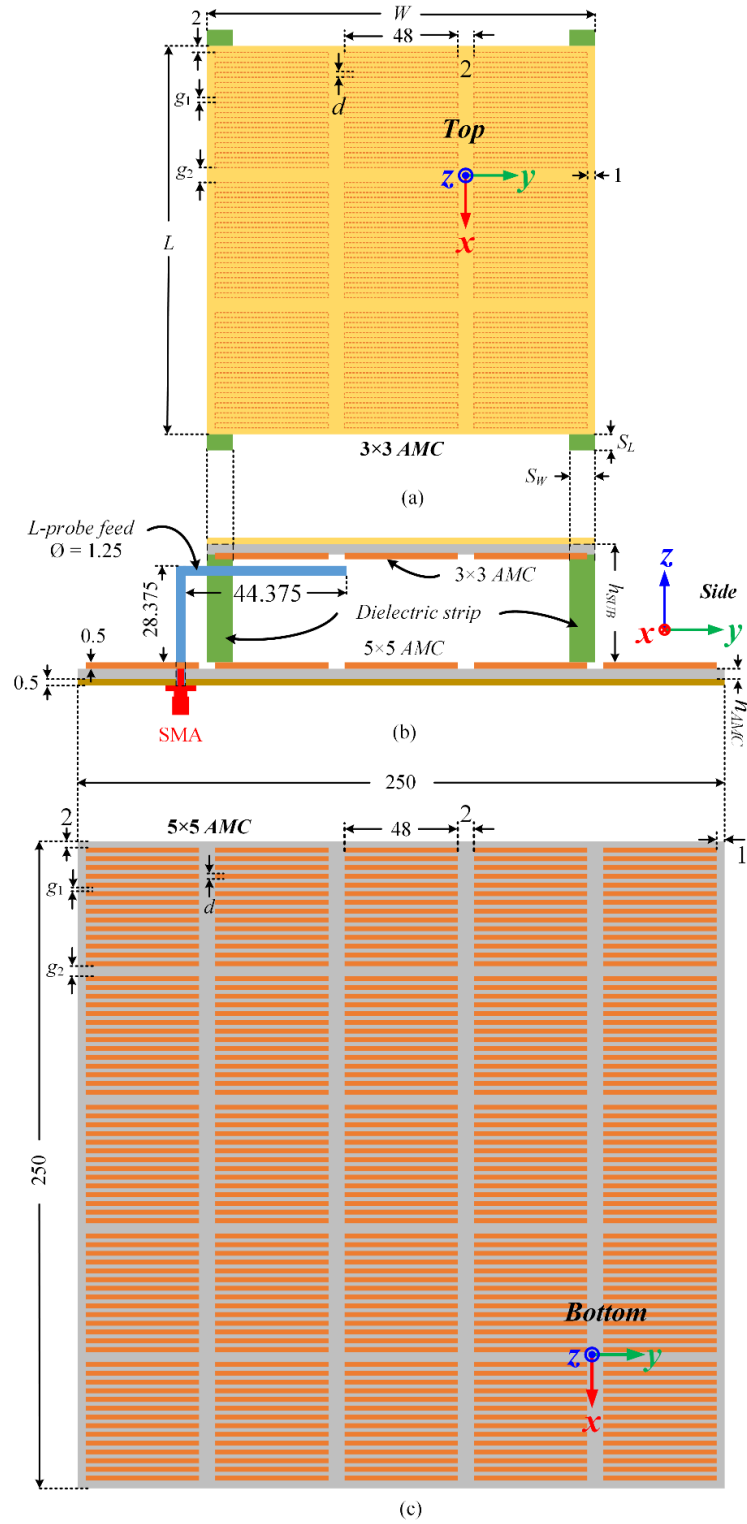


Fig. 5.4. Schematic representation of proposed antenna. (a) Top view, (b) side view (c) Bottom view. $w_s = 2$, $g_1 = 2$, $g_2 = 4$, $h_{SUB} = 30$, $h_{AMC} = 3.2$, $S_W = 5$, $S_L = 3.2$, $L_v = 28.3$, $L_h = 44.3$, $W = 150$, $L = 150$. Unit: mm.

L -probe (aligned along the y -axis) is to combine the radiation modes of both the AMC patch and L -probe.

5.4 AMC Integrated Antenna

A classical RMA with TM mode excitation is a lossy cavity resonator with PEC top and bottom walls and PMC side walls. In contrast, a TE patch is created by making the ground and patch PMC material, which makes the side walls PEC. This TE patch supports TE modes instead of TM modes, as is the case with a classical patch. The TE patch is the dual of the TM patch, and the field equations can be obtained using the duality theorem. The TE patch has more losses than the TM patch due to the use of AMC, but it has a wider bandwidth and lower directive gain. The dominant mode of the TE patch is TE_{10} mode, where the magnetic fields are vertical between the AMC patch and ground, while the electric fields form loops around the magnetic fields. The electric fields are entirely transverse to the z -direction, resulting in TE^z mode excitation. The magnetic fields oscillate back and forth along the patch length, and the radiation fields can be calculated using the electric current $\bar{J}_s = \hat{n} \times \bar{H}$ at the radiating slot aperture where \bar{J}_s is the surface current, \hat{n} is unit vector normal to the surface and \bar{H} is the magnetic field.

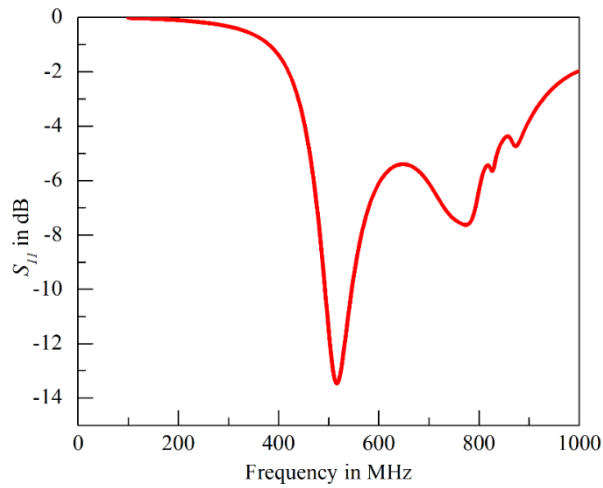
5.4.1 Frequency Impact of AMC Integrated Antenna

When an artificial magnetic conductor (AMC) is integrated with a patch antenna, the wavelength of operation becomes $\lambda_0 / \sqrt{\epsilon_r \mu_r}$ instead of $\lambda_0 / \sqrt{\epsilon_r}$. This is because the AMC patch is closer to the AMC ground, which creates a region of high magnetic field between them. This region resonates at a particular frequency, and at this frequency, the air within the patch cavity becomes weakly paramagnetic, with a permeability $\mu_r \geq 1$. As a result, the antenna patch becomes electrically larger in size, which reduces the overall frequency of the AMC-integrated antenna. The proposed AMC array design can excite two resonances at approximately 800 MHz and 860 MHz. When this AMC array is integrated with a patch antenna, the operating frequency may shift (or detune). The influence of the AMC resonance due to the patch cavity where patch cavity makes the AMC resonant at that frequency has been

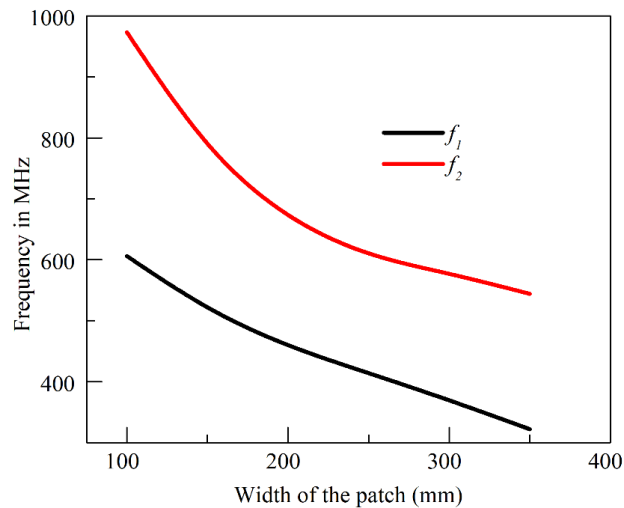
elaborated in previous chapter. As a result, the dual-band properties of the stand-alone AMC are shifted to the lower spectrum.

5.4.2 Evolution of Dual Band

A TE-RMA is constructed with dual periodic AMC patch and ground plane of size of $150 \text{ mm} \times 150 \text{ mm}$ and $250 \text{ mm} \times 250 \text{ mm}$ respectively with air substrate of height 30 mm. This dual band AMC is used to design the TE patch, top and bottom boundaries of patch cavity resemble magnetic properties at two frequencies.



(a)



(b)

Fig.5.5. (a) Reflection coefficient (S_{11}) profile of the AMC integrated TE patch. (b) Resonant frequency variations of the AMC integrated TE patch as a function of the patch width W (from 100 mm to 350 mm), while parameter L is kept constant at 150 mm.

This can excite a frequency of $f_1 = 517$ MHz with a 10-dB impedance bandwidth of 10.4% (492–546 MHz). In addition to the frequency f_1 these TE-RMA has tendency to excite a second frequency at the $f_2 = 778$ MHz as depicted in the Fig. 5.5(a). It can be observed from the Fig 5.3(a) that these second frequency at $f_2 = 778$ MHz is excited but with undesirable impedance matching. Furthermore, this TE-RMA has been thoroughly examined for various Lengths (L) and widths (W) of the patch. Interestingly it is observed that the resonant frequency (f_r) not only depends on the Length but also width of the patch. This effect of width on resonant frequency variation is in fact, due to the loss of TE property outside the cavity. Here, it is interesting to realize that in every case, two bands are found and the ratio of f_2 to f_1 is rather stable at approximately 1.5. In fact, the lower frequency f_1 is excited due to the full patch width W and the higher frequency f_2 is due to the reduced patch width W_r . The variation of both the frequencies are studied as a function of the width W of the patch and is presented in Fig.5.5(b). The physical insight into the formation of two cavities with widths W and W_r is elaborately explained in the section 5.4.3

5.4.3 Evolution of dual width cavity

The present antenna has been designed in such a way that it germinates two cavities of different widths from a single patch and thereby evolving two frequencies f_1 and f_2 . As the frequency shifts from lower to higher spectrum AMC loses its properties. This perturbs the boundary walls of the resonant cavity. Therefore, with in the two resonances f_1 and f_2 the top and bottom walls of cavity are no longer PMC which consequently making the four side walls of cavity no longer a PEC.

These perturbed PEC side walls fluster the adjacent sections of top and bottom boundaries of the cavity with are along the width of cavity. The H field vector distribution along the surface of the 3×3 AMC at bottom side of AMC patch is depicted in Fig. 5.6 which elaborately corroborates the conjecture. It can be observed from the Fig.5.6 (a) that at the frequency $f_1 = 517$ MHz full cavity width (W) under the patch is acting as AMC whereas at frequency $f_2 = 778$ MHz as depicted in Fig 5.6(b) only fraction of width (W_r) of the cavity under the patch is acting as AMC. As explained earlier this introduces perturbation in the patch cavity.

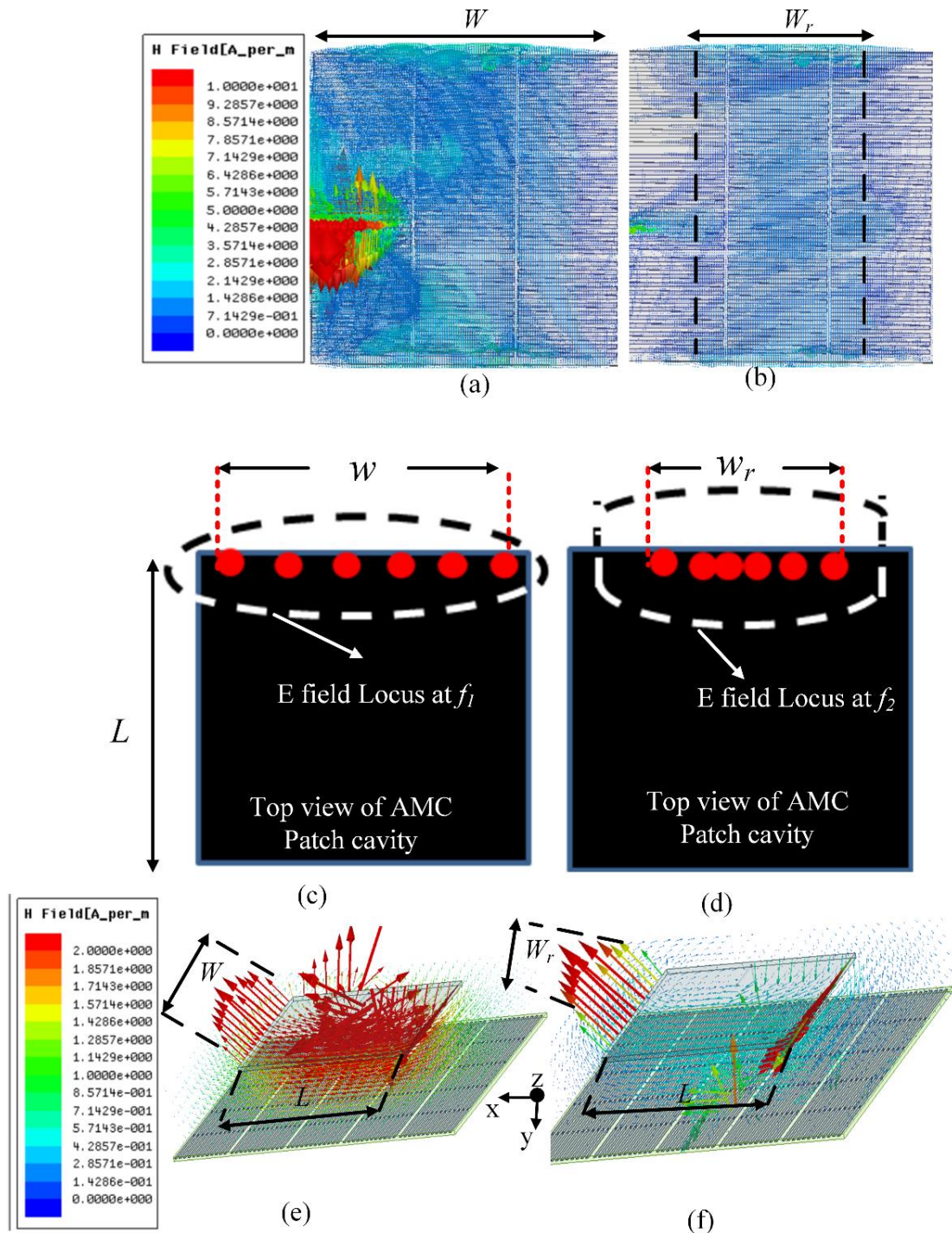


Fig.5. 6. (a) Approximately zero Magnetic field vector distribution on the entire 3×3 AMC surface at $f_1 = 517$ MHz, indicating the entire patch is having AMC properties. (b) Approximately zero Magnetic field vector distribution on the central section of the 3×3 AMC surface at $f_2 = 778$ MHz, indicating the central portion of the patch retains the AMC property. (c) Physical illustrations of upper radiating edge magnetic field vector at $f_1 = 517$ MHz, (d) same as (c) at $f_2 = 778$ MHz, (e) simulated fringing magnetic field vector at radiating edge at $f_1 = 517$ MHz, (f) same as (e) at $f_2 = 778$ MHz

This perturbation of cavity changes the boundary condition, which is manifested as a smaller Electric field loop as shown in Figs.5.6 (c) and 5.6(d). This makes central part of radiating edge densely populated with magnetic field components which are vertical between top-bottom PMC walls. It may be noted that,

$$\vec{\nabla} \cdot \vec{H} = \rho_m / \mu \quad (5.1)$$

$$\vec{\nabla} \times \vec{E} = \vec{M} + \mu \partial \vec{H} / \partial t \quad (5.2)$$

is valid only between two PMC walls. The conditions mentioned in equations (5.1) and (5.2) are maintained at the central section of the cavity, as depicted in Figs. 5.4 (e) and 5.4 (f). Hence, two cavities have been formed with $L \times W$ and $L \times W_r$, corresponds to two different frequencies f_1 and f_2 .

The resonance condition for a TE patch as indicated in [13] can be represented as

$$W = L/1.5 \quad \text{and} \quad L = 0.5\lambda_0 \quad (5.3)$$

The proposed TE-RMA is thoroughly investigated by keeping the length fixed at $L = 0.5 \lambda_0$, and varying the width W of the patch. The resonance frequency significantly changes as depicted in Fig.5. 5(b). Hence the resonant frequency as a function of width W can be approximated as

$$f_1 \cong \frac{c}{2W\sqrt{\epsilon_r\mu_r}} \quad (5.4)$$

Therefore, judicious selection of patch geometry plays a crucial role in the present antenna structure to yield dual-band operation. As the proposed antenna's geometry is square, it becomes advantageous to support dual-band characteristics. Here, low frequency resonance f_1 is excited due to $L = W = 0.5 \lambda_0$, and high frequency resonance f_2 is induced due to $W = L/1.5$, and can be denoted as

$$f_2 = \frac{c}{2(L/1.5)\sqrt{\epsilon_r\mu_r}} = 1.5 \frac{c}{2W\sqrt{\epsilon_r\mu_r}} = 1.5f_1 \quad (5.5)$$

These two resonances at $f_1 = 517$ MHz and $f_2 = 778$ MHz maintains the ratio of 1.5 which is confirmed from Fig. 5.5(b).

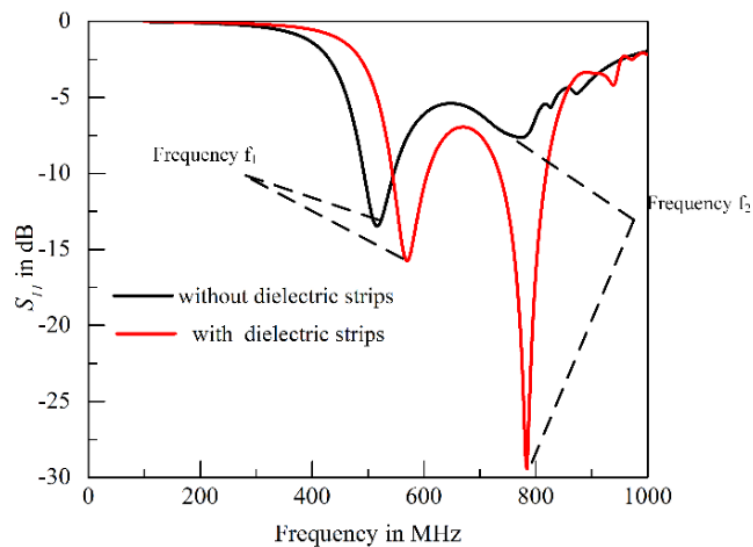
5.5 Dual Band Impedance Matching

In general Impedance matching in the case of TE antenna is a tedious task as it is made up of artificial magnetic ground and patch (AMC) instead of perfect magnetic

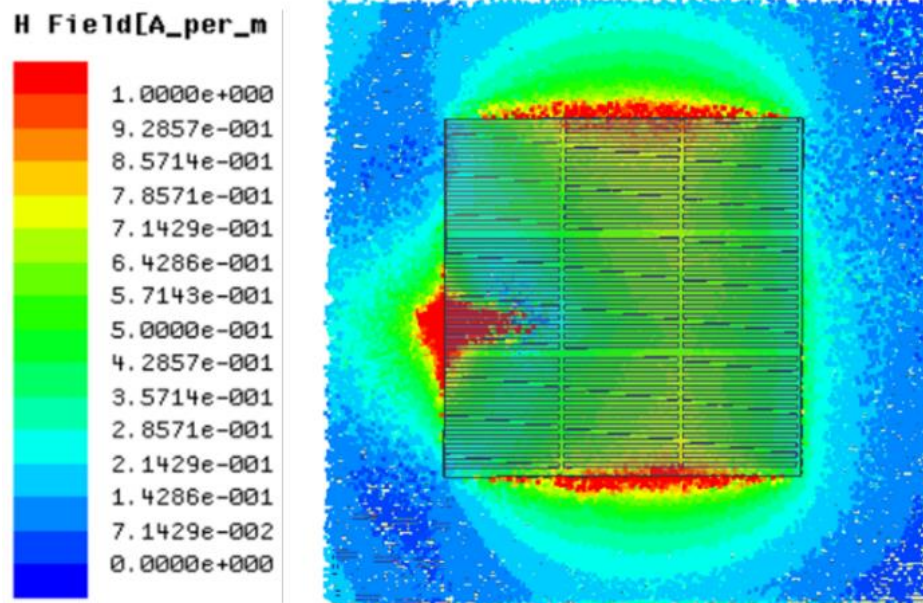
patch and ground (PMC). The impedance matching critically depends on the design of AMC structure and its periodicity that forms TE antenna. Furthermore, AMC design structures, its periodicity vary from one design to another. In conventional TM patch impedance matching can be obtained by offsetting the probe position along the length of the patch. This will not be applicable in the case of TE antenna for the aforementioned reasons in design of AMC.

In the present structure the of L-probe is judiciously adjusted longitudinally and laterally to attain the impedance matching at the lower frequency $f_1=517$ MHz. This position of L- probe is unable to provide impedance matching at the higher frequency $f_2 = 778$ MHz. This is observed from the S_{11} profile depicted in Fig. 5.5(a). This impedance mismatching is due to the fact that the capacitive effects near the L-probe feed enhances at $f_2 = 778$ MHz. This capacitive effect is compensated by careful modulation the magnetic fields in the cavity by placing four corner dielectric strips of alumina substrate $\epsilon_r = 10.2$ of height 30 mm with a cross-sectional area of $S_L \times S_W = 3.2 \text{ mm} \times 5 \text{ mm}$, as shown in Fig. 5.4. at the corners of the patch.

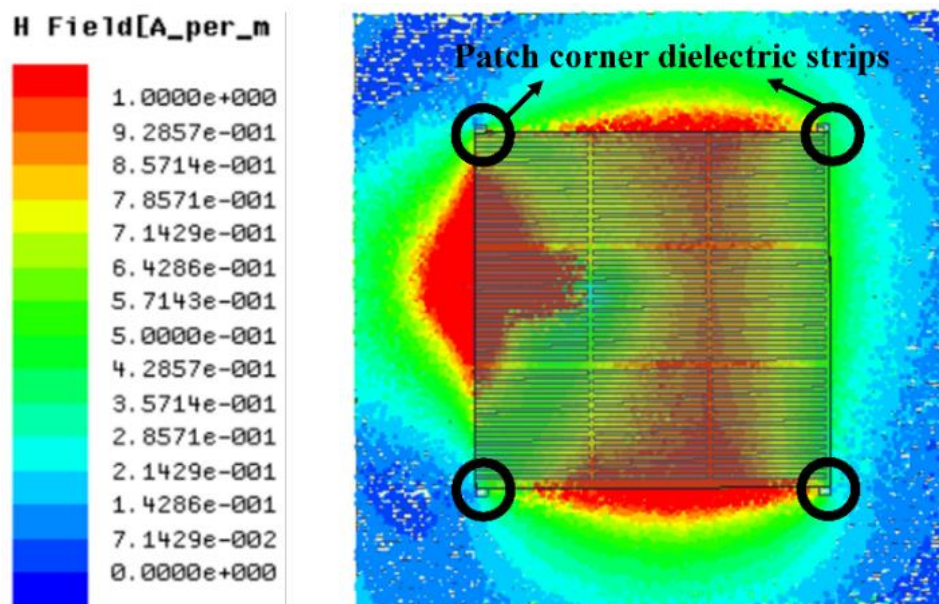
The simulated effects on the proposed TE-RMA, with and without four dielectric strips are depicted in Fig. 5.7. With the incorporation of corner dielectric strips, it is observed from Fig. 5.7(a) that the frequency f_1 is shifted from 517 MHz to 569 MHz and f_2 from 778 MHz to 782 MHz with good impedance matching. The shift in the frequency at higher frequency f_2 is slightly affected compared to that of frequency f_1 .



(a)



(b)

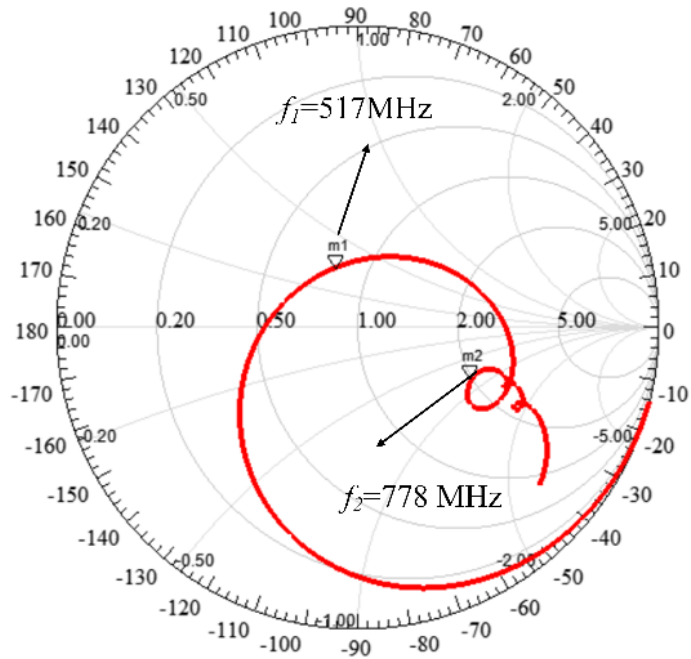


(c)

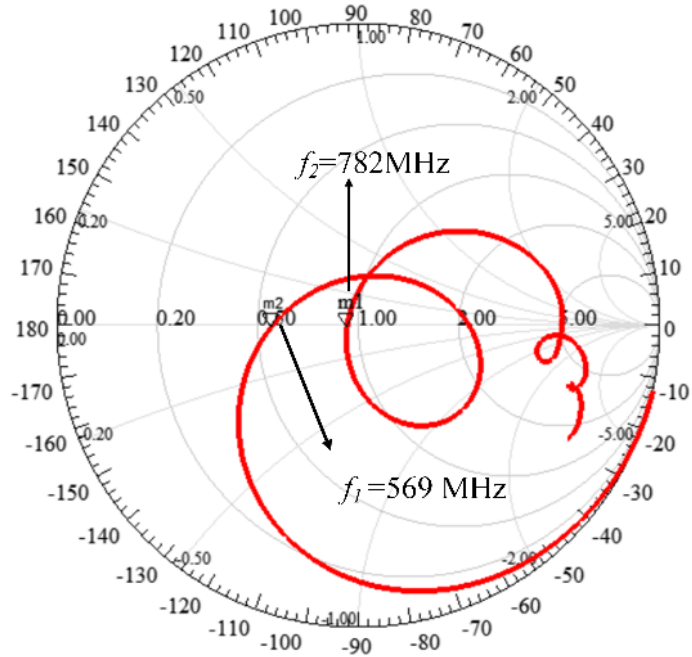
Fig. 5.7. Simulated results of the proposed TE-RMA with and without loading the four corner dielectric strips, (a) reflection coefficient, (b) magnetic-field (H-field) distribution under the 3×3 AMC patch cavity at higher frequency band (f_2) for TE-RMA without corner dielectric strips, (c) magnetic-field (H-field) distribution under the 3×3 AMC patch cavity Proposed TE-RMA with corner dielectric strips at higher frequency band (f_2).

The modulation of the electric field loop locus at higher frequency f_2 enhances with the loading of these four corner dielectric strips which is depicted in Figs.5.7(b) and 5.7(c). This pushes the H field towards the centre of patch cavity and hence field redistribution occurs. This in fact, enhances the magnetic energy near the L-probe feed

as is evident from Figs. 5.7(b) and (c) for the TE-RMA. To comprehend the above phenomenon smith charts with and without dielectric strips are plotted as shown in Figs. 5.8(a) and 5.8(b), respectively



(a)

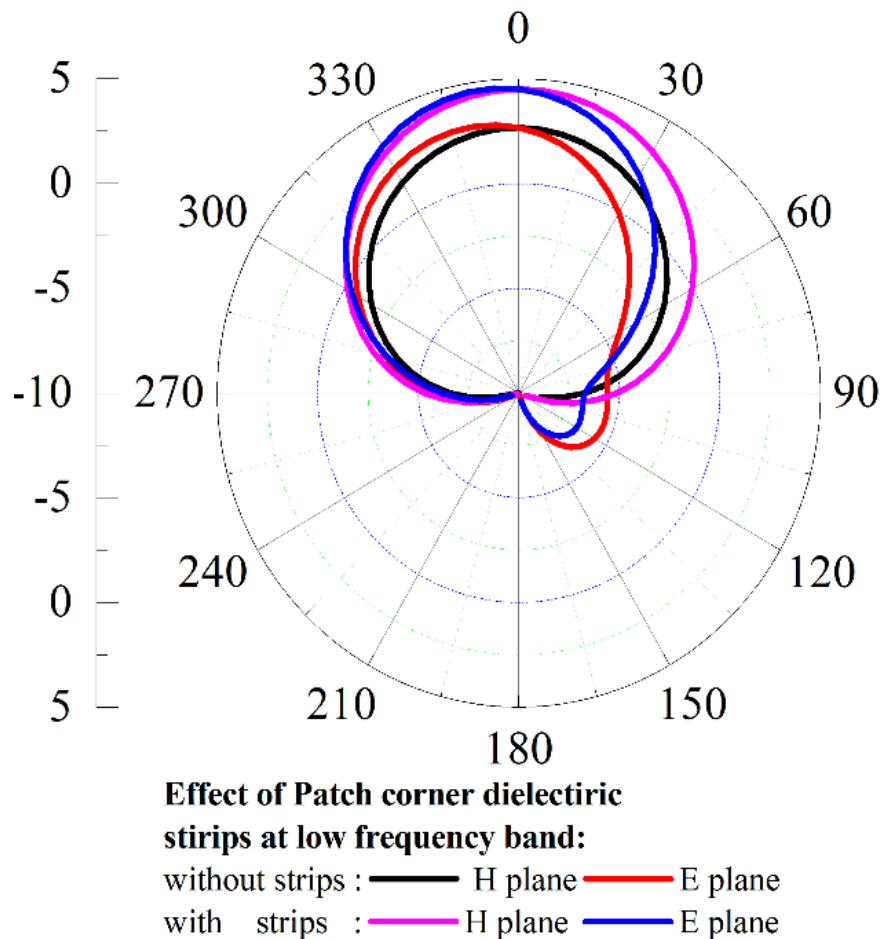


(b)

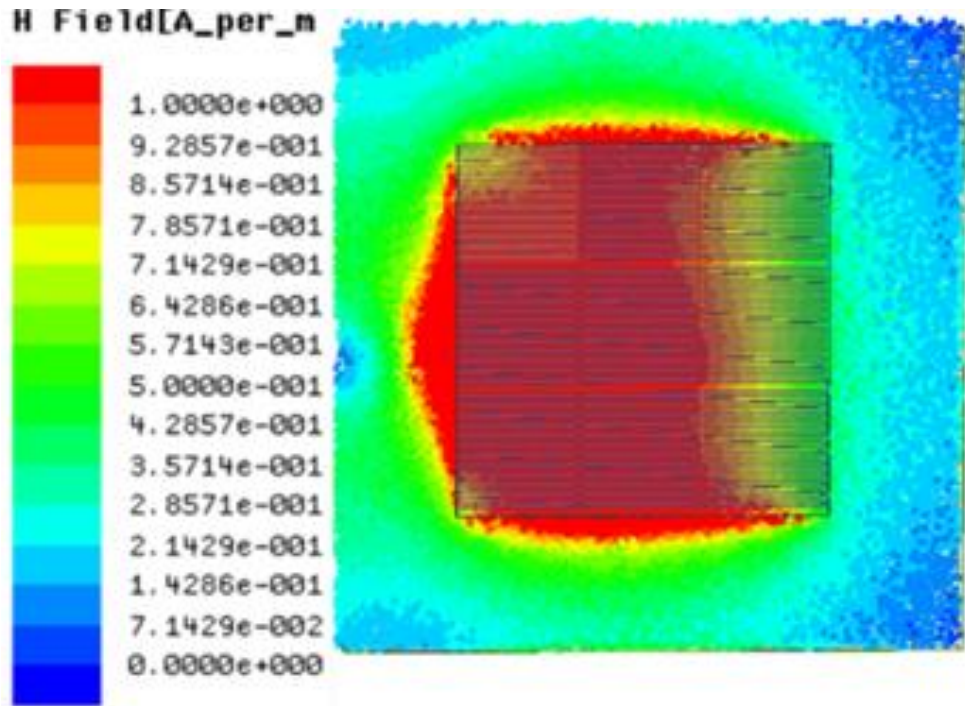
Fig. 5.8 Smith chart diagrams (a) without dielectric strips, and (b) with dielectric strips

5.6 Radiation Characteristics of TE RMA

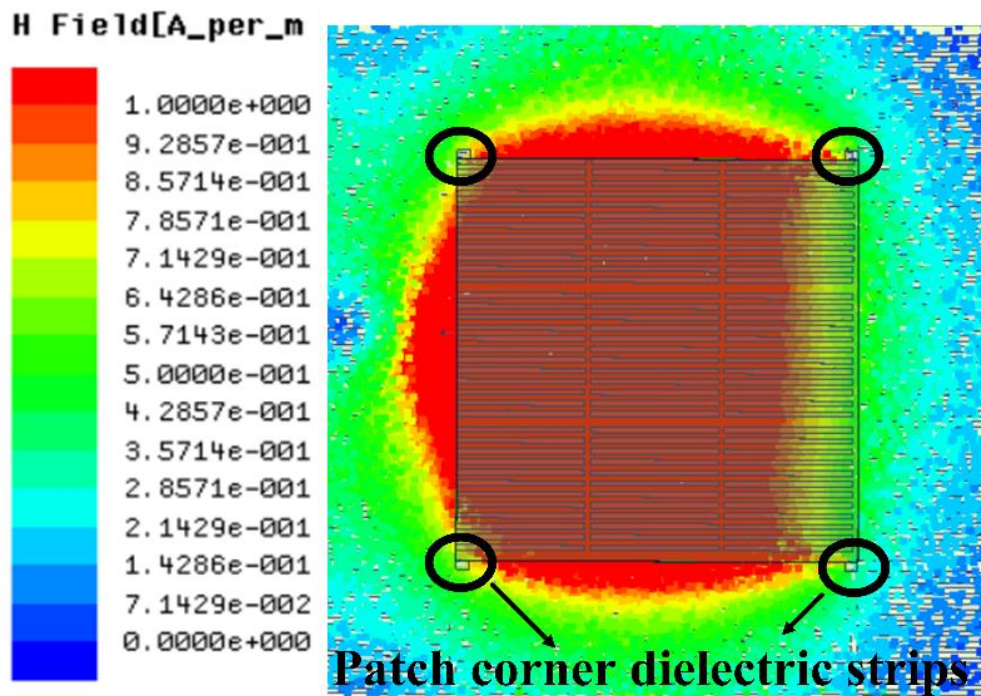
In this section the radiation characteristics of TE RMA with and without dielectric have thoroughly been studied. In both the cases, broadside radiations are observed at both the frequencies. However, it may be noted that, the gains for TE RMA without corner dielectric strips at $f_1= 517$ MHz and $f_2= 778$ MHz are 2.6 dBi and 4.8 dBi while the same for proposed TE RMA with corner dielectric strips are 4.5 dBi and 6.5 dBi at $f_{1p}= 569$ MHz and $f_{2p}= 782$ MHz respectively. As such, two-fold improvement is inferred with the incorporation of four corner dielectric strips. i.e. (i) Enhancement of impedance matching as well as gain improvement up to 6.5 dBi at higher frequency, (ii) Drastic improvement in antenna gains at lower frequency up to 4.5 dBi.



(a)



(b)



(c)

Fig. 5.9. Simulated results of the proposed TE-RMA at low frequency (f_1), (a) radiation patterns, with and without loading the four dielectric strips, (b) H-field distribution under the 3×3 AMC patch cavity without loading the four dielectric strips, (c) H-field distribution under the 3×3 AMC patch cavity with loading the four dielectric strips.

H-field magnitude at the substrate of TE RMA without and with dielectric strip is shown in Fig. 5.7(b) and (c) respectively. The modulation of the magnetic fringing field aperture at the patch's radiating edges due to the incorporation of corner dielectric strips causes an improvement in gain at both the frequencies. When we compare the magnetic fringing field aperture in the Fig 5.7(b) and Fig. 5.7(c) for high frequency and Fig 5.9(b) and Fig. 5.9(c) for low frequency, at both the frequencies for TE RMA with and without corner dielectric strips, the bulging of fringing fields at the radiating edges are observed and hence enhancing the fringing fields in the case of TE RMA with corner dielectric strips than in the case without corner dielectric strips. Notably, the inclusion of dielectric strips aids in higher frequency impedance matching too.

The simulated radiation patterns of the proposed TE-RMA with dielectric strips at the two frequencies $f_{1p} = 569$ MHz and $f_{2p} = 782$ MHz are exhibiting good broadside gain of 4.5 dBi and 6.5 dBi, respectively as depicted in the Fig.5.10.

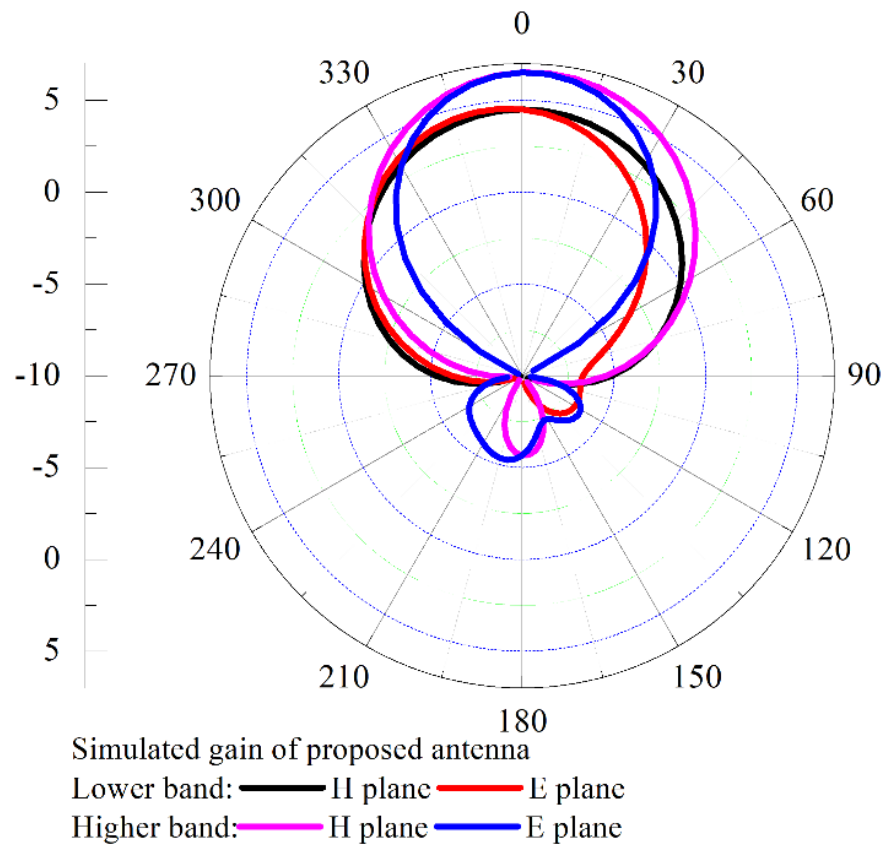


Fig. 5.10. Simulated radiation patterns of the proposed antenna (TE-RMA) at low frequency $f_{1p} = 569$ MHz and high frequency $f_{2p} = 782$ MHz

It is interesting to note that the resonance of magnetic field in case of present antenna happens along the x direction only at both the frequencies $f_{1p}= 569$ MHz and $f_{2p}= 782$ MHz. Therefore, the fringing H_x along with E_y produces power ($E_y \times H_x$) at broadside direction at both the frequencies. Hence, at both the frequencies the polarization is linear as there is no H_y component or E_x component accompanied with broad side radiation at both the frequencies. The resonating magnetic field along the length (x direction) as shown in Fig 5.6(e) and Fig. 5.6(f) confirm the linear polarization from the proposed structure at both the frequencies.

As discussed above, the radiation from the AMC radiating patch (of width W) at $f_{1p} = 569$ MHz is due to the fundamental TE-RMA resonance (or TE₁₀ mode). By further applying the duality theorem, the field pattern in E- and H-planes can be respectively computed from

$$E_{\theta|\phi=90} = 2 \left(\frac{2\pi W}{\lambda} \right) \cos \theta \frac{\sin\left(\frac{k_0 W}{2}\right) \sin \theta}{\left(\frac{k_0 W}{2}\right) \sin \theta} \quad (5.6)$$

$$E_{\phi|\phi=0} = 2 \left(\frac{2\pi W}{\lambda} \right) \cos \left(\frac{k_0 L}{2} \sin \theta \right) \frac{\sin\left(\frac{k_0 h}{2}\right) \sin \theta}{\left(\frac{k_0 h}{2}\right) \sin \theta} \quad (5.7)$$

For $f_{2p} = 782$ MHz, the 3×3 AMC patch cavity with reduced width W_r radiates as discussed above, and the contribution of the patch cavity radiation, in this case, can also be computed from equations (5.6) and (5.7), by substituting W with W_r . Notably, the two AMC structures namely, 3×3 AMC radiating patch (Top) and 5×5 AMC reflector (Bottom), will, in turn, creates images of the ‘‘horizontal section of the L-probe feed’’ (now denoted as ‘‘HSLP’’), which constitutes three elements in-phase non-equidistant array of the array factor

$$AF = 1 + e^{j\varphi} + e^{j\varphi_1} \quad (5.8)$$

were

$$\varphi = \frac{2\pi}{\lambda} d \cos \theta \quad \text{and} \quad \varphi_1 = \frac{2\pi}{\lambda} d_1 \cos \theta \quad (5.9)$$

Here, the parameter d is the image distance between the HSLP and the 3×3 AMC array, while parameter d_1 is the image distance between the HSLP and the 5×5 AMC reflector (bottom). It is noteworthy that the two aforementioned image distances ($d =$

0.005λ and $d_1 = 0.15 \lambda$) are difficult to project and draw; thus, they cannot be shown using appropriate diagrams or figures. Consequently, the magnitude of the three elements (HSLP, and its images on 3×3 and 5×5 array) in-phase non-equidistant array is denoted as

$$|AF| = \sqrt{(1 + \cos \varphi + \cos \varphi_1)^2 + (\sin \varphi + \sin \varphi_1)^2} \quad (5.10)$$

As the radiation field profile from a quarter-wavelength L-probe feed can be written as

$$E_\gamma = \frac{\cos\left(\frac{\pi}{2} \cos(\gamma)\right)}{\sin(\gamma)} \quad (5.11)$$

where,

$$\cos \gamma = \widehat{a}_y \cdot \widehat{a}_r = \sin \theta \sin \varphi \quad \text{and} \quad \sin \gamma = \sqrt{1 - \sin^2 \theta \sin^2 \varphi}$$

As the L-probe feed (with a ratio of $L_v/L_h = 0.63$) may be considered aligned along the y -axis direction [176], and it radiates in patch mode. Therefore, the pattern factors in the E- and H-planes can be obtained from equation (5.11) as

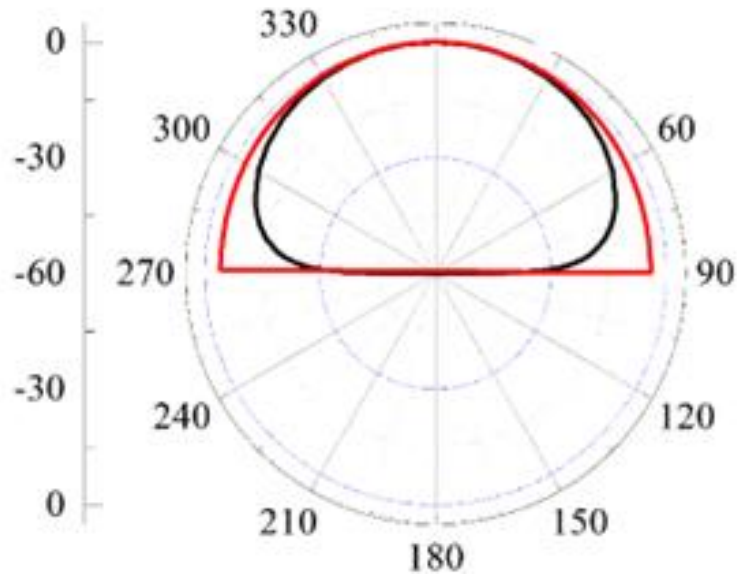
$$\left. \begin{aligned} [E_\gamma^{PL}]_{E \text{ Plane}} &= K \frac{\cos\left(\frac{\pi}{2} \cos \theta\right)}{\sqrt{1 - \sin^2 \theta}} \\ [E_\gamma^{PL}]_{H \text{ Plane}} &= K \end{aligned} \right\} \quad (5.12)$$

where K is the constant factor. Therefore, from equations (5.10) and (5.12), the contribution in radiation from the array can be written as

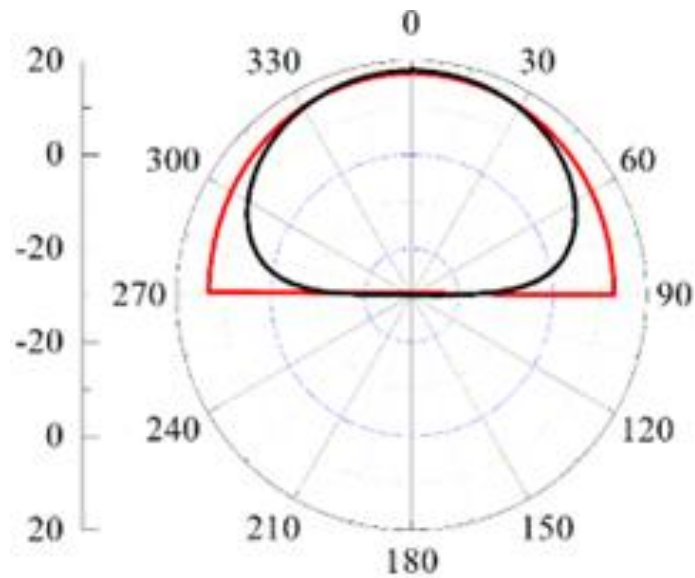
$$\left. \begin{aligned} [E_\gamma^{AL}]_{E \text{ Plane}} &= [E_\gamma^{PL}]_{E \text{ Plane}} \times |AF| \\ [E_\gamma^{AL}]_{H \text{ Plane}} &= [E_\gamma^{PL}]_{H \text{ Plane}} \times |AF| \end{aligned} \right\} \quad (5.13)$$

Now, the overall radiation profile (at $f_{2p} = 782$ MHz) due to the AMC radiating patch, L-probe feed, and its image (dissimilar sources) may be obtained from below

$$\begin{aligned}
 E_E &= [E_Y^{AL}]_{E\ Plane} + [E_{\theta|\phi=90}]_{W=W_r} \\
 E_H &= [E_Y^{AL}]_{H\ Plane} + [E_{\phi|\theta=0}]_{W=W_r}
 \end{aligned}
 \tag{5.14}$$



(a)



(b)

— E Plane — H Plane

Fig. 5.11. Computed radiation profile for E- and H-planes of the proposed antenna, (a) $f_{1p} = 569$ MHz, and (b) $f_{2p} = 782$ MHz.

Based on the above equations, the computed radiation profiles at broadside (upper hemisphere) for E- and H-planes at $f_{1p} = 569$ and $f_{2p} = 782$ MHz are depicted in Fig. 5.11. Unlike the classical patch, here, for the TE patch, the H-plane beam is broader than the one plotted in the E-plane, and it is valid for both the frequency band. It is very interesting to note that, at lower frequency, the L probe (L wire monopole) length $\approx 0.1\lambda_0$. In contrast, at higher frequency, the length of the same attains its proper resonant length i.e. $\approx 0.25\lambda_0$. Therefore, although unexcited, the higher frequency (2nd band) produces quite good gain of 4.8 dBi. Hence, radiation from HSLP at higher frequency should not be omitted. Now, besides patch, HSLP along with its images can contribute in broadside radiation and can give much higher gain than obtained at higher frequency. This is due to the screening of radiation field at the top metal layer of AMC patch. Hence comparatively lower gain of 6.3 dBi is achieved at higher frequency which is quite good for underground WUSN communication.

The effect of ground plane size on the radiation of the proposed antenna is also important. In general, the proposed TE RMA antenna produces wider H plane and narrower E plane pattern as is seen from Fig. 9 and also from [13]. It is observed that, as ground plane size increases, H plane and E plane beams become narrower and wider respectively and eventually attains symmetry while ground plane size is $\approx 0.8 \lambda_0 \times 0.8 \lambda_0$. The observation is similar as indicated in [179].

5.7 Results and Discussion

The pictures of the fabricated prototype of the proposed antenna are shown in Figs. 5.12(a) and 5.12(b). This prototype was used to measure its reflection coefficient (S_{11}) and radiation characteristics. The simulated and measured reflection coefficients of the proposed antenna are depicted in Fig. 5.13. In this figure, the measured dual resonances at f_1 (572 MHz) and f_2 (768 MHz) have demonstrated broad 10-dB bandwidths of 12.4% (543–615 MHz) and 12.7% (708–804 MHz), respectively. Both the simulation [147] and measurement results are in good agreement, and the slight discrepancy between the two results (especially for f_2) may be attributed to slight fabrication tolerance. Therefore, the practicality of applying the proposed TE patch for low frequency WUSN antenna is evident from Fig. 5.13.

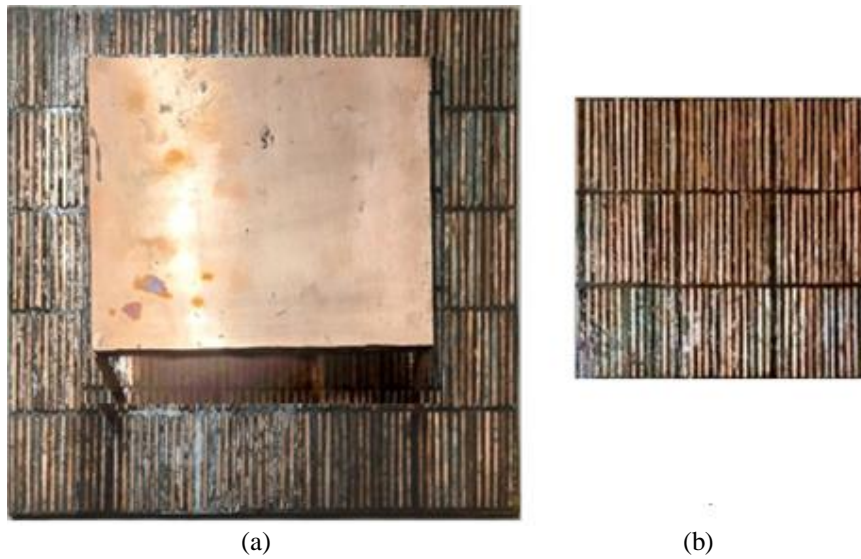


Fig. 5.12. Pictures of the fabricated prototype, (a) top view of proposed antenna, and (b) bottom view of 3×3 AMC (Top), revealing the 3×3 AMC patch structure.

The simulated and measured radiation patterns across the E- and H-planes for the two frequencies (f_{1p} and f_{2p}) are depicted in Figs. 5.14(a) to 5.14(d), and the two results (simulated and measured) have shown good validations.

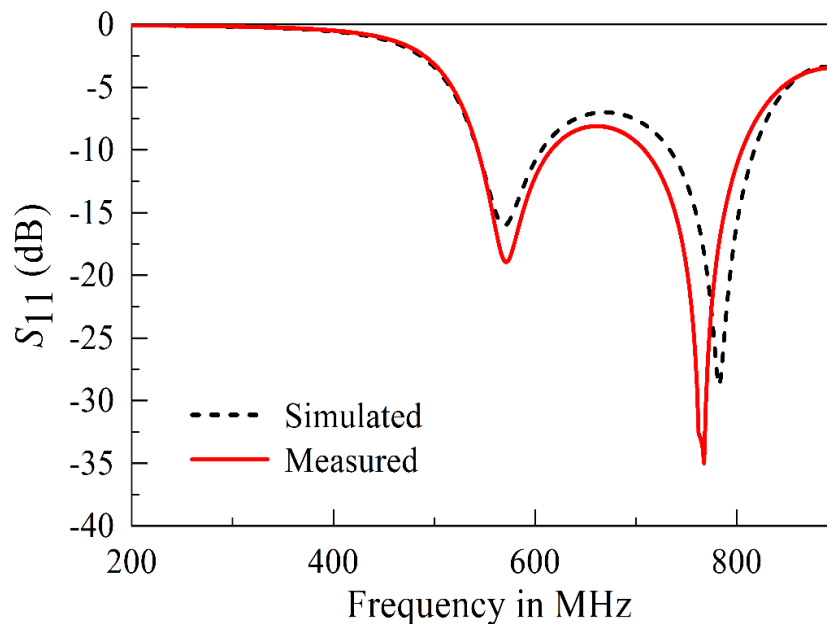
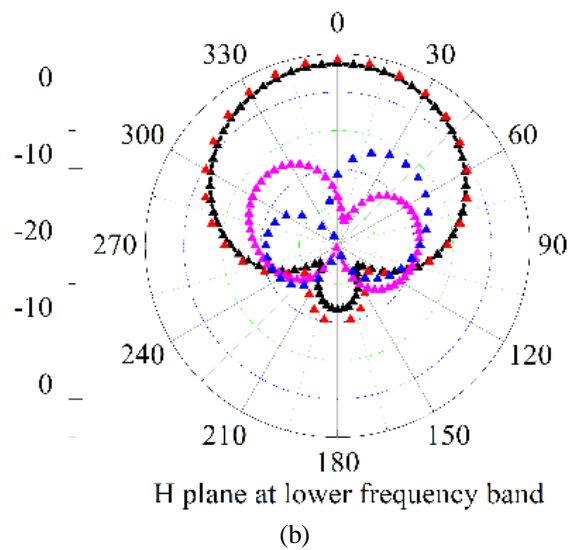
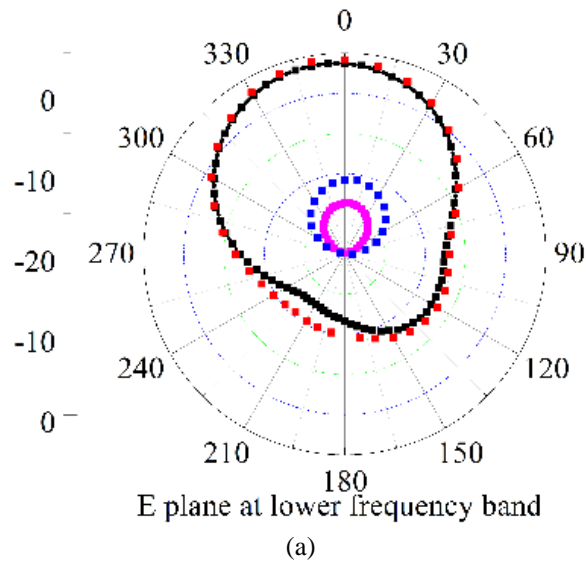
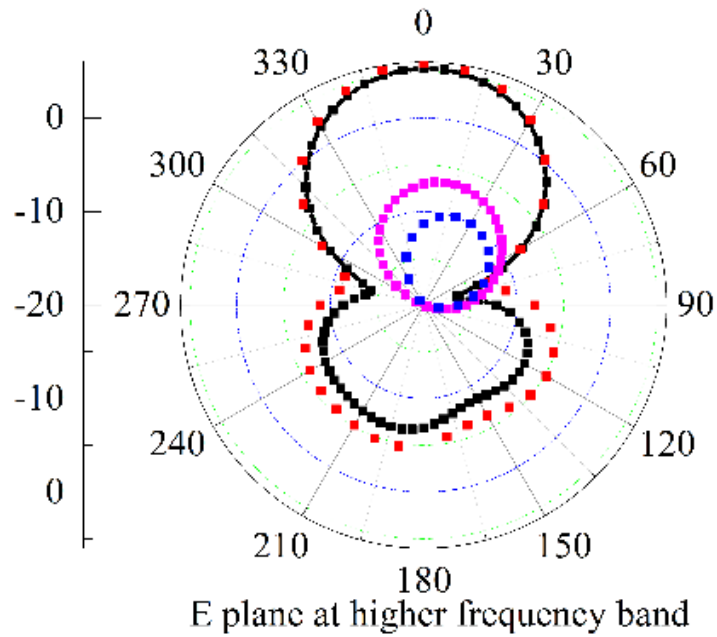


Fig. 5.13. Simulated and measured reflection coefficient (S_{11}) of the proposed antenna

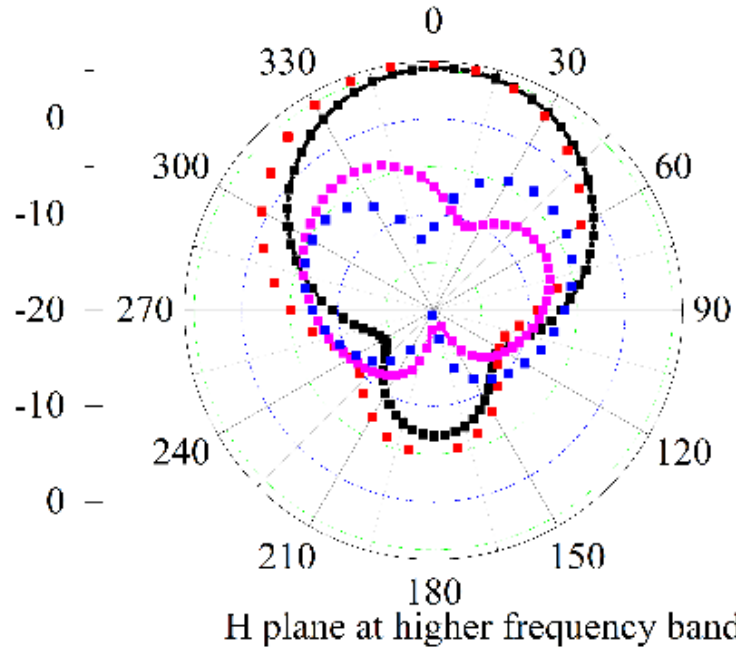
At both the frequency bands, one can see good positive gains (especially in the boresight direction) are achieved with wide H-plane and narrow E-plane beams, as is expected from duality. Here, desirable measured peak gains of 4.3 dBi and 6.1 dBi (with good boresight radiation) at 572 MHz and 768 MHz are observed. The measured

gain and efficiency of the proposed antenna as a function of frequency across the two operating bands are plotted in Figs. 5.15(a) and (b), respectively. In Fig. 5.15(a), it is noteworthy that the gain variation of the proposed antenna across the low frequency band (3.9–4.5 dBi) and high frequency band (5.2–6.3 dBi) is very small, with a variation of no more than 1 dB. As for its corresponding measured radiation efficiency, the efficiency variation across the low frequency band (68%–73%) and high frequency band (69%–78%) are also very small, with a variation of no more than 10%. Furthermore, the measured efficiency at f_1 (572 MHz) was approximately 71%, and the one at f_2 (768 MHz) was approximately 73%.





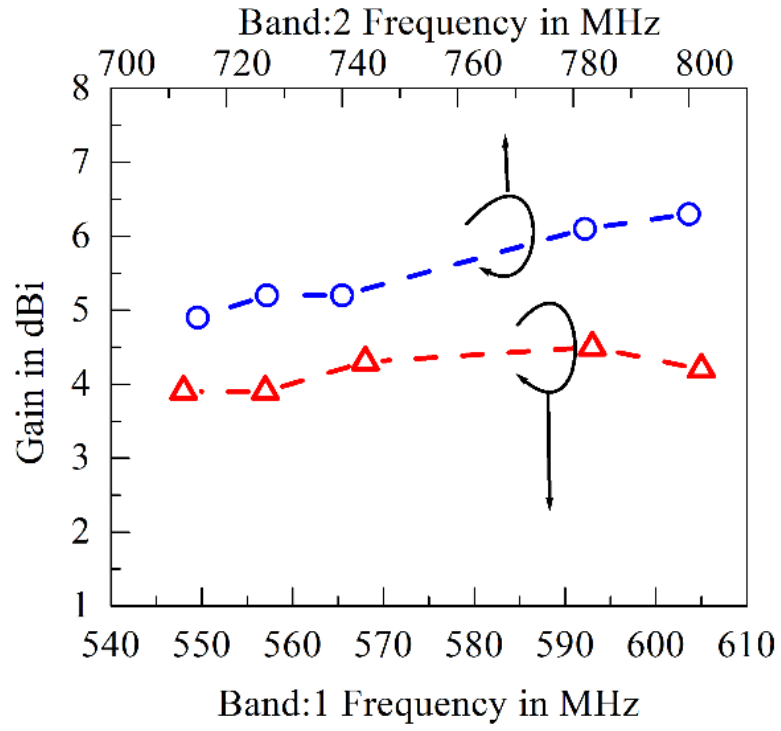
(c)



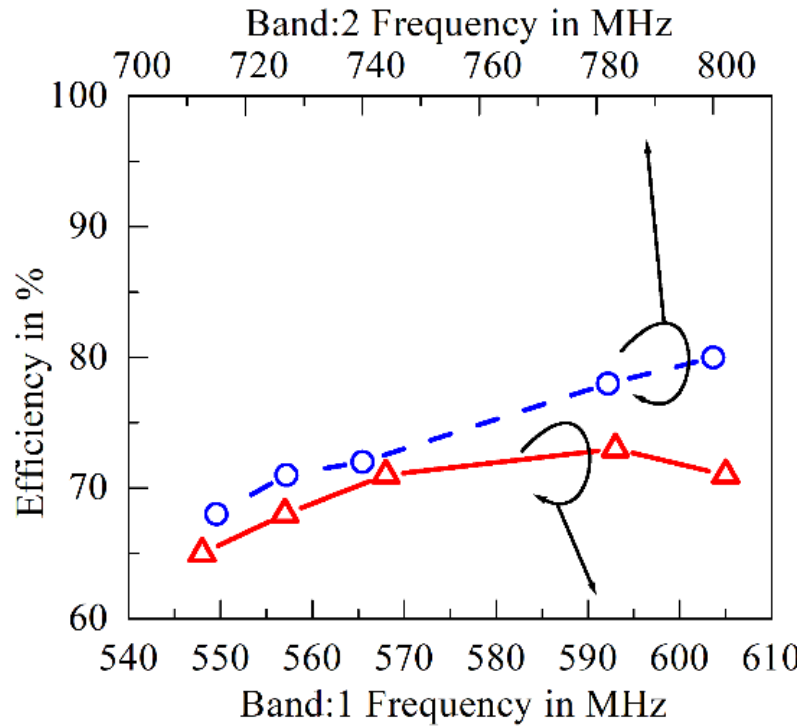
(d)

co pole : —▲— simulated —▲— measured
 cross pole: —▲— simulated —▲— measured

Fig. 5.14. Simulated and measured radiation patterns (co-pol and cross-pol) across the E- and H-planes, where the simulated $f_1 = 570$ MHz and $f_2 = 782$ MHz, and the measured $f_1 = 572$ MHz and $f_2 = 768$ MHz, (a) E-plane (f_1), (b) H-plane (f_1), (c) E-plane (f_2), and (d) H-plane (f_2).



(a)



(b)

Fig.5. 15. Variation of radiation performances of the proposed antenna across the two operating frequency bands (f_1 and f_2), (a) gain variation, and (b) efficiency variation.

These results confirm that the proposed antenna yields consistent good broadside radiations with good positive gain values and desirable efficiency.

The novelties of present TE-RMA design are listed as follows

➤ A dual-wideband TE-RMA configuration operating at a lower frequency band below 800 MHz for wireless underground communication is reported for the first time. Both operational bands achieve much higher gains than all previous designs for wireless underground communication, WUSN, or WIoT applications.

➤ A novel AMC design structure with dual periodicity is used to excite a second operating band (higher frequency band) in the present antenna structure.

➤ Efficient perturbation of the AMC radiating patch cavity walls is achieved by loading four dielectric strips at the four corners of the patch. This provides structural rigidity as well as better impedance matching at the high frequency band. Additionally, it can effectively modulate the fringing aperture, which in turn enhances the gain at the low frequency band.

➤ Credible modulation of the fringing field aperture is achieved with the compression of the magnetic field within the 3x3 AMC patch cavity. By concurrently applying the two proposed AMC structures, carefully positioning the four dielectric strips, and properly optimizing the L-probe feed, the antenna structure is versatile and efficient for low-frequency underground communication.

The reported works relevant to TE mode excited RMA is depicted in Table 5.1. The overall performance comparison of the present antenna with other reported structures usable for different low frequency wireless underground communication is presented in Table 5.2. Here, the structures operating between 500 MHz and 920 MHz are reported [148][171][178]. In [148], a compact Vivaldi antenna with a circular folded patch operates at 500 MHz for Ground Penetrating Radar (GPR) applications is proposed, but the peak gain is very low at -13 dBi. In [171], a CubeSat Antenna working at 435 MHz with a dipole-like radiation pattern is reported; however, besides showing a negative peak gain of -1 dBi, it has a very narrow bandwidth of 0.6%. A UHF RFID tag antenna (consisting of a parasitic patch and metal cavity) that can be embedded into a concrete floor is reported in [178].

Table 5.1
Comparison Of Existing Reports of TE-MA

Ref	Freq (MHz)	BW (%)	No. of Bands	L/W ratio	PG (dBi)	Remarks
[174]	4200	6.2	1	1.5	8.7	Use of single periodic AMC of complex structure to yield moderately higher gain and single wider band antenna following conventional design methodology of $L/W=1.5$. Primary analysis using duality is presented. Experimental validation for proof of concept is documented. [High frequency antenna: not compatible with underground communication]
[175]	4100	12	1	1.3	8.5	Use of single periodic simple square AMC to yield high gain single wider band antenna based on simulation study. [High frequency antenna: not compatible with underground communication]
[179]	9800	6	1	1.5	6.2	Use of single periodic simple square AMC to yield single wider band antenna based on simulation study following conventional design methodology of $L/W=1.5$. [High frequency antenna: not compatible with underground communication]
PA	$f_1: 572$ $f_2: 768$	12.4 12.7	2	1	4.3 6.1	Use of dual periodic AMC with patch corner dielectric strips to yield dual wide banding with good gain and efficiency. Through and methodical analysis is presented which is validated through simulation and measurement. [Low frequency antenna: compatible for underground communication]

Even though it has yielded a positive peak gain of 3.6 dBi at 919 MHz, it has yielded narrow bandwidth of 0.6 % and a low antenna efficiency of 49%. In comparison, the proposed antenna has yielded two operating bands with broad bandwidths (larger than 12%) and good positive gains (larger than 4.5 dBi). Furthermore, the two operating bands demonstrate a high antenna efficiency of >70%. Therefore, the proposed antenna confirms its versatility of operation for WUSN /WIOT or other wireless underground low frequency communication.

Table 5.2

Performances Comparison of Proposed Antenna with Other Relevant Reports for Low Frequency Underground Communications

Ref	Size (λ_0) ³ ;	Frequency (MHz)	PG (dBi)	BW (%)	Eff. (%)
[150]	0.15×0.14×0.24,	900	-7	4.4	NA
[173]	0.12×0.06×0.005	450	2.5	2	69
Previous chapter Air-AMC (PA)	0.16×0.20×0.01	413	3.1	2	75
[148]	0.11×0.10×0.002	500	-13	2	NA
[171]	0.13×0.05×0.001	435	-1	0.6	55
[178]	Ø0.35×0.123	919	3.6	0.7	49
Proposed TE Antenna	0.33×0.33×0.007	f_1 : 572;	4.5	12.4	71
		f_2 : 768	6.3	12.7	73

5.8 Conclusion

A thorough, insightful investigation into a TE mode excited RMA has been successfully performed, and a new TE-RMA is proposed for dual wideband operation with high gain and efficiency. The AMC with dual periodicity embedded on patch and ground makes antenna operating at dual frequency and TE characteristics. The proposed antenna is constructed with two AMC array structures in both patch with 3x3 arrays and ground plane with 5x5 arrays; The patch is fed by an L-probe feed. The proposed antenna is simple to manufacture and exhibits versatility in terms of frequency. This antenna works well below 1 GHz frequency range with a good bandwidth and high gain characteristics. The proposed structure works at 572 MHz and 768 MHz with bandwidth of 12.4% and 12.7% respectively. The gain of antenna at 572 MHz and 768 MHz are 4.5 dBi and 6.3 dBi respectively. The high gain and larger bandwidth of proposed antenna at the two operating bands and its analysis will surely benefit the scientific community who are looking for low frequency applications.

CHAPTER

6

Conclusion and Scope for Future Studies

In this research work a detailed study on low frequency underground sensor network antennas are presented. The proposed antennas work in the range of (300 - 1000 MHz) frequency that suits well for underground propagation.

Initially simulation and experiments are conducted to determine the frequency range suitable for underground propagation. Simulation is conducted using two antenna model in Electromagnetic simulation software HFSS. The same has been verified by performing experiments in air medium and underground medium. The results depicts that low frequency is feasible for the underground Electromagnetic wave propagation for different condition of soil (different dielectric constant).

The size of conventional antenna size becomes voluminous at the low operating frequency in Mega Hertz ranges. A miniaturization technique using shorting vias is thoroughly analyzed. The effect on the operating frequency with change in number and position of shorting vias are observed and concluded. With this technique we can obtain miniaturized antenna.

To enhance the performance of the above miniaturized antenna a meta material called Artificial Magnetic Conductor (AMC) is embedded with the antenna. This AMC possess in phase reflection properties which enhance the gain if properly utilized. In this thesis AMC is utilized to make a composite substrate for the first time for the low frequency range. The antenna with air-AMC composite substrate has been designed, analyzed, fabricated and measured. This antenna is first of its kind to make use of AMC as composite substrate and producing overall gain of 3.1 dBi at frequency of 413 MHz.

A novel design of dual band Transverse Electric (TE) mode excited square patch antenna is designed. The dual band is obtained with incorporation of a dual periodic AMC design. The usage of dual periodic AMC array for attaining dual band frequency operation at the frequency below 1000 MHz is the first work to be reported as far as the authors' knowledge. A 3×3 AMC array is used to form a patch of size $150 \text{ mm} \times 150 \text{ mm}$ and 5×5 array to form a ground plane of $250 \text{ mm} \times 250 \text{ mm}$ for the proposed TE antenna. This proposed TE antenna is judiciously designed to modulate the fringing fields to obtain the impedance matching, gain and radiation characteristics. This is achieved by incorporating four corner dielectric strips. The proposed structure works at 572 MHz and 768 MHz with bandwidths of 12.4% and 12.7% respectively. The gain of the antenna at 572 MHz and 768 MHz are 4.5 dBi and 6.3 dBi respectively. The high gain and larger bandwidth of the proposed antenna at the two operating bands and its analysis will surely benefit the scientific community who are looking for low frequency applications.

In future, the Low frequency planar antenna can be further exploited as it is a relatively new field of research in the antenna domain. Low frequency antennas are useful in many applications such as agriculture, landmine detection, defence and underwater. The scope of these antennas can be further extended to other fields such as space and satellite applications for exploration of surface properties of the Moon, Mars etc. The design aspects can be further explored for making the antennas more compact and higher gain.

Other metamaterials can be embedded to enhance the antenna characteristics. Specifically, use of metamaterial as composite substrate has a lot of scope for further exploration. AMC with different shapes such as circle, triangle can be further explored to exploit its advantages in antenna performance. The effects of AMC on other shapes of patch antennas can be investigated in future. The design of Transverse Electric (TE) patch antennas is very interesting and it is seldom explored. The antenna community may explore new structures of AMC in patch and ground plane for new designs of TE patch antennas. The possibility of Multiband antennas may be explored with different periodic structures of AMC to meet the multiple applications in versatile soil conditions.

References:

- [1] D. D. Greig and H. F. Engleman, "Microstrip—a new transmission technology for the kilomegacycle range," *Proc. IRE*, vol. 40, pp. 1644-1650, 1952.
- [2] G. A. Deschamps, "Microstrip Microwave Antennas", *3rd USAF Symposium on Antennas*, 1953.
- [3] H. Gutton, and G. Baissinot, "Flat Aerial for Ultra High Frequencies", French Patent No. 703113, 1955.
- [4] E. G. Fubini, "Stripline radiators," *IRE Transac. on Microwave Theory and Tech.*, vol.3, no. 2, pp. 149-156, 1955
- [5] J.A. McDonough, R. G. Malech, and J. Kowalsky, "Recent developments in the study of printed antennas," *IRE Int. Conv. Rec.*, pp. 173-176, New York, 1957.
- [6] L. Lewin, "Radiation from discontinuities in strip lines," *Proc. IEE-Part C*, vol. 107, no. 12, pp 163-170, 1960.
- [7] E. J. Denlinger, "radiation from microstrip resonators," *IEEE Transac. on Microwave Theory and Tech.*, vol.17, no. 4, pp. 235-236, 1969.
- [8] E.V. Byron, "A new flush mounted antenna element for phased array applications", *Proc. Phased Array Antenna Symp.*, pp.187-192, 1970.
- [9] J. Q. Howell, "Microstrip antennas," *Dig. IEEE Int. Symp. Antennas Propagat.*, pp.177-180, Dec. 1972.
- [10] H. D Weinschel, "Progress report on development of microstrip cylindrical arrays for sounding rockets", *Phys. & Sci. Lab.*, New Mexico State Univ., Las Cruces, 1973.
- [11] G. G Sanford, "Conformal microstrip phased array for aircraft tests with ATS-6", *Proc. Nat. Electronic Conf.*, vol.29, pp. 252-257, 1974.
- [12] R. E. Munson, "Conformal microstrip antennas and microstrip phased arrays," *IEEE Trans. Antennas Propagat.*, Vol. 22, pp. 74-78, 1974.
- [13] R. E. Munson, "Dual slot microstrip antenna device," U.S. patent No. RE29296, 1975.
- [14] J. Q. Howell, "Microstrip antennas," *IEEE Trans. Antennas Propag.* vol. AP-23, no. 1, pp. 90-93, 1975.
- [15] J. R James, and G.J Wilson, "New design technique for microstrip antenna arrays", *Proc. 5th European Microwave Conf.*, pp-102-106, Hamburg, 1975.
- [16] G. W Garvin, R.E Munson, L.T Ostwald, and K.G Schroeder, "Low profile electrically small missile base mounted microstrip antennas", *Dig. Int. Symp. Antennas Propag. Soc.*, Urbana, IL, pp-244-247, 1975.
- [17] J. P. Seaux, A. Reineix, B. Jecko, and J. H. Hamelin, "Transient analysis of a space-borne microstrip patch antenna illuminated by an electromagnetic pulse," *IEEE Trans. Electromagnetic Compatibility*, Vol.33, pp. 224-233, Aug.1991.
- [18] P.K.Bondyopadhyay, "Spherical microstrip arrays for mobile satellite communication," *Dig. IEEE Int. Symp. Antennas Propagat.*, Vol. 3, pp.1438–1441, 1995.

- [19] R. E. Thomas and J. Huang, "Ultra-wideband UHF microstrip array for Geo SAR application," *Dig. IEEE Int. Symp. Antennas Propag.*, Vol. 4, pp.2096-2099,1998.
- [20] J. Huang, "Miniaturized UHF microstrip antenna for a Mars mission," *IEEE Int. Symp. Antennas Propag.*, Vol. 4, pp. 486 –489, 2001.
- [21] J. T. Bernhard, R. Wang, R. Clark, and P. Mayes, "Stacked reconfigurable antenna elements for space-based radar applications," *Dig. IEEE Int. Symp. Antennas Propag.*, Vol.1, pp. 158 -161, 2001.
- [22] I. J. Bahl and P. Bhartia, *Microstrip Antennas*, Artech House, Dedham, MA, 1980.
- [23] J. R. James, P. S. Hall, and C. Wood, *Microstrip Antennas: Theory and Design*, London, UK, Peter Peregrinus, 1981.
- [24] K. Carver and J. Mink, "Microstrip antenna technology," *IEEE Trans. Antennas Propag.*, Vol. 29, pp. 2-24, Jan. 1981.
- [25] A. G. Derneryd, "Linear microstrip array antennas," *Chalmer Univ. Technol.*, Goteborg, Sweden, Tech. Rep. TR 7505, 1975.
- [26] Y. T. Lo, D. D. Harrison, D. Solomon, G. A. Deschamps, and F. R. Ore, "Study of microstrip antennas, microstrip phased arrays, and microstrip feed networks," *Rome Air Development Center, Tech. Rep. TR-77-406*, 1977.
- [27] Y.T Lo, D. Solomon, and W.F Richards, "Theory and experiment on microstrip antennas," *IEEE AP-S Symposium (Japan)*, pp.53-55, 1978.
- [28] W.F Richards, Y.T Lo, and D.D Harrison, "Improved theory for microstrip antennas," *Electron. Lett.*, vol.15, no. 2, pp.42-44, 1979.
- [29] Y.T Lo, D. Solomon, and W.F Richards, "Theory and experiment on microstrip antennas," *IEEE Trans. Antennas Propag.*, vol.27, no. 2, pp.137-145, 1979.
- [30] L. C. Shen and S. A. Long, "Low profile printed circuit antennas," *Dept. Elec. Eng., Univ. Houston*, Houston, TX, Contract DAAG-29-75-0187, Final Rep., 1977.
- [31] K. R. Carver and E. L. Coffey, "Theoretical investigation of the microstrip antenna," *Physic. and Sci. Lab.*, New Mexico State Univ., Las Cruces, Tech. Rep. PT-00929, 1979.
- [32] K.R Carver, "A modal expansion theory for the microstrip antenna", *Dig. Int. Symp. Antennas Propaga. Soc.*, Seattle, WA, pp.101-104, 1979.
- [33] K.R Carver and E.L Coffey, "Theoretical investigations of the microstrip antenna", *Tech. Rept. PT 00929, Physical Science Lab.*, New Mexico Science Univ., Las Cruces, 1979.
- [34] E.L Coffey and T.H Lehman, "A new analysis technique for calculating the self and mutual impedance of microstrip antennas", *Proc. Workshop on Printed Circuit Antennas*, New Mexico State Univ., pp.31/1-21, 1979.
- [35] J.R James and C.J Wilson, "Microstrip antennas and arrays part i fundamental action and limitations", *IEE Proc. Microwaves, Opt. & Antennas*, vol.1, pp. 165-174, 1977.

- [36] J.R Mosig and F.E Gardiol, "The near field of an open microstrip structure", *IEEE AP-S, Int.Symp. Digest*, pp.379-381, 1979.
- [37] P.K Agarwal and M.C Bailey, "An analysis technique for microstrip antennas", *IEEE Trans. Antennas Propagat.*, vol. 25, no. 6, pp.756-759, 1977.
- [38] N.G. Alexopoulose, N.K Uzunoglu, and I. E. Rana, "Radiation by microstrip patches," *Dig. Int. Symp. Antennas Propagat.*, pp.722-727, 1979.
- [39] C. A. Balanis, *Antenna Theory: Analysis and Design*, John Wiley & Sons, NY, 1997.
- [40] R. Garg *et. al.*, *Microstrip Antenna Design Handbook*, Artech House, Boston, 2001.
- [41] G. Kumar and K. P. Ray, "*Broadband microstrip antennas*," Boston, Artech House, 2002.
- [42] K.L.Wong, *Planar Antennas for Wireless Communications*, Wiley, 2003.
- [43] Rod Waterhouse, *Microstrip Patch Antennas: A Designer's Guide*, Springer,2003.
- [44] Randy Bancroft, *Microstrip and Printed Antenna Design*, Noble Publishing, 2004.
- [45] Z. N. Chen and M. Y. W. Chia, *Broadband Planar Antennas: Design and Applications*, Wiley, 2006.
- [46] I. Bulu, H. Caglayan, K. Aydin and E. Ozbay, "Compact size highly directive antennas based on the SRR metamaterial medium," *New Journal of Physics*, Vol. 7, 2005.
- [47] C. A. Allen, K. Leong, C. Caloz, T. Itoh, "A two-dimensional edge excited metamaterial-based leaky wave antenna," *IEEE Antennas and Propagation Society International Symposium*, pp.320-323, 2005.
- [48] J. L. Volakis et.al, "Miniaturization methods for narrowband and ultra-wideband antennas," *IEEE International Workshop on Antenna Technology: Small Antennas and Novel Metamaterials*, 2005.
- [49] T.Kokkinos,C.D.Sarris, G.V. Eleftheriades, "Finite-difference time-domain analysis of metamaterial-based leaky-wave antennas," *IEEE Antennas and Propagation Society International Symposium*, pp. 26-29, 2005.
- [50] A.Erentok, R.W. Ziolkowski, "Metamaterial-Inspired Efficient Electrically Small Antennas" *IEEE Transactions on Antennas and Propagation*, vol. 56, no.3, pp. 691 –707, 2008.
- [51] M. A. Hui Feng, Chen Xi, Yang Xin Mi, X U Hong Sheng, Cheng Qiang and Cui Tie Jun, "A broadband metamaterial cylindrical lens antenna," *Chinese Science Bulletin.*, vol. 55, no.19, pp. 2066–2070, 2010.
- [52] D. Guha, Y. M. M. Antar (Eds.), *Microstrip and Printed Antennas: New Trends, Techniques and Applications*, Ch. 11, Wiley, 2011.
- [53] D. Guha, M. Biswas, and Y. M. M. Antar, "Microstrip patch antenna with defected ground structure for cross polarization suppression," *IEEE Antennas Wireless Propag. Lett.*, vol. 4, pp. 455–458, 2005.

- [54] D. Guha, S. Biswas, T. Joseph and M. T. Sebastian, "Defected ground structure to reduce mutual coupling between cylindrical dielectric resonator antennas", *Electronic Lett.*, vol. 44, no.14, pp. 836-837, July 2008.
- [55] H. Moghadas, A. Tavakoli, M. Salehi, "Elimination of scan blindness in microstrip scanning array antennas using defected ground structure," *Int. J. Electron. Commun.*, Vol. 62, pp.155 – 158, 2008.
- [56] D. B. Hou, *et al.*, "Elimination of scan blindness with compact defected ground structures in microstrip phased array," *IET Microwave Antennas propag.*, Vol. 3, no. 2, pp. 269-275, 2009.
- [57] D. Guha, C. Kumar, and S. Pal, "Improved Cross-Polarization Characteristics of Circular Microstrip Antenna Employing Arc-Shaped Defected Ground Structure (DGS)," *IEEE Antennas Wireless Propag. Lett.*, Vol. 8, pp. 1367–1369, 2009.
- [58] D. Guha, S. Biswas, and C. Kumar, "Annular Ring-Shaped DGS to Reduce Mutual Coupling Between Two Microstrip Patches," *IEEE Applied Electromagnetics Conf. AEMC 2009*, pp. 1-4, Kolkata, India, 2009.
- [59] C. Kumar, and D. Guha, "A New Look into the Cross-Polarized Radiation form a Circular Microstrip Antenna and Suppression Using Dot-Shaped DGS," *IEEE AP-S Symp.*, Toronto 2010.
- [60] F. Y. Zulkili, E. T. Rahardjo, and D. Hartanto, "Mutual coupling reduction using dumbbell defected ground structure for multiband microstrip antenna array," *Progress In Electromagnetics Research Letters*, Vol. 13, pp. 29-40, 2010.
- [61] A. K. Shackelford, K.F. Lee, and K. M. Luk, "Design of Small-Size Wide-Bandwidth Microstrip Patch Antennas," *IEEE Antennas and Propagation Magazine*. Vol. 45, no. 1, February 2003.
- [62] S.I. Latif, L. Shafai, and S. K. Sharma, "Bandwidth Enhancement and Size Reduction of Microstrip Slot Antennas," *IEEE Transaction on Antennas and Prop.*, Vol. 53, no. 3, March 2005.
- [63] R. Głogowski and C. Peixeiro, "Multiple Printed Antennas for Integration Into Small Multistranded Handsets," *IEEE Antennas and Wireless Propagation Letters*, Vol. 7, 2008.
- [64] L. Han, W. Zhang, G. Han, R. Ma and L. Li, "Differential Dual-Frequency Antenna for Wireless Communication," *ETRI journal*, Vol. 30, no. 6, pp. 877-879, 2008.
- [65] S. K. Rajgopal and S. K. Sharma, "Investigations on Ultrawideband Pentagon Shape Microstrip Slot Antenna for Wireless Communications," *IEEE Transaction on Antennas and Propagat.*, Vol. 57, no. 5, 2009.
- [66] P. Rakluea, N. Anantrasirichai, K. Janchitrapongvei, and T. Wakabayashi, "Multiband Microstrip-Fed Right Angle Slot Antenna Design for Wireless Communication Systems," *ETRI journal*, Vol. 31, no. 3, pp. 271-281, 2009.
- [67] A. Foroozesh and L. Shafai, "Performance Enhancement of the Compact Microstrip Antennas Using AMC Ground Planes," *IEEE International Symposium on Antennas and Propagation and the USNC/URSI National Radio Science Meeting*, 2009.

- [68] D. R. Jackson *et. al.*, Computer-Aided Design of Rectangular Microstrip Antennas, in *Advances in Microstrip and Printed Antennas*, K. F. Lee and W. Chen (*Eds.*), Wiley, NY, 1997.
- [69] C.T. Lee, and K.L. Wong, “Uniplanar Printed Coupled-Fed PIFA with a Band-Notching Slit for WLAN / Wi MAX Operation in the Laptop Computer,” *IEEE Transaction on Antennas and Propagat.*, Vol. 57, no. 4, 2009.
- [70] J. Siden, P. Jonsson, T. Olsson, and G. Wang, “Performance Degradation of RFID system due to the distortion in RFID tag antenna”, *11th International Conference on Microwave and Telecommunications Technology (CriMiCo 2001)*, Sevastopol, Crimea, Ukraine, 2001.
- [71] P. Nikitin, S. Lam, and K. Rao, “Low cost silver ink RFID tag antennas,” *IEEE Antennas and Propagation Society International Symposium*, Vol. 2B, p. 353, 2005.
- [72] K. Rao, P. Nikitin, and S. Lam, “Antenna design for UHF RFID tags: a review and a practical application,” *IEEE Transactions on Antennas and Propagation*, vol. 53, no. 12, p. 3870, 2005.
- [73] S. R. Aroor and D. D. Deavours, “Evaluation of the State of Passive UHF RFID: An Experimental Approach,” *IEEE Systems Journal*, Vol. 1, no. 2, pp. 168-176, 2007.
- [74] D. M. Dobkin, *The RF in RFID*, Elsevier-News, Chapter 7, 2007.
- [75] M. Sivakumar and D. Deavours, “A Dual-Resonant Microstrip Antenna for Paper board in the Cold Chain,” *IEEE Symposium*, 2008.
- [76] D. D. Deavours, “Analysis and Design of Wideband Passive UHF RFID Tags Using a Circuit Model,” *IEEE RFID*, April 27–28, Orlando, FL, 2009.
- [77] N. A. Mohammed, M. Sivakumar, and D. D. Deavours, “An RFID Tag Capable of Free-Space and On-Metal Operation”, *IEEE Radio and Wireless Symposium*, January 18-22, San Diego, CA, 2009.
- [78] M. T. Hallikainen and F. T. Ulaby, “Microwave Dielectric Behavior of Wet Soil - Part I: Empirical Models and Experimental Observations,” *IEEE Trans. Geosci. Remote Sens.*, vol. GE-23, no. 1, pp. 25–34, 1985.
- [79] M. C. Dobson, F. T. Ulaby, M. T. Hallikainen, and M. A. El-Rayes, “Microwave Dielectric Behavior of Wet Soil-Part II: Dielectric Mixing Models,” *IEEE Trans. Geosci. Remote Sens.*, vol. GE-23, no. 1, pp. 35–46, 1985, doi: 10.1109/TGRS.1985.289498.
- [80] N. R. Peplinski, F. T. Ulaby, and M. C. Dobson, “Dielectric Properties of Soils in the 0.3–1.3-GHz Range,” *IEEE Trans. Geosci. Remote Sens.*, vol. 33, no. 3, pp. 803–807, 1995, doi: 10.1109/36.387598.
- [81] J. R. Holdem, R. B. Keam, and J. A. Schoonees, “Estimation of the number of frequencies and bandwidth for the surface measurement of soil moisture as a function of depth,” *IEEE Trans. Instrum. Meas.*, vol. 49, no. 5, pp. 964–970, 2000, doi: 10.1109/19.872915.

- [82] J. Burrell, T. Brooke, and R. Beckwith, "Vineyard Computing: Sensor Networks in Agricultural Production," *IEEE Pervasive Comput.*, vol. 3, no. 1, pp. 38–45, 2004, doi: 10.1109/MPRV.2004.1269130.
- [83] R. Cardell-Oliver, M. Kranz, K. Smettem, and K. Mayer, "A Reactive Soil Moisture Sensor Network: Design and Field Evaluation," *Int. J. Distrib. Sens. Networks*, vol. 1, no. 2, pp. 149–162, 2005, doi: 10.1080/15501320590966422.
- [84] M. J. Tiusanen, "Wideband antenna for underground Soil Scout transmission," *IEEE Antennas Wirel. Propag. Lett.*, vol. 5, no. 1, pp. 517–519, 2006, doi: 10.1109/LAWP.2006.887549.
- [85] E. P. Stuntebeck, D. Pompili, and T. Melodia, "802-15-4_Underground-Measurements.Pdf," *IEEE Conf.*, pp. 1088–1090, 2006.
- [86] I. F. Akyildiz and E. P. Stuntebeck, "Wireless underground sensor networks: Research challenges," *Ad Hoc Networks*, vol. 4, no. 6, pp. 669–686, 2006, doi: 10.1016/j.adhoc.2006.04.003.
- [87] L. Li, M. C. Vuran, and I. F. Akyildiz, "Characteristics of underground channel for wireless underground sensor networks," *Proc. Med-Hoc-Net*, vol. 7, pp. 13–15, 2007.
- [88] M. C. Vuran and I. F. Akyildiz, "Cross-Layer Packet Size Optimization for Wireless Terrestrial, Underwater, and Underground Sensor Networks," pp. 226–230, 2008, doi: 10.1109/infocom.2008.54.
- [89] I. F. Akyildiz, Z. Sun, and M. C. Vuran, "Signal propagation techniques for wireless underground communication networks," *Phys. Commun.*, vol. 2, no. 3, pp. 167–183, 2009, doi: 10.1016/j.phycom.2009.03.004.
- [90] Z. Sun and I. F. Akyildiz, "Underground wireless communication using magnetic induction," *IEEE Int. Conf. Commun.*, pp. 1–5, 2009, doi: 10.1109/ICC.2009.5199549.
- [91] J. A.L. Riquelme, F. Soto, J. Suardíaz, P. Sánchez, A. Iborra, and J. A. Vera, "Wireless Sensor Networks for precision horticulture in Southern Spain," *Comput. Electron. Agric.*, vol. 68, no. 1, pp. 25–35, 2009, doi: 10.1016/j.compag.2009.04.006.
- [92] H. R. Bogena, J. A. Huisman, H. Meier, U. Rosenbaum, and A. Weuthen, "Hybrid Wireless Underground Sensor Networks: Quantification of Signal Attenuation in Soil," *Vadose Zo. J.*, vol. 8, no. 3, pp. 755–761, 2009, doi: 10.2136/vzj2008.0138.
- [93] A. Salam and M. C. Vuran, "EM-Based Wireless Underground Sensor Networks," *underground sensing . Elsevier Inc*, pp.247-287,2018.
- [94] T. E. Abrudan, O. Kypris, N. Trigoni, and A. Markham, "Impact of Rocks and Minerals on Underground Magneto-Inductive Communication and Localization," *IEEE Access*, vol. 4, pp. 3999–4010, 2016, doi: 10.1109/ACCESS.2016.2597641.
- [95] A. Salam, M. C. Vuran, and S. Irmak, "Pulses in the sand: Impulse response analysis of wireless underground channel," *Proc. - IEEE INFOCOM*, vol. 2016-July, 2016, doi: 10.1109/INFOCOM.2016.7524457.
- [96] H. R. Bogena, M. Herbst, J. A. Huisman, U. Rosenbaum, A. Weuthen, and H. Vereecken, "Potential of Wireless Sensor Networks for Measuring Soil Water

- Content Variability,” *Vadose Zo. J.*, vol. 9, no. 4, pp. 1002–1013, 2010, doi: 10.2136/vzj2009.0173.
- [97] Z. Sun and I. F. Akyildiz, “Channel modeling and analysis for wireless networks in underground mines and road tunnels,” *IEEE Trans. Commun.*, vol. 58, no. 6, pp. 1758–1768, 2010, doi: 10.1109/TCOMM.2010.06.080353.
- [98] M.C. Vuran and A.R. Silva, “Communication through soil in wireless underground sensor networks-theory and practice,” G. Ferrari(ed.), *Sensor Networks, Signals and Communication Technology*, Springer-Verlag Berlin Heidelberg, pp. 309–347,2010.
- [99] N. Chaamwe, W. Liu, H. Jiang, and I. Engineering, “Wave Propagation Communication Models for Wireless Underground Sensor Networks,” no. 60803115, pp. 9–12, 2010.
- [100] X. Dong and M. C. Vuran, “A channel model for wireless underground sensor networks using lateral waves,” *GLOBECOM - IEEE Glob. Telecommun. Conf.*, 2011, doi: 10.1109/GLOCOM.2011.6134437.
- [101] M. Johannes Tiusanen, “Soil Scouts: Description and performance of single hop wireless underground sensor nodes,” *Ad Hoc Networks*, vol. 11, no. 5, pp. 1610–1618, 2013, doi: 10.1016/j.adhoc.2013.02.002.
- [102] X. Dong, M. C. Vuran, and S. Irmak, “Autonomous precision agriculture through integration of wireless underground sensor networks with center pivot irrigation systems,” *Ad Hoc Networks*, vol. 11, no. 7, pp. 1975–1987, 2013, doi: 10.1016/j.adhoc.2012.06.012.
- [103] X. Yu P. Wu, Z. Zhang, N. Wan, and W. Han," Electromagnetic Wave Propagation In Soil for UnderGround Sensor Networks ,"*Progress In Electromagnetics Research M*, vol. 30, vol. 30, pp. 11–23, 2013.
- [104] X. Dong, M. C. Vuran, and S. Irmak, “Autonomous precision agriculture through integration of wireless underground sensor networks with center pivot irrigation systems,” *Ad Hoc Networks*, vol. 11, no. 7, pp. 1975–1987, 2013, doi: 10.1016/j.adhoc.2012.06.012.
- [105] H. Guo and Z. Sun, “Channel and energy modeling for self-contained wireless sensor networks in oil reservoirs,” *IEEE Trans. Wirel. Commun.*, vol. 13, no. 4, pp. 2258–2269, 2014, doi: 10.1109/TWC.2013.031314.130835.
- [106] J. Gutierrez, J. F. Villa-Medina, A. Nieto-Garibay, and M. A. Porta-Gandara, “Automated irrigation system using a wireless sensor network and GPRS module,” *IEEE Trans. Instrum. Meas.*, vol. 63, no. 1, pp. 166–176, 2014, doi: 10.1109/TIM.2013.2276487.
- [107] Z. Zhang, X. Yu, P. Wu, and W. Han, “Survey on Water-saving Agricultural Internet of Things based on Wireless Sensor Network,” *Int. J. Control Autom.*, vol. 8, no. 4, pp. 229–240, 2015, doi: 10.14257/ijca.2015.8.4.23.
- [108] A. Salam and M. C. Vuran, “Impacts of soil type and moisture on the capacity of multi-carrier modulation in internet of underground things,” *2016 25th Int. Conf. Comput. Commun. Networks, ICCCN 2016*, 2016, doi:10.1109/ICCCN.2016.7568532.

- [109] A. Salam and M. C. Vuran, "Wireless underground channel diversity reception with multiple antennas for internet of underground things," *IEEE Int. Conf. Commun.*, 2017, doi: 10.1109/ICC.2017.7996893
- [110] A. Salam and M. C. Vuran, "Smart underground antenna arrays: A soil moisture adaptive beamforming approach," *Proc. - IEEE INFOCOM*, 2017, doi: 10.1109/INFOCOM.2017.8056990.
- [111] S. Jabbar *et al.*, "Analysis of Factors Affecting Energy Aware Routing in Wireless Sensor Network," *Wirel. Commun. Mob. Comput.*, vol. 2018, 2018, doi: 10.1155/2018/9087269.
- [112] Y. Xiaoqing, Z. Zenglin, and H. Wenting, "Experiment measurements of RSSI for wireless underground sensor network in soil," *IAENG Int. J. Comput. Sci.*, vol. 45, no. 2, pp. 237–245, 2018.
- [113] A. Salam, M. C. Vuran, X. Dong, C. Argyropoulos, and S. Irmak, "A Theoretical Model of Underground Dipole Antennas for Communications in Internet of Underground Things," *IEEE Trans. Antennas Propag.*, vol. 67, no. 6, pp. 3996–4009, 2019, doi: 10.1109/TAP.2019.2902646.
- [114] A. Salam, M. C. Vuran, and S. Irmak, "Di-Sense: In situ real-time permittivity estimation and soil moisture sensing using wireless underground communications," *Comput. Networks*, vol. 151, pp. 31–41, 2019, doi: 10.1016/j.comnet.2019.01.001.
- [115] A. Salam, "Underground environment aware MIMO design using transmit and receive beamforming in internet of underground things," vol. 11519 LNCS. Springer International Publishing, 2019.
- [116] A. Salam and S. Shah, "Urban underground infrastructure monitoring iot: The path loss analysis," *IEEE 5th World Forum Internet Things, WF-IoT 2019 - Conf. Proc.*, pp. 398–401, 2019, doi: 10.1109/WF-IoT.2019.8767358.
- [117] A. Salam, "An underground radio wave propagation prediction model for digital agriculture," *Inf.*, vol. 10, no. 4, 2019, doi: 10.3390/info10040147.
- [118] N. Shutimarrungson and P. Wuttidittachotti, "Realistic propagation effects on wireless sensor networks for landslide management," *Eurasip J. Wirel. Commun. Netw.*, vol. 2019, no. 1, 2019, doi: 10.1186/s13638-019-1412-6.
- [119] N. Saeed, M. S. Alouini, and T. Y. Al-Naffouri, "Toward the Internet of Underground Things: A Systematic Survey," *IEEE Commun. Surv. Tutorials*, vol. 21, no. 4, pp. 3443–3466, 2019, doi: 10.1109/COMST.2019.2934365.
- [120] A.J.Compston,J.D. Fluhler, and H.G. Schantz, " A fundamental limit on antenna gain for electrically small antennas,". *2008 IEEE Sarnoff Symposium* pp. 1-5, IEEE,2008.
- [121] M.Howlader, Md.O. Faruq, and T.P. Sattar, "Miniaturization of dipole antenna for low frequency ground penetrating radar," *Progress In Electromagnetics Research C (PIER C)* no.61 pp.161-170,2016.
- [122] A.Babar,L. Ukkonen, M. Soini, and L. Sydanheimo. "Miniaturized 433 MHz antenna for card size wireless systems." *2009 IEEE Antennas and Propagation Society International Symposium*, pp. 1-4. IEEE, 2009.

- [123] Tripathi, N.Mani, "Miniaturized meander PCB antenna for 433MHz," *2015 IEEE Applied Electromagnetics Conference (AEMC)*, pp. 1-2, IEEE, 2015.
- [124] T.Malika, K. Abdennaceur, A.Rahma, and A.Frédéric, "Miniaturized on-body patch antenna for 430MHz wireless digestive monitoring system," *2014 IEEE Workshop on Biometric Measurements and Systems for Security and Medical Applications (BIOMS) Proceedings*, pp. 57-60. IEEE, 2014.
- [125] Kunsei, Herman, K. S. Bialkowski, Md. S.Alam, and A.M. Abbosh. "Improved communications in underground mines using reconfigurable antennas," *IEEE Transactions on Antennas and Propagation*, vol.66, no. 12, pp.7505-7510,2018.
- [126] U.Raza, and A. Salam,"A survey on subsurface signal propagation," *Smart Cities*, vol.3,no.4, pp.1513-1561,2020.
- [127] X.Q.Yu, Z.L. Zhang, and W.T. Han, "Evaluation of communication in wireless underground sensor networks," *IOP Conference Series: Earth and Environmental Science* ,vol. 69, No. 1, p.012083. IOP Publishing,2017.
- [128] M.N.Alam,R.A. Dougal and M.Ali, "Electrically small broadband VHF/UHF planar antenna matched using a non-foster circuit" *Microwave and Optical Technology Letters*, vol.55,no.10, pp.2494-2497,2013.
- [129] A. K. Skriversvik, J.F. Zurcher, O. Staub and J. R. Mosig, "PCS antenna design: the challenge of miniaturization," in *IEEE Antennas and Propagation Magazine*, vol. 43, no. 4, pp. 12-27, Aug. 2001, doi: 10.1109/74.951556.
- [130] R.Saad and K.L.Ford, "A triple band Artificial Magnetic Conductor surface incorporating a split ring resonator antenna," *2014 Loughborough Antennas and Propagation Conference (LAPC)* ,pp. 717-720, IEEE,2014.
- [131] A. Erentok, P. L. Luljak and R. W. Ziolkowski, "Characterization of a volumetric metamaterial realization of an artificial magnetic conductor for antenna applications," in *IEEE Transactions on Antennas and Propagation*, vol. 53, no. 1, pp. 160-172, Jan. 2005, doi: 10.1109/TAP.2004.840534.
- [132] M.E.de Cos and F.Las Heras, Novel uniplanar flexible artificial magnetic conductor," *Applied Physics A*, vol.109, pp.1031-1035,2012
- [133] I. T.Reyes and E. R.Iglesias, "Comparative study on different AMC ground planes and its application to low profile wire antennas," *2009 IEEE Antennas and Propagation Society International Symposium*, North Charleston, SC, USA, 2009, pp. 1-4, doi: 10.1109/APS.2009.5171632.
- [134] G.Harine,S. Abirami,B. Harini, S.E.Florence, and I. Subramaniam, "Design and Analysis of Novel EBG/AMC Unit Cell," *2019 5th International Conference on Advanced Computing & Communication Systems (ICACCS)*, pp. 684-688, IEEE,2019.
- [135] R.Dewan, M.K.Rahim, M.R.Hamid, M.F.Yusoff, N.A. Samsuri,N.A. Murad,and K. Kamardin,Artificial magnetic conductor for various antenna applications," An overview. *International Journal of RF and Microwave Computer-Aided Engineering*, vol.27, no.(6),e.21105.2017

- [136] S. S. Hubbard, J.E Peterson, E.L.Majer , P.T.Zawislanski, K.H. Williams, J.Roberts, and F.Wobber, “Estimation of permeable pathways and water content using tomographic radar data,” *The Leading Edge*, vol.16, pp.1623-1628, 1997.
- [137] M.A.Akkas, and R.Sokullu,”Wireless underground sensor networks: channel modeling and operation analysis in the terahertz band,” *International Journal of Antennas and Propagation*,Vol.2015,pp.1-12,Article ID.780235,2015. . doi:10.1155/2015/780235.
- [138] K.Priyanka and N.Rajesh, “Review and Survey of Compact and Broadband Microstrip Patch Antenna,” *IEEE International Conference on Advances in Engineering & Technology Research (ICAETR-2014)*, pp.1-5, 2014.
- [139] U.K.Muhammad,S.S.Mohammad and M. Raj, “Microstrip patch antenna miniaturisation techniques: a review,” *IET Microwaves, Antennas & Propagation*, vol. 9, Issue. 9, pp. 913–922,2015.
- [140] R.Li,G. Dejean,M.M.Tentzeris and J Laskar, “Development and analysis of a folded shorted-patch antenna with reduced size,” *IEEE Trans. Antennas Propagation*, no. 52, Vol.2 pp. 555–562, 2004.
- [141] C.G.Kakoyiannis, P.Constantinou, ”A compact microstrip antenna with tapered peripheral slits for CubeSat RF payloads at 436 MHz: miniaturization techniques, design, and numerical results,” *IEEE Int. Workshop on Satellite and Space Communications*. pp. 255–259, 2008.
- [142] J.Anguera,L.Boada,C.Puente, C.Borja, and J.Soler, “Stacked H-shaped microstrip patch antenna,” *IEEE Trans. Antennas Propagation*, vol.4, no. 52, pp. 983–993,2004.
- [143] S.A.Bokhari,J.F Zurcher, J.R.Mosig, and F.E Gardiol, “A small microstrip patch antenna with a convenient tuning option,” *In: IEEE Trans. Antennas and Propagation*, Vol.44, no.11, pp. 1521–1528,1996.
- [144] P.Rebeka, “Theory of Miniaturized Shorting-post Microstrip Antennas, *IEEE Transaction on Antennas and Propagation*, 48, vol.1, pp.41-47,2000.
- [145] S. Chatterjee, K. Ghosh, J. Paul, S.K. Chowdhury, D. Chanda, P.P. Sarkar,” Compact microstrip antenna for mobile communication,” *Microw.Opt. Technol.Lett*,vol. 55, no.5, pp. 954–957 ,2013.
- [146] C.Filippo and M.Agostino,”Closed-Form Analysis of Reflection Losses in Microstrip Reflect array Antenna,” *IEEE Transaction in Antenna and Propagation*, vol.60, no.10, pp.4650-4660,2012.
- [147] HFSS: High Frequency Structure Simulator V. 14, Ansoft Corp.,Pittsburgh, PA, USA.
- [148] S. Warathe, R. K. Tanti, and N. Anveshkumar, “Compact vivaldi antenna design at 500MHz for GPR applications,” *2019 IEEE Indian Conf. Antennas Propagation, InCAP 2019*, pp. 1–5, 2019.
- [149] M. Biancheri-Astier, A. Diet, Y. Le Bihan, and M. Grzeskowiak, “UWB Vivaldi antenna array lower band improvement for ground penetrating radar applications,” *Radioengineering*, vol. 27, no. 1, pp. 92–98, 2019.

- [150] G. Castorina, L. Di Donato, A. F. Morabito, T. Isernia, and G. Sorbello, "Analysis and Design of a Concrete Embedded Antenna for Wireless Monitoring Applications [Antenna Applications Corner]," *IEEE Antennas Propag. Mag.*, vol. 58, no. 6, pp. 76–93, 2016.
- [151] J. Owusu, M. R. Bin Hamid, S. Tweneboah-Koduah, and S. Afoakwa, "Omnidirectional antenna with modified ground plane for wideband DVB in handheld devices," *Sci. African*, vol. 13, p. e00872, 2021.
- [152] "ISM 315MHz Helical Antenna ISM 315MHz Helical Antenna," Pulse Finland Oy, *ISM Helical Antenna*, pp. 6–9, Datasheet Version, 2008.
- [153] J. Buckley, D. Gaetano, K. G. McCarthy, L. Loizou, B. O'Flynn, and C. O'Mathuna, "Compact 433 MHz antenna for wireless smart system applications," *Electron. Lett.*, vol. 50, no. 8, pp. 572–574, 2014. doi: 10.1049/el.2013.4312.
- [154] W. Liu, Z. Zhang, and Z. Feng, "ISM 433-MHz miniaturized antenna using the shielding box of mobile terminals," *IEEE Antennas Wirel. Propag. Lett.*, vol. 11, pp. 330–333, 2012.
- [155] T. Zhou, Y. Cao, Z. Cheng, M. Le Berre, and F. Calmon, "A High-Efficiency Compact Planar Antenna for ISM Wireless Systems," *Int. J. Antennas Propag.*, vol. 2017, 2017.
- [156] C. T. Rodenbeck, "Planar miniature RFID antennas suitable for integration with batteries," *IEEE Trans. Antennas Propag.*, vol. 54, no. 12, pp. 3700–3706, Dec. 2006.
- [157] A. Jafargholi, and B. Ghalamkari, "Dual-Band Slim Microstrip Patch Antennas," *IEEE Trans. Antennas Propag.*, vol. 66, no. 12, pp. 6818–6825, 2018.
- [158] X. Zhang, L. Zhu, and N.-W. Liu, "Pin-loaded circularly-polarized patch antennas with wide 3-dB axial ratio beamwidth," *IEEE Trans. Antennas Propag.*, vol. 65, no. 2, pp. 521–528, 2017.
- [159] X. Zhang and L. Zhu, "High-gain circularly polarized microstrip patch antenna with loading of shorting pins," *IEEE Trans. Antennas Propag.*, vol. 64, no. 6, pp. 2172–2178, Jun. 2016.
- [160] X. Zhang and L. Zhu, "Gain-enhanced patch antennas with loading of shorting pins," *IEEE Trans. Antennas Propag.*, vol. 64, no. 8, pp. 3310–3318, May 2016.
- [161] T. Sarkar, A. Ghosh, L. L. K. Singh, S. Chattopadhyay, and C. Y. D. Sim, "DGS-integrated air-loaded wideband microstrip antenna for X- and Ku-band," *IEEE Antennas Wireless Propag. Lett.*, vol. 19, no. 1, pp. 114–118, Jan. 2020.
- [162] T. Sarkar, A. Ghosh, S. Chakraborty, L. L. K. Singh, and Sudipta Chattopadhyay, "A new insightful exploration into a low profile ultra-wide-band (UWB) microstrip antenna for DS-UWB applications," *Journal Electromag. Waves App.*, vol. 35, no. 15, pp. 2001–2019, 2021.
- [163] Zonunmawii, A. Ghosh, L. L. K. Singh, and S. Chattopadhyay, "Cavity Field Modulation with Modulating Circular Patch Antenna Surface: A Key to Realize Reduced Horizontal Radiation and Omni-Present Improvement in Radiation Performance," *IEEE Access*, vol. 10, pp. 18434–18444, 2022.

- [164] H. Mosallaei and K. Sarabandi, "Antenna miniaturization and bandwidth enhancement using a reactive impedance substrate," *IEEE Trans. Antennas Propag.*, vol. 52, no. 9, pp. 2403–2414, Sept. 2004.
- [165] Y. Gong, S. Yang, B. Li, Y. Chen, F. Tong, and C. Yu, "Multi-band and high gain antenna using AMC ground characterized with four zero-phases of reflection coefficient," *IEEE Access*, vol. 8, pp. 171457–171468, 2020.
- [166] F. Rahmadani and A. Munir, "Microstrip patch antenna miniaturization using artificial magnetic conductor," *6th International Conference on Telecommunication Systems, Services, and Applications (TSSA)*, pp. 219–223, 2011.
- [167] A. P. Feresidis, G. Goussetis, S. Wang, and J. C. Vardaxoglou, "Artificial magnetic conductor surfaces and their application to low-profile high-gain planar antennas," *IEEE Trans. Antennas Propag.*, vol. 53, no. 1, pp. 209–215, 2005.
- [168] F. Costa and A. Monorchio, "Closed-form analysis of reflection losses in microstrip reflectarray antenna," *IEEE Trans. Antenna Propag.* vol. 60, no.10. pp. 4650–4660, 2012.
- [169] S.A. Tretyakov and C.R. Simovski, "Dynamic model of artificial reactive impedance surfaces," *Journal Electromag. Waves App.*, vol. 17, no.1, pp. 131–145, 2003.
- [170] S. K. Podilchak, A. P. Murdoch, and Y. M. M. Antar, "Compact, microstrip-based folded-shortened patches: PCB antennas for use on microsatellites," *IEEE Antennas Propag. Mag.*, vol. 59, no. 2, pp. 88–95, 2017.
- [171] A. Narbudowicz, R. Borowiec, and S. Chalermwisutkul, "No-need-to-deploy UHF antenna for CubeSat: design based on characteristic modes," *IEEE Antennas Wireless Propag. Lett.*, vol. 20, no. 4, pp. 508–512, 2021.
- [172] D.F. Sievenpiper, D.C. Dawson, M.M. Jacob, T. Kanar, S. Kim, J. Long, and Quarfoth, "Experimental validation of performance Limits and Design Guidelines for Small Antennas," *IEEE Transaction on Antenna and Propagation*, Vol.60, no.1 pp.8-19, 2012.
- [173] T. Alam, A. F. Almutairi, M. Samsuzzaman, M. Cho, and M. T. Islam, "Metamaterial array based meander line planar antenna for cube satellite communication," *Sci. Rep.*, vol. 11, no. 1, pp. 1–12, 2021.
- [174] Yang, S. L. Steven, A. A. Kishk, and K. F. Lee, "Rectangular patch antenna based on TE modes supported by artificial magnetic conducting surfaces," *Proc. URSI Gen. Assem.*, 2008.
- [175] T. Mitha and M. Pour, "Investigation of dominant transverse electric mode in microstrip patch antennas," *IEEE Trans. Antennas Propag.*, vol. 67, no. 1, pp. 643–648, Jan. 2019.
- [176] A. Andújar, J. Anguera, C. Puente, and A. Pérez, "On the radiation pattern of the L-shaped wire antenna," *Progress in Electromagnetics Research M*, no. 6, pp. 91–105, 2009.

- [177] K. M. Luk, L. K. Au Yeung, C. L. Mak, and K. F. Lee, "Circular patch antenna with an L-shaped probe," *Microw. Opt. Technol. Lett.*, vol. 20, no. 4, pp. 256–257, Feb. 1999.
- [178] S. H. Jeong and H. W. Son, "UHF RFID tag antenna for embedded use in a concrete floor," *IEEE Antennas Wireless Propag. Lett.*, vol. 10, pp.1158–1161, Oct. 2011.
- [179] T. H. Mitha and M. Z. A. Pour, "Effect of ground plane size on a rectangular microstrip patch antenna based on TE modes supported by perfect magnetic conducting surface," *IEEE International Symposium on Antennas and Propagation & USNC/URSI National Radio Science Meeting*, pp. 2237–2238, 2017.

BIO-DATA OF THE CANDIDATE

Name of Candidate : Sarath Kumar Annavarapu
Date of Birth : 15/01/1986
Contact : 9160429450
Saratkumar.annavarapu@gmail.com
Permanent Address : S/O: A. Hanumaiah,
Hno:92-2-212, 7th lane, A.T Agraharam
Wardno:26, Guntur.
Dist: Guntur
Pin: 522004
State: Andhra Pradesh

Married : Yes

Educational Details

BE : Anna University ,Chennai, with 65%
M.Tech :Electronics and Communication Engineering, JNTUK
Kakinada, Andhra Pradesh with 65 %

Ph.D Course work : Mizoram University ,SGPA of 9.3

LIST OF PUBLICATIONS

Referred Journals (SCI)

1. **S. K. Annavarapu**, A. Ghosh, L. L. K. Singh, S. Chattopadhyay and C. -Y. - D. Sim, "Fringing Aperture Modulation of Transverse Electric Mode Excited Microstrip Antenna for Wireless Underground Sensor Networks," in *IEEE Transactions on Antennas and Propagation*, vol. 71, no. 9, pp. 7250-7260, Sept. 2023, doi: 10.1109/TAP.2023.3295508.
2. **S. K. Annavarapu**, A. Ghosh, L. Lolit Kumar Singh, S. Chattopadhyay, and C. Y. D. Sim, "Application of Dielectric-Artificial Magnetic Conductor Composite Substrate to Design Miniaturized P-Band Microstrip Antenna for Wireless Underground Sensor Network," *IEEE Antennas Wirel. Propag. Lett.*, vol.21,no. 12, pp. 2352–2356, 2022, doi: 10.1109/LAWP.2022.3193415.

International Conferences

1. **S.K. Annavarapu**, L.L.K. Singh, Chattopadhyay, and A. Ghosh, "Miniaturization of Rectangular Microstrip Antenna using Shorting Posts for low frequency Wireless Underground Sensor Networks, "presented in *International Conference on Intelligent Computing Systems and Applications (ICICSA 2022)*, NIT-Silchar Assam, India, September.2022.
2. **S.K. Annavarapu**, L.L.K. Singh, Chattopadhyay, and A. Ghosh, "Determination of Suitable frequency for underground Electromagnetic Wave Propagation," in *International Conference on Data Science and Communication (ICTDsC-2023)*, Siliguri Institute of Technology, West Bengal, India, March.2023.
3. **S. K. Annavarapu**, A. Ghosh, L. L. K. Singh and S. Chattopadhyay, "Artificial Magnetic Conductor based Composite substrate Antenna for Low Frequency Wireless Underground Sensor Networks," 2023 3rd International conference on Artificial Intelligence and Signal Processing (AISP), VIJAYAWADA, India, 2023, pp. 1-3, doi: 10.1109/AISP57993.2023.10134897.

PARTICULARS OF THE CANDIDATE

Name of Candidate : Sarath Kumar Annavarapu
Degree : Ph.D.
Department : Electronics and Communication Engineering

Title of Thesis : Design and Analysis of Antennas for Wireless
Underground Propagation

Date of Admission : 12th AUGUST 2019
Approval of Research Proposal :
 1.DRC : 4th MARCH 2020
 2.BOS : 22nd APRIL 2020
 3.School Board : 13th MAY 2020

MZU Regn No : 1900103
Ph.D Regn No : MZU/Ph.D/ 1446 of 12.08.2019
Extension : No

Head

Department of Electronics and Communication Engineering

ABSTRACT

**DESIGN AND ANALYSIS OF ANTENNAS FOR WIRELESS
UNDERGROUND PROPAGATION**

**AN ABSTRACT SUBMITTED IN PARTIAL FULFILLMENT OF
THE REQUIREMENTS FOR THE DEGREE OF DOCTOR OF
PHILOSOPHY**

SARATH KUMAR ANNAVARAPU

MZU REGN NO: 1900103

Ph. D REGN NO: MZU/Ph.D./ 1446 of 12.08.2019



**DEPT. OF ELECTRONICS & COMMUNICATION
ENGINEERING
SCHOOL OF ENGINEERING AND TECHNOLOGY**

OCTOBER 2023

**DESIGN AND ANALYSIS OF ANTENNAS FOR WIRELESS
UNDERGROUND PROPAGATION**

BY

Sarath Kumar Annavarapu

Department of Electronics & Communication Engineering

Name of Supervisor : Prof. L. Lolit Kumar Singh

Name of Joint Supervisor : Prof. Sudipta Chattopadhyay

Submitted

In partial fulfillment of the requirement of the Degree of Doctor of Philosophy in
Electronics & Communication Engineering of Mizoram University, Aizawl.

ABSTRACT

In the present era of Technology, the wireless communication is grabbing the importance and has become an interesting field of research. Wireless Sensing applications requires a sensor node that consists of a processing unit, memory and antenna (Transmitter and receiver) as important components. These sensor nodes are useful in many applications for Internet of things. One of such application is wireless underground sensing.

Electromagnetic wave propagation depends on parameter of the medium of in which they propagate. For Underground environment factors such as volumetric water content of soil, rocks, roots of the trees and depth plays a key role. Determining the suitable frequency and designing suitable antennas for underground wireless communication is the main objective of this research work. It is found from the literature that low frequencies in the range of Mega Hertz (MHz) preferably in P-Band is suitable. This is due to the fact that higher frequency signal gets more attenuation in the underground. Decrease in the operating frequency of antenna affects the antenna parameter such as size, gain etc. The design of small size, good performance antenna for low frequency communication is one of challenges for antenna design. In this research work the design and analysis of planar rectangular microstrip antennas for low frequency (below 1 GHz) with good performance is reported.

The gain of a miniaturized patch antenna decreases dramatically as its size decreases. As a result, designing miniaturized high gain antennas is a difficult task. Various methods can be used to improve the gain of such miniaturized antennas, one of such methods is the usage of meta material backing. In order to maximize the benefits of metamaterials, their properties must be investigated so that these characteristics must be compatible for the gain enhancement of antenna. In this thesis, an artificial magnetic conductor (AMC) is embedded with the antenna to improve its performance. AMC is a meta material having in phase reflection properties that, the gain of an antenna can be increased when it utilized properly.

This thesis investigates the suitable frequency for communication in underground environment using simulation and experimental validation. The findings obtained in all of the cases reveal that the received signal strength at low frequency is found to be better than high frequency. This initially validates the feasibility of low frequencies in MHz range for underground electromagnetic wave propagation.

As the low frequencies are preferred, antenna size increases at such low frequencies. As a result, a miniaturization approach must be integrated into the antenna design in order to make it small. This work investigates the quarter wave patch (QWP) with shorting vias in depth. The effect of varying the number and position of shorting vias on operating frequency is explored. This QWP with shorting vias offers a more suitable alternative for miniaturized antenna structures. The miniaturized version is achieved by reducing the number of shorting vias to at the QWP's edge. The frequency of operation can also change by adjusting the position of the shorting vias from the edge of the QWP.

Even if downsizing is achieved using QWP and shorting vias, the gain is substantially reduced. In the thesis four number of shorting vias are used to get our desired QWP structure. The inclusion of metamaterial with the aforementioned QWP improves antenna gain. In the current study, an artificial magnetic conductor (AMC) having in phase reflection properties is used. The AMC is used as composite substrate in one of the proposed structures. Usage of AMC as composite substrate to attain gain of 3.1 dBi at 413 MHz is probably the first work to be reported as per the authors knowledge.

Soil conditions varies with different parameters such as location, climate, water content and depth. To perform multiple task, multi frequency antennas are preferred. In this work a dual band Transverse Electric (TE) mode Exited antenna is designed and analyzed. A dual periodic AMC array is integrated to form a 3×3 AMC patch of size $150 \text{ mm} \times 150 \text{ mm}$ and 5×5 AMC ground of size $250 \text{ mm} \times 250 \text{ mm}$ respectively. Furthermore, the TE structure is modified by incorporating dielectric strips at the four corners of the patch. Because of incorporation of strips the fringing aperture modulation is obtained which make the antenna properly matched and also

producing good gains in both the operating bands. This antenna operates at frequencies of 572 MHz and 768 MHz with gain of 4.5dBi and 6.3 dBi respectively. The bandwidth of the antenna at operating bands are 12.4 % and 12.7 % respectively.

Finally, the thesis ended with a conclusion and future scopes. The significance of low frequency antenna applications is emphasized in the chapters wherever needed. This might aid researchers and scientists working on low frequency antenna designs for specific purposes.